Department of Engineering,

School of Civil Engineering

Thermal-hydro-mechanical Coupled Model for Energy Pile in Mudstone Area

Dissertation of M.Phil.

Author

Jiahui Zhou

ID：201444543

University of Leeds

Date

01/05/2024

Abstract

Energy piles, a novel energy-saving technology leveraging shallow geothermal resources, play a crucial role in addressing energy shortages and environmental pollution. This technology integrates the buried heat exchange pipes from conventional ground-source heat pump systems with building pile foundations, forming underground heat exchangers that can both bear structural loads and exchange thermal energy. This study, focusing on a shallow mudstone layer in the Woodsmith project, examines the heat exchange efficiency, thermo-mechanical (TM) coupling, and thermal-hydraulic-mechanical (THM) effects during temperature cycles of energy piles. A 3D thermal-hydro (TH) coupling model was developed in COMSOL to evaluate their heat exchange efficiency and longevity, and to investigate thermal interference in pile groups. A 3D TM model was also created to assess the coupling effects in mudstone, while a 2D THM model explores the mechanical responses and pore water pressure variations during temperature cycles.

Simulation results reveal that mudstone's low permeability minimally impacts the heat transfer efficiency of energy piles due to density-driven pore water flow. Factors like mudstone’s thermal properties, and the flow velocity of the working fluid inside the heat exchange pipes, influence the efficiency of energy piles. TM coupling simulations indicate that thermal disturbances cause notable displacements in energy piles, particularly cooling contraction or heating expansion, with maximum displacements at the pile head and minimized, constrained displacements at the centre. Mudstone's thermal expansion coefficient, elastic modulus, and thermal conductivity critically influence these mechanical responses. THM coupling simulations show the pile head moves upward during heating and downward during cooling, with minimal impact on the surrounding layer's pore water pressure. The temperature setting of the heat exchanger crucially affects these displacements and pressure changes.

Publication

During my MPhil studies, in addition to the research described in this paper, I also collaborated with colleagues at the University of Leeds on deep geothermal energy extraction. The focus of this study was to derive the fully coupled thermo-hydro-mechanical (THM) governing equations for dual-porosity geothermal reservoirs, addressing the interaction between strain, pore/fracture pressure, and temperature. We explored the feasibility and long-term environmental impacts of Enhanced Geothermal Systems (EGS) for harnessing geothermal energy in hot dry rock (HDR) formations (Wang et al., 2023). In this part, I primarily participated in data collection before modelling, contributed to some modelling work, drafted sections of the literature review, and conducted proofreading in the later stages. Then we published the paper in "Applied Thermal Engineering," which is a Q1 journal. The journal mainly covers research in the field of thermal engineering, including aspects such as heat transfer, thermodynamics, and fluid mechanics. With an impact factor of 6.4 and a Cite Score of 11.8, it demonstrates the high impact and recognition of the journal in the academic community:

WANG, K., ZHOU, J., MA, Y., DING, A. & CHEN, X. 2023. Constitutive and numerical modelling for the coupled thermal-hydro-mechanical processes in dual-porosity geothermal reservoir. *Applied Thermal Engineering,* 223, 120027.

The research results of chapters 6, and 7 are expected to be submitted to the journal "Geothermics" for review. "Geothermics" is an international journal focused on research and applications in the field of geothermal energy.

ACKNOWLEDGMENTS

Firstly, I would like to thank my friend Rouqi for her unwavering support and encouragement. Her companionship and concern have been invaluable to me throughout my whole study life at the University of Leeds, and I am deeply grateful for her presence in my life. Rouqi has always been able to offer valued advice whenever I have felt lost or unsure, and I have learned and grown from her over the past few years. I feel truly lucky to have met such a wonderful friend.

I would also like to express my gratitude to my supervisor, Professor Chen, for his guidance and mentorship. Dr. Chen has been a respected mentor, and I am deeply grateful for his advice. Whenever I encountered difficulties, Dr. Chen would patiently analyse the causes of the challenges and help me overcome them. His encouragement and feedback have been instrumental in my research, and I feel privileged to have had the opportunity to be mentored by him.

Finally, I would like to thank my parents for their support and encouragement. Their love and support have been the driving force behind my perseverance, and I am truly grateful for their unconditional love for me. I feel very lucky to have such lovely parents.

Content

List of Figure

List of Table

Nomenclature

EP-Energy Pile

FEA-Finite Element Analysis

GSHP-Ground Source Heat Pumps

GWL-Ground Water Level

HRD-Hot Dry Rock

HEP-Heating Exchanger Pipes

TH-Thermal Hydro

TM-Thermal Mechanical

THM- Thermal Hydro Mechanical

1 Introduction

1.1 Background

In order to mitigate global warming, the development of various clean energy sources has become one of the hot topics in academia. Energy piles, geotechnical structures that utilize geothermal energy for heating and provide foundation support, have been used in Australia and the USA for over 40 years. While the safety and efficiency of energy piles are widely recognized by researchers, their operation in mudstone ground conditions has received little attention. Specifically, mudstone is characterized by low permeability, low strength, and fragility.

Currently, research on installing energy piles in mudstone formations is rare. Most studies on energy piles focus on clay or sandy soils. However, mudstone is widely distributed globally, found in regions such as the Sichuan Basin in China and the Marcellus Shale in the United States. In the United Kingdom, mudstone underlies much of central and southern England, serving as the bedrock for many urban areas and their infrastructure. Therefore, the findings of this study could provide references for future installation and construction of energy piles in mudstone regions.

1.2 Objectives and Aims

The aim of this study is to establish a finite element analysis (FEA) model to investigate the installation of energy piles in mudstone environments, considering the effects of TH, TM, and THM coupling. The results from these models will contribute to the design and analysis of energy piles in mudstone areas.

The objectives of this report are as follows:

1. To collate and analyze the properties of mudstone, review the history of energy piles, and assess the advantages and disadvantages of various types of energy piles.

2. To construct a conceptual model of energy pile THM coupling, gather geological and experimental data to select suitable mudstone parameters, and perform numerical simulations.
3. To use 3D TH-coupled and TM-coupled models to predict and assess the efficiency of energy piles in mudstone areas. Additionally, to develop 2D THM-coupled models to predict the long-term operation of energy piles, aiming to simplify computational complexity.

1.3 The Structure of Dissertation

1.3.1 Literature Review

This section aims to review the literature on the fundamental classifications and characteristics of energy piles in mudstone. Additionally, it will consolidate the findings of finite element simulation analyses on the interplay of thermal, hydraulic, and mechanical factors in energy piles. Through this review, the objective is to identify gaps in our understanding and to establish a theoretical foundation for the formulation of conceptual models.

1.3.2 Ground Conditions

This section discusses the geological models derived from Cleveland stratigraphic survey reports (Timmen et al., 2023) and the Woodsmith project report (Gschnitzer et al., 2020). It includes stratigraphic classification, rock characteristics, and hydrological conditions.

1.3.3 Methodology

The main contents of this chapter include selecting finite element analysis software, the rationale behind creating conceptual models, and a discussion of the study's limitations. The selection of coupling equations varies according to the research objectives.

1.3.4 Data Analysis

These sections employ TH, TM, and THM coupling models to analyse heat transfer performance, pore water seepage, thermal-mechanical responses, and deformation of energy piles in mudstone. The TH model assesses heat transfer and pore water seepage. The TM model studies thermal-mechanical response. The THM model simulates an annual operation (400 days), assessing thermal load effects on pile deformation and pore water pressure changes in the surrounding soil.

1.3.5 Conclusion and Future Expectations

Chapter 8 is the conclusion section, providing an overview of the primary findings derived from the model outcomes. It also addresses the current research limitations and suggests areas for future model improvements.

2 Literature Review

2.1 Background

With rapid population growth worldwide and economic shake-ups caused by epidemics and wars, the energy demand is more critical than ever before. Conventional energy sources such as fossil fuels are not only non-renewable but also generate significant amounts of greenhouse gases. Although in the short term, for economic and human survival reasons, reducing the use of large amounts of these traditional energy sources is not feasible, the development and use of clean energy sources can be recognized as an effective solution to this environmental challenge. In recent years, concern about energy shortages has been increasingly mentioned across various fields. Particularly considering the need to control carbon emissions, the demand for green energy is urgent. To address this concern, some geotechnical researchers have combined conventional structures with heat exchangers to develop energy piles (or thermal piles), achieving the dual purpose of supporting the superstructure and supplying energy (Arzanfudi et al., 2020). The energy source of the thermal pile mainly derives from geothermal energy; thus, energy piles are highly anticipated to achieve zero-emission energy buildings by extracting this type of renewable energy.

The approach was first used in Austria in the 1980s (Brandl, 2006), Since then, energy pile technology has been adopted in many countries, particularly the USA and Sweden. In the UK, although the adoption of this technology did not begin early, there has been substantial development in recent years. Figure 1 clearly illustrates the rapid adoption and use of energy piles in the UK from 2005 to 2019. By 2019, the total number of energy piles installed in the UK had increased by 4174%, resulting in approximately 7500 tonnes of annual carbon dioxide savings attributed to their installation.

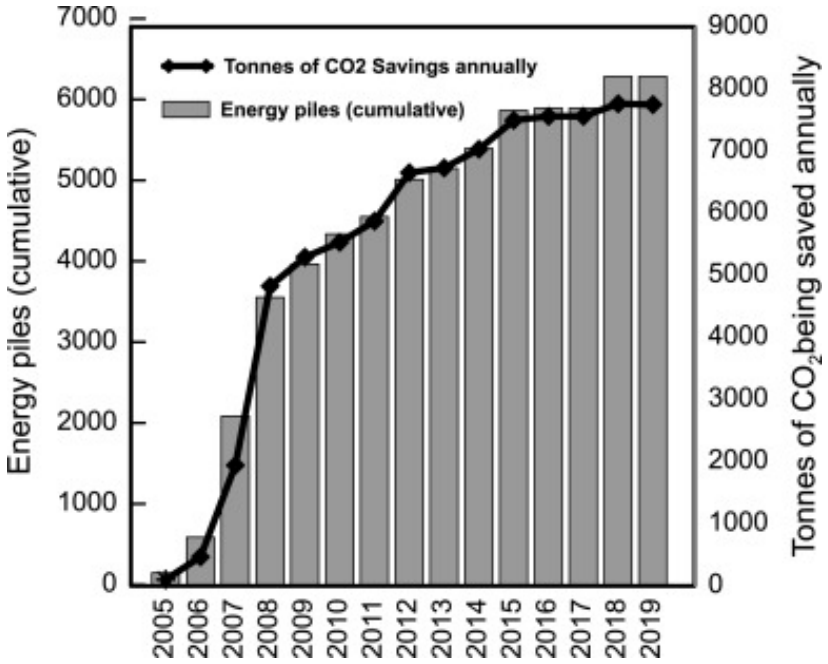

Figure 1. Energy piles installed in the UK and resultant Annual Co2 savings (to date in 2019) (Sadeghi and Singh, 2023)

2.2. Conception of Energy Piles

2.2.1 Ground-source Heat Pumps System

The operation of energy piles is based on ground-source heat pumps (GSHP). In a typical ground-source heat pump system (shown in Figure 2), three units (energy piles, heat pump, and distribution system) work together to achieve energy transfer (Sani et al., 2019). Energy piles, as the primary unit, have the function of extracting and injecting heat from the shallow earth. In winter, the heat extracted by the pile foundation passes through the heat pump unit to the distribution system (secondary unit) to supply the building with warmth. In summer, the process is reversed to keep the building cool, with excess heat discharged to the ground by energy piles.

In the GSHP system, the heat pump system changes the pressure to control the compression, condensation, and expansion evaporation of the working fluid. The working fluid brings heat flow into the evaporator, where the refrigerant absorbs this heat energy, causing its temperature to

increase. By increasing the pressure of the high-temperature refrigerant, the compressor converts it to a high-pressure and high-temperature state (vapour). The high-pressure, high-temperature refrigerant passes into the condenser, where it condenses and releases heat, which is used to heat the building. After condensing, the refrigerant's pressure and temperature are reduced by the expansion valve. It then leaves the expansion valve and returns to the evaporator, starting the next cycle.

After the above process, heat can be transferred from a low-temperature source to a higher-temperature sink (Rees, 2016). In other words, the function of the heat pump is to upgrade low-grade energy extracted from the ground to high-grade energy, providing heating and cooling for buildings.

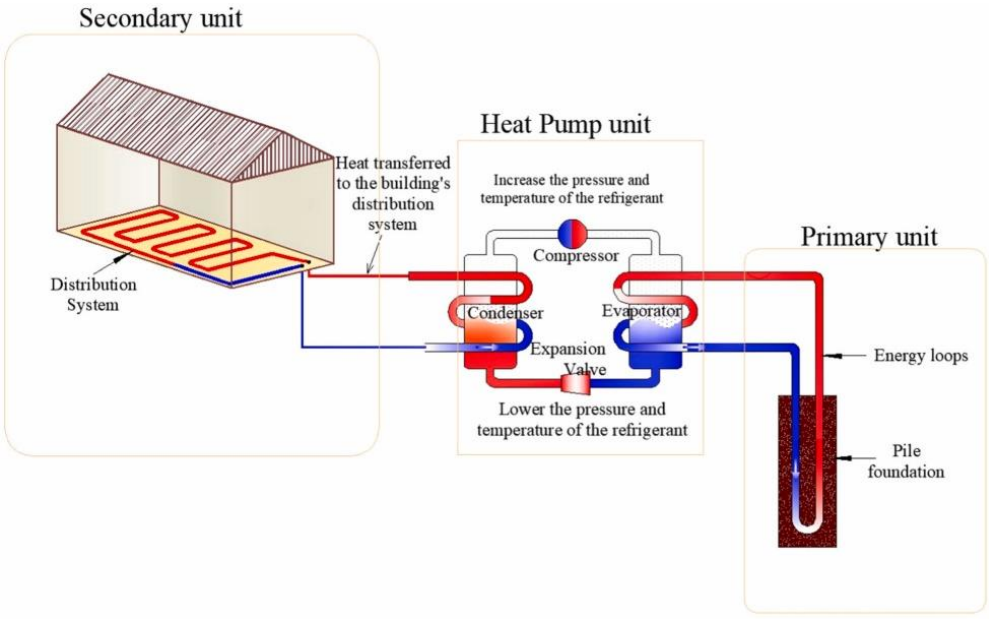

Figure 2. The typical ground-source heat pump system (Sani et al., 2019)

2.2.2 Component of Energy Piles

A typical configuration of an energy pile is shown in Figure 3, It comprises three main components, namely:

1. The heat exchanger tubes are connected to the heat pump and serve as the transmission path for the heat extracted from the ground.
2. The reinforcement cage is utilized to secure the heat exchanger tubes.
3. The backfill material collaborates with the reinforcement cage to support the superstructure and facilitate heat exchange.

In practice, the components and installation process of energy piles depend on the specific configurations; however, the above components are the most typical and common in practical projects.

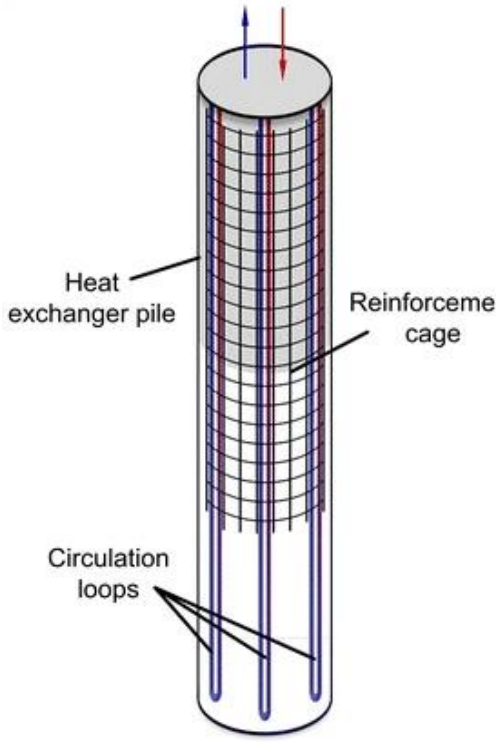

Figure 3. The typical configuration of energy piles (Olgun et al., 2015)

2.3. The Types of Energy Piles

The classification of ground heating exchanger pipes (HEP) is mainly based on the configuration of the heat exchanger pipes and the cross-sectional geometry of piles. Of these, the configuration of the pipes has a significant impact on performance. In practical GSHP system projects, U and

W-shaped pipes are most commonly used (shown in Figure 4), while spiral or helix-type exchangers are not popular in practice and are mostly mentioned in research. The next section details the characteristics of energy piles based on different shapes of heating exchanger tubes (Chen et al., 2021).

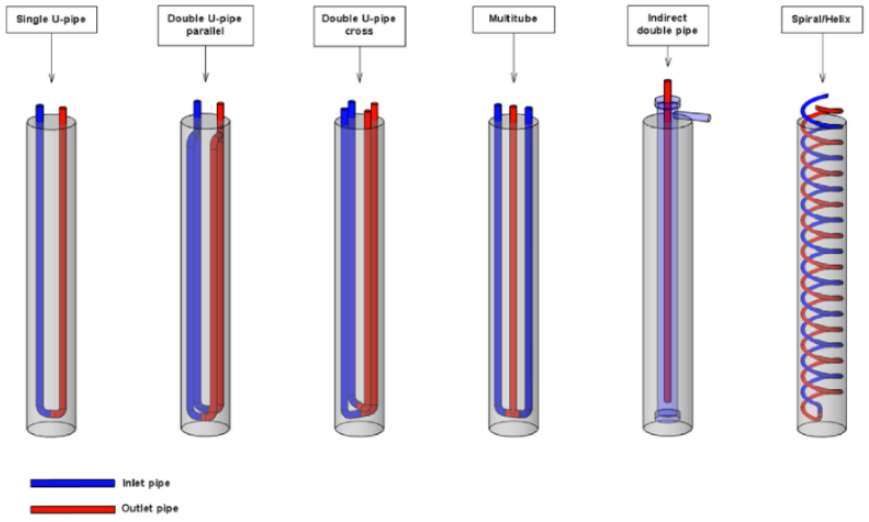

Figure 4. The common type of energy piles (Fadejev et al., 2017)

2.3.1 U-shaped Heat Changer Pipe and W-shaped Heat Changer Pipe

Compared to other shapes of heat exchangers, U-tube heat exchangers are more economical and easier to install. Therefore, the most popular heat exchanger type in the industry has been the single U-pipe for the past thirty years. To ensure the efficiency of U-tube energy piles, a series of studies has analyzed the parameters related to their thermal efficiency. These results identified the key factors that influence the U-tube pile energy efficiency (Bozis et al., 2011). These factors include the layout of the heat exchanger pipe, pile length, concrete conductivity, pile diameter, and concrete cover. It is also indicated that the most significant design parameter is the number of pipes because compared with extending the pile dimensions, the number of pipes increased more easily

(Cecinato and Loveridge, 2015). However, it is not the case that a higher number of pipes always results in a greater improvement in the thermal efficiency of the energy pile.

Numerical simulations indicate that doubling the number of pipes from 2 to 4 results in an increase in exchanged energy that falls significantly short of doubling (Mohamad et al., 2021). Further increasing the number of pipes from 6 to 12, the efficiency of exchanged energy was found to be even smaller. In addition to the concern about the number of pipes, other studies have been undertaken to analyse the impact of the connections of heat transfer pipes. A numerical model has been developed to predict energy flows and temperature changes in and around a borehole (Carotenuto et al., 2017). The model also analyses the efficiency of single and double U-tubes. The results indicate that regardless of the connections of heat transfer pipes, the double U-loop is always more efficient than the single pipe, and the efficiency of the in-series double U-tube is much higher than the parallel configuration.

However, it cannot be proven that the in-series configuration is always the best choice when designing energy piles. Previous research has shown that the efficiency of series U-tubes is slightly lower than parallel U-tubes. More pipes also show high potential for heat transfer, but a higher number of U-loops in series means higher construction costs (Gao et al., 2008). Multiple parallel U-tubes are commonly applied when designing pile heat exchangers due to their larger heat transfer area and simpler installation process. A recent study presented analytical and numerical heat transfer models separately to define the thermal effectiveness of the pile. The results also showed that increasing the number of U-tubes is beneficial for the overall thermal effectiveness of the energy pile. The reason for this is that increasing the number of U-tubes extends the heat transfer area. However, the increase in the number of U-tubes should be limited to an appropriate range because an excessive number of pipes may decrease overall thermal effectiveness due to

thermal interference among the U-tubes (Cui et al., 2020). The research discussed above points out that increasing the number of U-tubes in an energy pile can improve heat performance. However, the thermal interferences that occur between adjacent pipe loops should be considered, as they can limit heat efficiency.

W-pipe heat exchangers are also a popular type used in energy piles in addition to U-shaped tubes. The thermal transfer capacity of a single W-pipe is close to that of 3U-tube energy piles, and the installation cost of the W-shape is less than half that of the 3U-shape (Yoon et al., 2015). The reason the W-tube is not as widely used as the U-tube in practice is not only its more complicated construction process but also the risk of air accumulation at the top of the W-pipe (Zhang et al., 2017). There is currently very limited research focused on the performance of W-shaped heat exchanger pipe piles. An experiment indicates that the W-type heat exchange in the cooling process is much higher than in the heating operation, and similar to the U-pipes, a compact W layout can reduce the effectiveness of heat exchange due to thermal interferences (Park et al., 2017).

2.3.2 Spiral-shaped Heat Changer Pipe

Research on spiral (or helix) heat exchangers in energy piles has also garnered significant attention. The spiral-shaped energy pile, compared with other shapes, has better heat transfer efficiency, prevents air blocking, reduces the risk of thermal "short-circuiting", and simplifies the pipe connection process (Man et al., 2017). Based on these advantages, some researchers regard the spiral heat exchanger pipe as the best configuration for pile heat exchangers (Mohamad et al., 2021).

According to Zhao et al. (2015), in their thermal performance analysis of various types of energy piles, changes in temperature distribution indicate that the spiral heat exchanger achieves more uniform heat transfer compared to U-shaped and W-shaped heat exchanger pipes. The change distributions in temperature are more uniformly due to the layout of the coil, the coils are not simply placed vertically in the pile like W and U shapes but are fixed to the reinforcement cage in equally spaced wraps (Zhang et al., 2015). Therefore, the heat transfer ability greatly relies on the density of the coils. A higher density of coils means more coils arranged inside a pile, which can significantly increase the heat transfer capacity (Zhang et al., 2017).

Another research also proves that small coil pitch energy piles have better thermal efficiency, it compared 4 different spiral pitches (0.25, 0.5, 1.0, 2.0 m) of the heat transfer rate, which showed the difference between the maximum and minimum temperatures of the smallest spiral pitch is most closed (Zhao et al., 2017). This also indirectly explains why a small pitch usually has a better uniform distribution for the heat flux in the pile and is more energy-efficient than a large spiral pitch. However, this does not mean the spiral pitch can be reduced indefinitely. If the pitch size is smaller than 0.25 m, it can lead to thermal interferences and limit an increase in heat transfer performance (Carotenuto et al., 2017). In addition to pitch size, pipe dimensions also affect the thermal efficiency of spiral-type energy piles. Luo et al. (2016) tested the thermal efficiency of 25mm and 32mm diameters spiral pipes, the results in the short-term (operation of 72 h) are shown in Figure 5, the mean thermal exchange rate of 25mm diameters spiral pipes is 224.72 W/m and 32mm diameters spiral pipes is 296.3 W/m, which means that the larger diameter pipes of ground heat exchanger usually has higher thermal efficiency. (Luo et al., 2016).

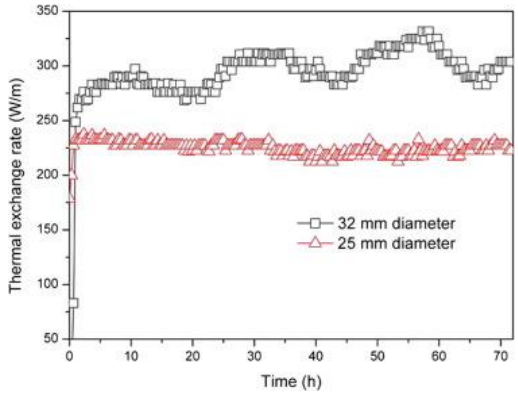

Figure 5. The thermal exchange rate of spiral-type ground heat exchangers with 25mm diameter pipe and 32mm diameter pipe (Luo et al., 2016)

2.4 Thermal Behaviour of Energy Piles

Understanding heat transfer can establish a basis for assessing the thermal performance of energy piles. The thermal process in energy piles is primarily based on two mechanisms: conduction and convection. Conduction occurs in solids due to the movement of atomic particles. The heat transfer conduction process occurs in the ground, pile concrete, and heat exchanger pipe walls. Convection involves diffusion mechanisms and the bulk movement of a fluid; it occurs inside the pipes (working fluid) and at the interface with the inner pipe walls, as shown below.

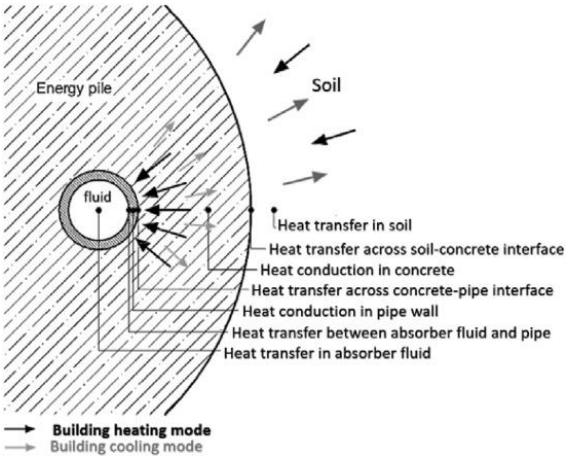

(a)

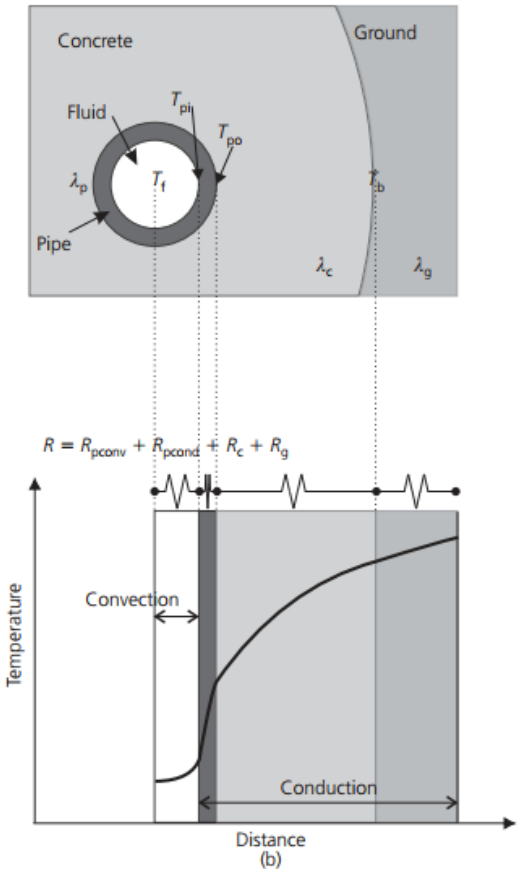

Figure 6. (a) the heat transfer mechanisms of an energy pile. (b). heat transfer pathway of an energy pile (Loveridge and Powrie, 2013)

Loveridge et al. (2013) illustrated the thermal pile heat transfer pathway for an energy pile, depicting the flow of heat transfer fluid through to the surrounding soil (Figure 6(b)). If groundwater flow is ignored in the heat transfer mechanisms, as depicted in Figure 6(b), conduction is viewed as the dominant process. However, this diagram represents a simplified linear heat transfer pathway and does not account for the more intricate factors present in practical structures. In reality, the exchanged heat interacts with pipe-to-ground, pipe-to-pipe, ground-to-concrete, and pipe-to-ground interfaces, all of which could influence the thermal behaviour of energy piles (Loveridge and Powrie, 2013).

2.5 Thermo-hydro-mechanical Behaviour in Energy Piles

Energy piles are a type of geotechnical infrastructure that utilizes the thermal energy stored in the ground to provide heating and cooling for buildings. These piles are designed to operate under complex coupled thermo-hydro-mechanical (THM) conditions, posing a challenge to their performance and long-term stability. In recent years, several studies have been conducted to investigate the THM behaviour of energy piles, providing valuable insights into their design and performance. This literature review examines recent studies that specifically focus on the thermal deformations of energy piles and their impact on performance.

Adinolfi et al. (2018) focused on the long-term performance of a single energy pile at a site in Napoli. The study used a numerical model to simulate three different conditions to analyse how they influence the thermal deformations of the pile. The three conditions were: mode 1, which considered daily temperature variations; mode 2, which ignored daily temperature variations (using min-max values); and mode 3, which used average temperature values. The study found that the axial loads of the pile greatly changed due to daily thermal cycles in mode 1, and the pore water pressure regime was also affected by these cycles. Compared with mode 1, the calculated pile head displacement in mode 2 is higher, and the axial load profiles changed due to the altered pore water pressure regime. Mode 3 uses average temperature values, and the thermal exchange with the ground is slightly undervalued. The study concluded that the influence on structural capacity due to pile head displacements, pore water pressure regime, and axial loads can be negligible. The results of the study also indicated that considering daily temperature variations, the thermally generated settlements are overestimated, and if only average values are considered, vertical displacements are underestimated. The study found that the generation of pore pressure is

not determined only by permeability but also influenced by the loading rate of thermal charges and stiffness of soils.

Rui and Soga (2019) conducted a study to analyse the THM behaviour of a long thermal pile (23m) based on in-site testing results from Lambeth College. The study adopted an advanced thermal-elastoplastic constitutive model to analyse the coupled THM behaviour of the pile. The research identified two primary factors significantly influencing pile head movement: the expansion/contraction coefficient of concrete piles caused by temperature fluctuations and the location of the neutral point, where the shaft friction direction transitions under mechanical loading conditions. The study also found that the axial stress change in the thermal pile due to heating and cooling cycles is affected by the reloading/swelling stiffness of the soil, as well as the relative coefficients of thermal expansion of the soil skeleton, the pile concrete, and pore water (Parkes et al., 2021). The study concluded that the thermal expansion of pore fluid (liquid phase) is more affected than that of the soil (solid phase). The study provides a comprehensive understanding of the effects of thermo-plasticity on the thermal pile's performance, particularly in the heavily over-consolidated nature of London Clay (New and Bowers, 1994).

Other research focuses on the freezing and thawing behaviour in energy piles and surrounding soil (Arzanfudi et al., 2020). The main reason for this research concern is the absence of understanding of the coupled thermo-hydro-mechanical forces that arise from freezing-thawing cycles of porous media and how they affect soil behaviour and the pile-soil interface. Freezing-thawing cycles in soil can cause a variety of physical processes, including compressibility of solids and fluids, fluid and heat flow, pore expansion, and permeability reduction due to ice formation. The existing numerical analysis models used for energy pile design do not accurately capture the coupling of these processes, necessitating the development of a new model. The study also presents a proposed

model that can capture these processes and their coupling behaviour on the integrity of energy pile systems. The newly developed model considers, in addition to conventional operating conditions, other risks such as the failure of mechanical components, operational errors in the system, or extreme weather changes. Additionally, this research highlights the effects of heat conduction-convection in the heat exchanger, causing axial and uneven radial thermal strain gradients in both the pile and the adjacent soil. According to numerical experiments, this gradient can result in localized damage and influence the integrity of the pile-soil interface. The line heat source model used in designing energy piles cannot capture this effect, necessitating a re-evaluation of its validity.

In conclusion, these studies provide valuable insights into the thermal deformations of energy piles under THM conditions. The studies demonstrate that the performance of energy piles is significantly affected by daily temperature variations and the properties of the pile concrete and soil. The studies highlight the importance of considering THM behaviour in the design of energy piles and the need for further research in this area.

2.6 Energy Pile in Mudstone Layer

The deformation and damage behaviour of soft ground conditions has significant implications for the safety and stability of energy piles, such as those in mudstone. Research shows that controlling the water content of mudstone during energy pile installation and understanding the mechanical behaviour of mudstone are crucial for ensuring the safety and stability of geotechnical engineering projects (Li et al., 2017, Liu et al., 2021).

The deformation and damage behaviour of mudstone, an unfavourable ground condition encountered during energy pile installation in soft ground, have significant implications for the design and safety of energy piles. Sissins and Paraskevopoulou (2021) suggested that

understanding the deformation and damage behaviour of mudstone is crucial for the design of geotechnical engineering projects. They proposed the use of multi-stage triaxial compression tests and discrete element modelling to investigate the mechanical response of mudstone specimens with varying degrees of damage. Yang et al. (2019) utilized particle flow code to simulate mudstone samples subjected to multi-stage triaxial compression. They identified that the degree of damage to the samples was related to the magnitude of cohesion and the angle of internal friction of the mudstone. They also developed exponential attenuation equations based on the numerical simulation results and verified the validity of these equations with experimental results (Yang et al., 2019).

Other studies have focused more on the water content of mudstone. In their research, Liu et al. (2020) investigated the impact of water content on the argillization of mudstone using rolling abrasion tests under different water content conditions. The results of this research showed that water acted as a lubricant initially, reducing frictional heat during the early stages of argillization. However, continual frictional heat generation and the water-weakening effect led to the uneven contraction of the mudstone, ultimately causing microstructure destruction and the formation of slaking mudstone (Liu et al., 2020),. Their findings emphasize the importance of controlling mudstone water content during energy pile installation to prevent slaking and ensure pile safety and stability.

2.7 Thermal Load Impact

When developing geothermal energy resources, it is usually necessary to inject working fluids into the subsurface to extract and utilize thermal energy resources. During this process, thermal disturbances inevitably affect the mechanical field of the rock/soil and energy piles, which in turn impacts the safety of the extraction process. Therefore, studying the thermo-mechanical coupling

effects during geothermal energy extraction is crucial. In the context of shallow geothermal energy extraction, some scholars have conducted extensive research and analysis on the mechanical field of energy piles subjected to thermal disturbances.

Laloui et al. (2006) conducted field experiments on energy piles in Switzerland, applying both mechanical and thermal loads to the piles. The results indicated that energy piles exhibit thermoelastic behaviour, with changes in the temperature field significantly affecting the additional stress on the energy piles while having a minimal impact on pore water pressure. AMATYA et al. (2012) analysed and summarized the field test results of Laloui et al. (2006) and Bourne-Webb et al. (2009) clarifying the load-bearing mechanism of single piles under thermal load. Hassani Nezhad Gashti et al. (2014) conducted a numerical analysis using a three-dimensional model to study the construction of end-bearing composite energy pile foundations. The results demonstrated that, under winter and summer conditions, the maximum stress in the energy piles occurred near the downward and upward-grounded heat exchanger pipes, respectively. During heating conditions, as the temperature of the circulating fluid decreases, the zero-displacement point of the pile gradually moves upward, and the change in pile-side friction is significant. However, under cooling conditions, there is no notable change in the zero-displacement point location or in pile-side friction.

Bourne-Webb et al. (2016) used the Abaqus finite element analysis software to simulate the interaction between energy piles and soil. The simulation results indicated that the initial temperature field of the soil, the length-to-diameter ratio of the energy piles, and the thermal expansion coefficients of both the piles and the soil significantly affect the thermo-mechanical coupling effects on the piles. In deep geothermal energy extraction, thermal disturbances have a greater impact on the mechanical properties of high-temperature rock masses under high-ground

stress. Vaziri (1988) developed a flow-solid coupling model based on non-isothermal single-phase flow and nonlinear elastic deformation, solved using the finite element method. This model was used to simulate the thermal recovery process of a single well. Tortike and Ali (1993) established a three-dimensional coupled model of elastic-plastic deformation, fluid flow, and heat transfer for geothermal extraction simulation. Gutierrez and Makurat (1997) developed a numerical model for three-field coupling, which was used to simulate the coupled process of cold-water injection into fractured reservoirs.

3 Methodology

3.1 Introduction

This study aimed to establish a conceptual model of energy piles based on the assumed ground conditions of the Wilton mine project's geological strata, characterized by extensive mudstone distribution. Utilizing finite element analysis software, the operation of the energy piles was simulated. The analysis focused on their working conditions under the combined effects of mechanical loads, thermal loads, changes in pore water pressure, and the deformation of the surrounding soil.

In order to achieve this objective, a 3D thermo-hydro coupled model, a 3D thermo-mechanical coupled model, and a 2D thermo-hydro-mechanical coupled model were developed and analysed using COMSOL Multiphysics software, utilizing Darcy's Law, the Solid Mechanics module, and the heat transfer module.

3.2 Constitutive Modelling

To study the operation of energy piles under different soil conditions, it is essential to determine the soil's constitutive model. This is because a suitable constitutive model provides the most realistic response to the behaviour of the soil under external loads, such as heat transfer between the soil and the energy pile, as shown in Figure 7.

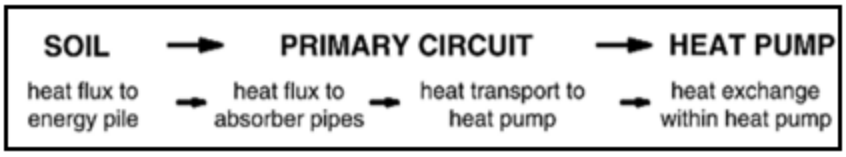

Figure 7. Energy pile system (Brandl, 2006)

The models need to be set depending on the situation. The advantages and limitations of the models need to be described. This study presents a 3D thermo-hydro (TH) coupled model, a 3D thermo-mechanical (TM) model, and a 2D thermo-hydro-mechanical (THM) model of the soil, particularly using the finite element analysis software COMSOL.

3.3 Coupling

To properly model the various physical properties of the surrounding soil for energy piles, different coupling characteristics must be considered according to the specific research objectives. In the thermal variation process of energy piles, six different interactions need to be considered, as shown in Figure 8. Chapter 5 considers TH coupling; Chapter 6 considers TM coupling; and Chapter 7 adopts the THM model.

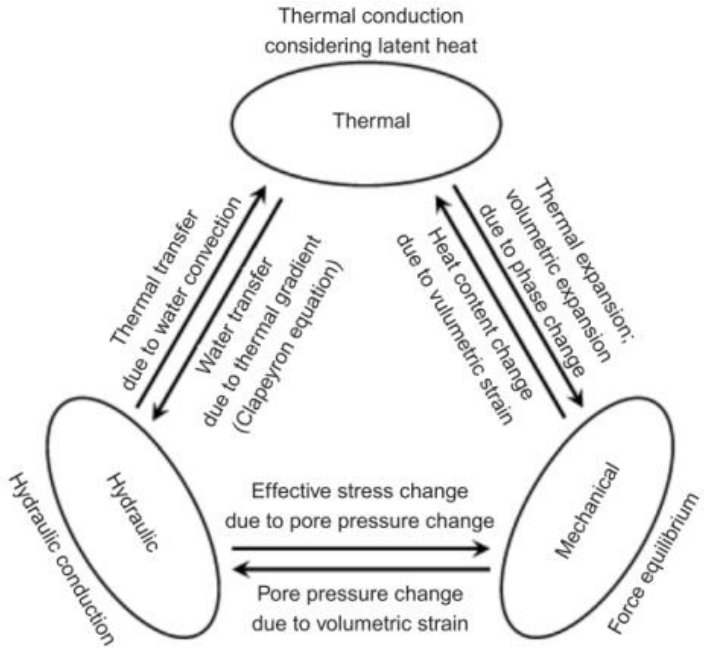

Figure 8. Coupling processes in soils when the energy pile works

These studies utilized the linear elasticity material model in the solid mechanics section, assuming that the energy pile and surrounding soil would not experience plastic deformation. However, since

the model incorporates thermal-hydro-mechanical coupling, adjustments are required for the original solid physical formulas. The fundamental equation is provided below, representing an exponential relationship between stress (σ), strain (ε), and displacement (u).

$$\rho \frac{\partial^2 u}{\partial t^2} = \nabla \cdot s + \boldsymbol{F}v \quad (3.1)$$

When considering the deformation of the soil, assuming it to be linear-elastic, the equation must be revised to align with both Biot's consolidation theory and Hooke's law.

Initially, the stress expression in the equilibrium condition is recognized as:

$$\nabla \cdot [\sigma] + \boldsymbol{F} = 0 \ (3.2)$$

where F represents the body force.

The stress equilibrium equation (3.2) can be transformed by incorporating the small strain assumption and the plane strain equation, resulting in the following equation:

$$\frac{E}{2(1+v)} \nabla^2 \boldsymbol{u} + \frac{E}{2(1+v)(1-v)} \nabla \cdot (\nabla \boldsymbol{u}) + \mathbf{F} = 0 \ (3.3)$$

The basic formulation of Darcy's law in COMSOL deviates slightly from the hydraulic equations of the Biot theory, requiring additional adjustments as outlined below:

$$\frac{\partial}{\partial t}\left(\in_p \rho\right) + \nabla(p\boldsymbol{u}) = Q_m \ (3.4)$$

Where $\boldsymbol{u} = -\frac{K}{\mu} \nabla \rho$

By incorporating the storage model into Darcy's law, we can obtain the hydraulic equation of Biot's theory.

$$\frac{\partial}{\partial t}\left(\in_p \rho\right) + \nabla(p\boldsymbol{u}) = Q_m, \frac{\partial}{\partial t}\left(\in_p \rho\right) = \rho s \frac{\partial p}{\partial t} \quad (3.5)$$

Where $\boldsymbol{u} = -\frac{K}{\rho g}(\nabla\rho + \rho\boldsymbol{g})$

3.5 Model Selection

Chapters 5-7 of this paper each focus on numerical simulation analyses, with each chapter dedicated to a distinct simulation model. The three computational models each focus on different aspects of energy pile systems. The 3D TH coupling model encompasses the entire energy transfer process, including multi-layered geothermal heat transfer, solid heat conduction in concrete piles, and convective heat transfer via the working fluid. This model primarily investigates heat transfer pathways and efficiency. Additionally, it assesses how geological characteristics and operational rate affect heat transfer efficiency and operational cycles, aiming to guide the efficient and durable deployment of energy piles in mudstone regions. The analysis indicates that in low-permeability mudstone, buoyancy-driven pore water flow has a minimal effect on the heat transfer efficiency of energy piles, allowing the influence of seepage heat transfer through the multi-layered geology to be disregarded.

Building on these findings, the 3D TH coupling model simplifies the heat transfer process by focusing on solid heat conduction. It examines the mechanical responses of energy piles to thermal disturbances and analyses how parameters like mudstone's thermal expansion coefficient, elastic modulus, and thermal conductivity influence the stress and strain within the pile, thus assessing the operational safety of energy piles in mudstone regions. However, in engineering practice, the temperature, seepage, and mechanical fields often interact and influence one another. Due to computational power limitations and model convergence challenges, this study establishes a 2D energy pile THM coupling model. This model specifically examines the mechanical responses of

energy piles under temperature cycles and variations in soil pore water pressure to better align with actual working conditions.

3.5 Research Approaches

The purpose of this research is to investigate the performance of energy piles under unfavoured ground conditions. Numerous studies and experiments have already demonstrated the safety and economic feasibility of energy piles as a new type of pile foundation, particularly in clay and sand. However, there is limited research on the behaviour of energy piles in certain special ground conditions, such as mudstone formations.

Since energy piles are not commonly installed in mudstone strata, finite element analysis software can be employed to simulate their performance based on soil parameters. However, given that energy piles utilize geothermal energy, their behaviour differs from that of conventional pile foundations and thus requires consideration of thermo-hydraulic coupling and thermo-mechanical behaviour. To comprehensively assess the operation of energy piles in mudstone areas, it is necessary to simulate different operating conditions. The entire research approach is shown in the flow chart.

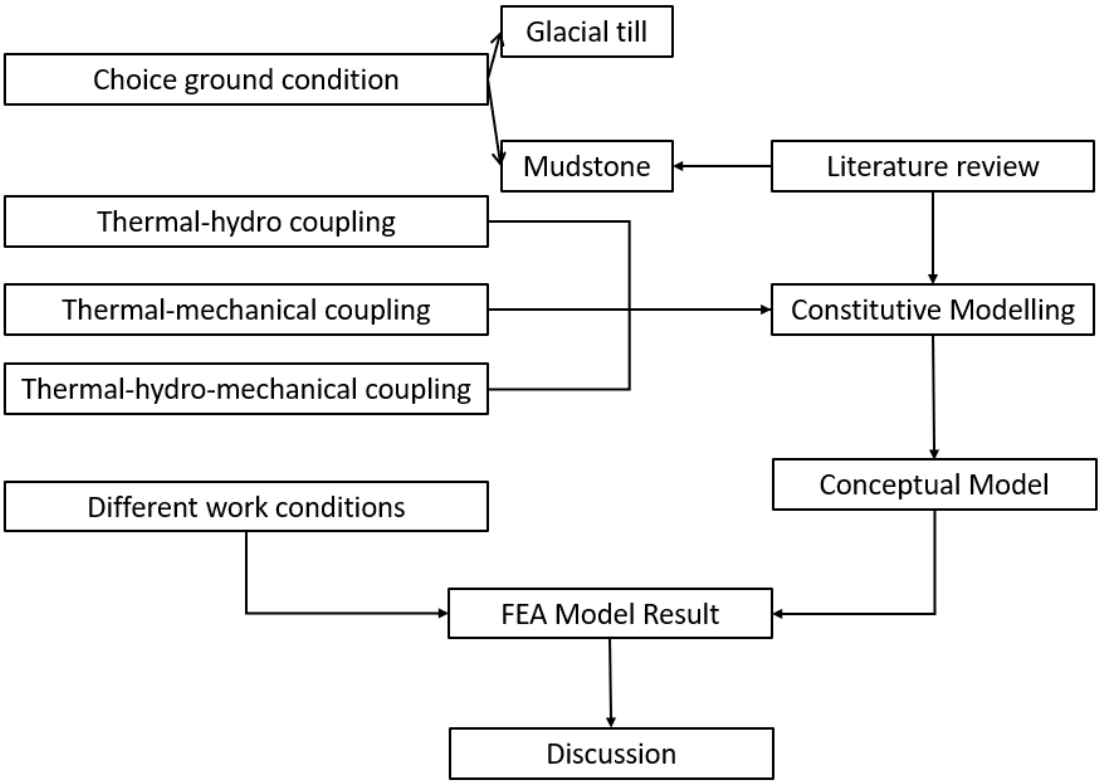

Figure 9. Flow Chart of methodology for coupling models for energy plie project in mudstone area

3.6 Limitation

There are still some limitations to this methodology, including:

1. Constitutive Model: The selected site for this study has a low probability of experiencing landslides and does not bear significant loads. Therefore, the impact of plastic deformation in the mudstone is minimal. Consequently, the mudstone in this study is represented using a linear elastic constitutive model, rather than an elastoplastic model. This approach does not capture the nonlinear, strain-hardening, elastoplastic, and dilatant mechanical characteristics of the rock.
2. Model Simplifications: Due to computational limitations and challenges in model convergence, a 2D model is employed for the THM coupling analysis of energy piles.

Compared to 3D models, the temperature of the heat exchanger pipe wall in this model is simplified as a constant boundary condition and does not vary over time. The model also fails to depict the stress and strain evolution of the energy pile under triaxial ground stress conditions.

3. Pile-Soil Interface: In all coupling models used in this study, the energy pile and the surrounding media form a unified system. The contact surfaces between them share common nodes and maintain conformal deformation. Frictional contact (relative sliding) between the energy pile and the surrounding media is not considered in these models.

4 Ground Conditions

This chapter focuses on the geological conditions and parameter selection for energy piles. Due to the limited availability of experimental monitoring results for energy piles in mudstone regions, this study assumes the installation of energy piles in the Woodsmith Mine project area. The geological model used in this study refers to the survey reports of the Woodsmith Project (Gschnitzer et al., 2020), integrating information from surveys of the Lias Group (Hobbs et al., 2012) and Mercia Mudstone Group (Sumbler et al., 2000, Hobbs et al., 2002). Geological profiles and slope diagrams for the Wilton Mine site are shown in Figure 10.

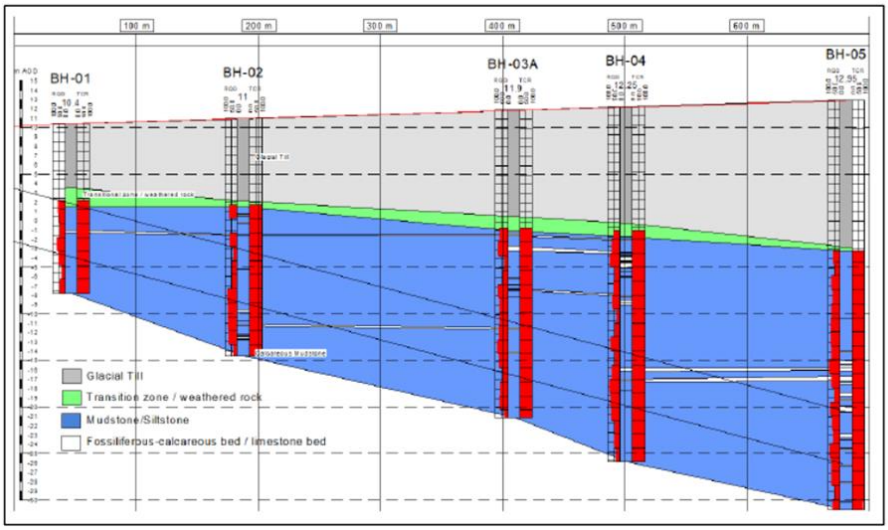

Figure 10. Geological landscape of the mudstone areas (Gschnitzer et al., 2020)

The geological profile above indicates that the soils in the area are mainly composed of shallow superficial deposits and mudstone layers. Based on the referenced information, this study has simplified some geological layers, and the conceptual geological model required for modelling is depicted in Figure 11.

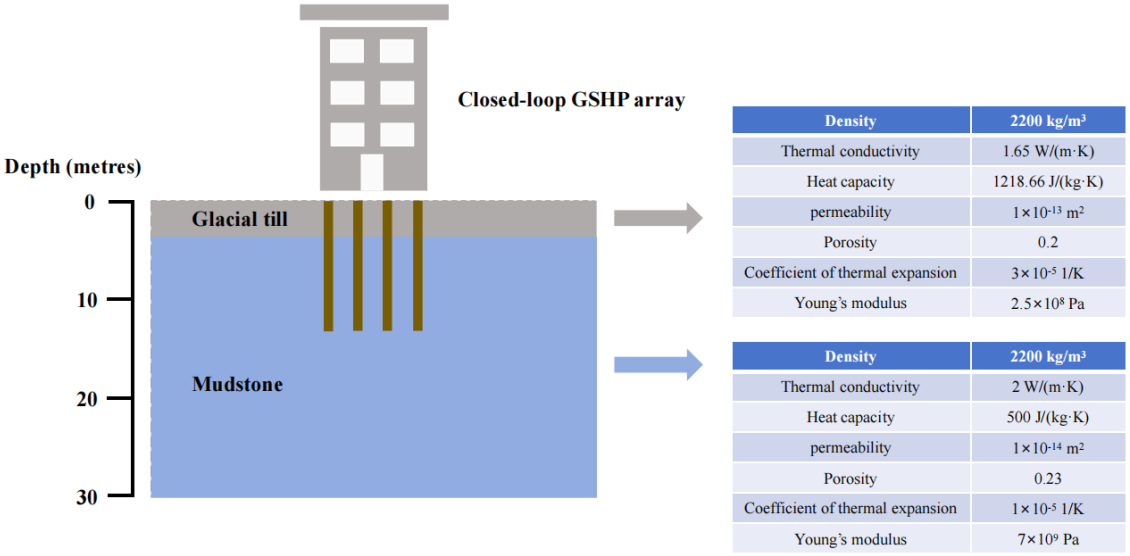

Density	2200 kg/m³
Thermal conductivity	1.65 W/(m·K)
Heat capacity	1218.66 J/(kg·K)
permeability	1×10^{-13} m²
Porosity	0.2
Coefficient of thermal expansion	3×10^{-5} 1/K
Young's modulus	2.5×10^{8} Pa

Density	2200 kg/m³
Thermal conductivity	2 W/(m·K)
Heat capacity	500 J/(kg·K)
permeability	1×10^{-14} m²
Porosity	0.23
Coefficient of thermal expansion	1×10^{-5} 1/K
Young's modulus	7×10^{9} Pa

Figure 11. Geological Profile of the Simplified Stratigraphy

4.1 Glacial Till

The superficial deposits mainly consist of Glacial Till, which is predominantly found in areas near the coastline, both at low and high altitudes (Agar, 1954). According to Hesselbo and Jenkyns (1998) and Hobbs et al. (2012), the glacial deposits in the soil model for this study are assumed to be 3 meters thick. Clarke (2018) published a paper highlighting the challenges in testing and classifying the geotechnical properties of Glacial Till soil, which is a complex composite soil (Clarke, 2018).

The design parameters for the soil properties of the glacial deposits were established based on their depositional characteristics, lithology, and engineering properties. Detailed characteristics of glacial tills are provided below.

Table 1. Geotechnical characteristics of glacial till layer

Parameters of glacial till layer	Value
Thermal conductivity	1.65 W/(m·K) (Tinsley and Pavía, 2019)
Heat capacity	1218.66 J/(kg·K) (Tinsley and Pavía, 2019)
Permeability	1×10^{-13} m^2 (Hobbs et al., 2012)
Porosity	0.2 (Clarke, 2018)
Coefficient of thermal expansion	3×10^{-5} 1/K (Reiter et al., 2023)
Young's modulus	2.5×10^{8} Pa (Tinsley and Pavía, 2019)

4.2 Mudstone

The Strabag company has established observation points along the Woodsmith project to determine the geological conditions, since this type of mudstone is predominantly found in the Lias Group and is divided into the Redcar Mudstone and the Whitby Mudstone. The Redcar Mudstone is typically light to dark grey and exhibits a weak to very weak rock class, with a very fine-grained texture and numerous fractures that affect its structural stability.

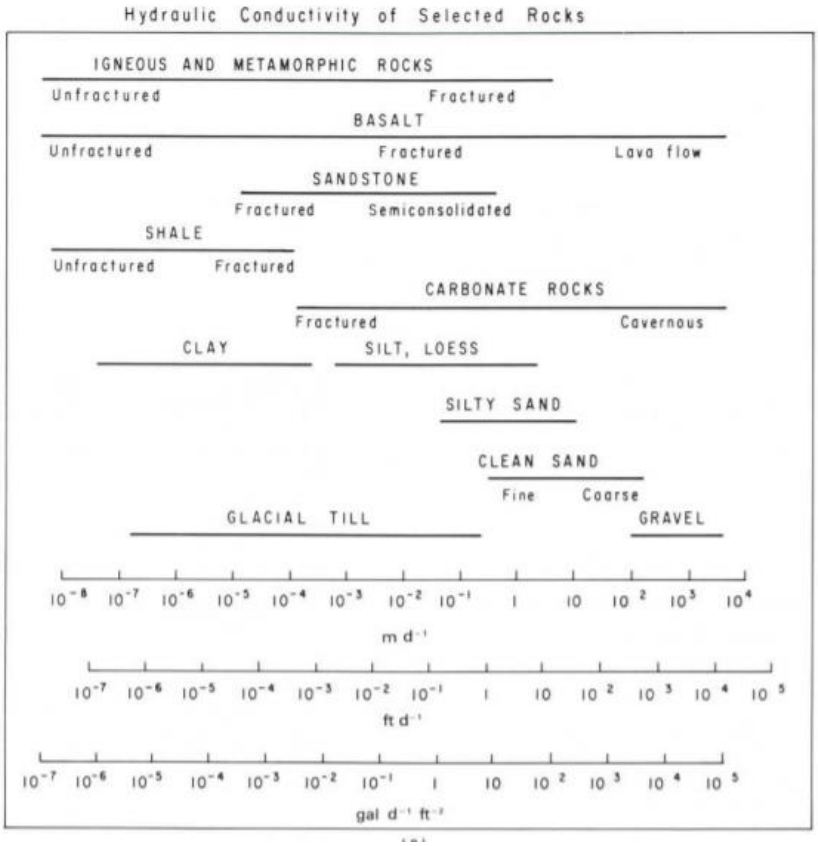

Figure 12. Hydraulic conductivity of typical geotechnical units (Slater et al., 2018)

Furthermore, laboratory experiments have demonstrated that when mudstone interacts with limestone strata with a high calcium carbonate content, the resulting mudstone complex can withstand higher compressive stresses (Zhang et al., 2010). The most notable characteristic of mudstone primarily centers on its remarkably low permeability, with a hydraulic conductivity of around 2.0 x 10^{-7} m/s, and its restricted ductility, with Young's modulus significantly inferior to that of other brittle rocks (1-40 MPa). Detailed parameters of the mudstone layer involved in the modelling are shown in Table 2.

Table 2. Geotechnical characteristics of mudstone layer

Parameters of mudstone layer	Value
Thermal conductivity	2.0 W/(m·K) (Parkes et al., 2021)
Heat capacity	500 J/(kg·K) (Boon et al., 2021)
Permeability	1×10^{-14} m^2 (Houben et al., 2020)
Porosity	0.23(Yang and Aplin, 2010)
Coefficient of thermal expansion	1×10^{-5} 1/K (Boon et al., 2021)
Young's modulus	7×10^{9} Pa(Parkes et al., 2021)

4.3 Hydrological Conditions

The study's conceptual model of energy piles is informed by hydrological conditions near the tunnel project site at Wilton. Findings suggest that the rock mass's characteristics are markedly influenced by its anisotropy, resulting in directional differences in observations. The fine-grained nature of the Lias Group rock mass inhibits water flow when the rock mass is intact.

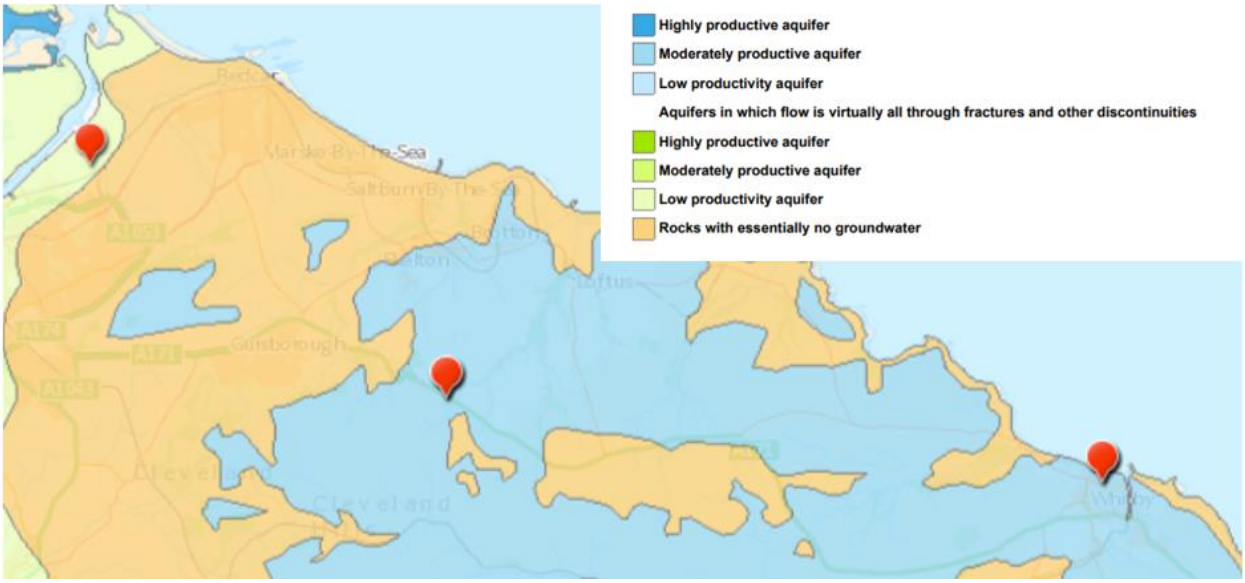

Figure 13. Aquifer distribution map (BGS, 2021)

5 3D FEA Thermal-hydro Coupling Modelling of Energy Pile

In this case study, it is assumed that energy piles are built in mudstone areas where the permeability of the soil is very low. The energy piles work by circulating fluid through a network of underground pipes embedded in the piles. The piles act as heat exchangers, absorbing and transferring heat to and from the glacial till layer and mudstone layer. The piles can be drilled to a depth of 18 meters and connected to a heat pump system. The heat pump system can extract heat from the ground during the winter months. During the summer months, the heat pump system can reverse the process and use the energy piles to cool the building. The area around the Woodsmith Mine project includes tunnels and other underground structures. Therefore, if there are plans to construct energy piles in the future, it is essential to ensure high stability in the foundation and energy pile design. Before constructing the energy piles, an analysis of thermal behaviour is necessary to confirm that this type of structure will not compromise the safety of adjacent buildings.

5.1 Numerical model

In this section, a three-dimensional transient finite element numerical model is developed in COMSOL Multiphysics software to simulate the heat exchange process between the energy pile (EP) and the surrounding soil layers (glacial till and mudstone) under two operating conditions: summer and winter. Additionally, the model investigates the seepage pattern of pore water within the mudstone driven by natural convection. The model utilizes the heat transfer and Darcy's Law modules for porous media to simulate the behaviour of the soil, the solid heat transfer module for the pile, and the non-isothermal pipe flow module for the heat transfer process in the U-shaped heat exchanger tube.

The model consists of a U-shaped heat transfer pipe, a concrete energy pile, and the surrounding soil layers. The size of the ground model is 40m × 40m × 50m, ensuring that the model's outer boundary remains unaffected by the heat exchange of the energy pile during system operation. The diameter of the concrete energy pile is 0.6m, and the length of the pile is 18m. The U-type heat exchanger pipe is simplified as a one-dimensional line with a length of 17.5m.

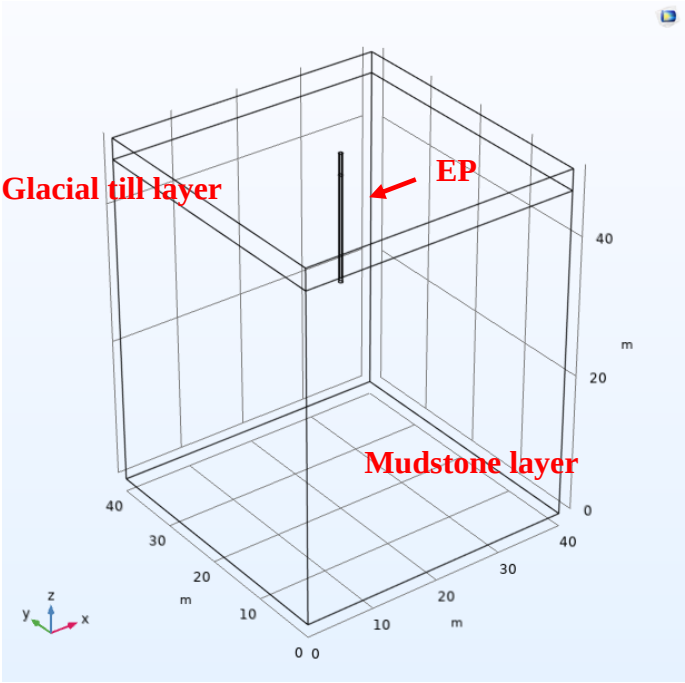

Figure 14. Diagram of the energy pile and ground thermal-hydro model in COMSOL

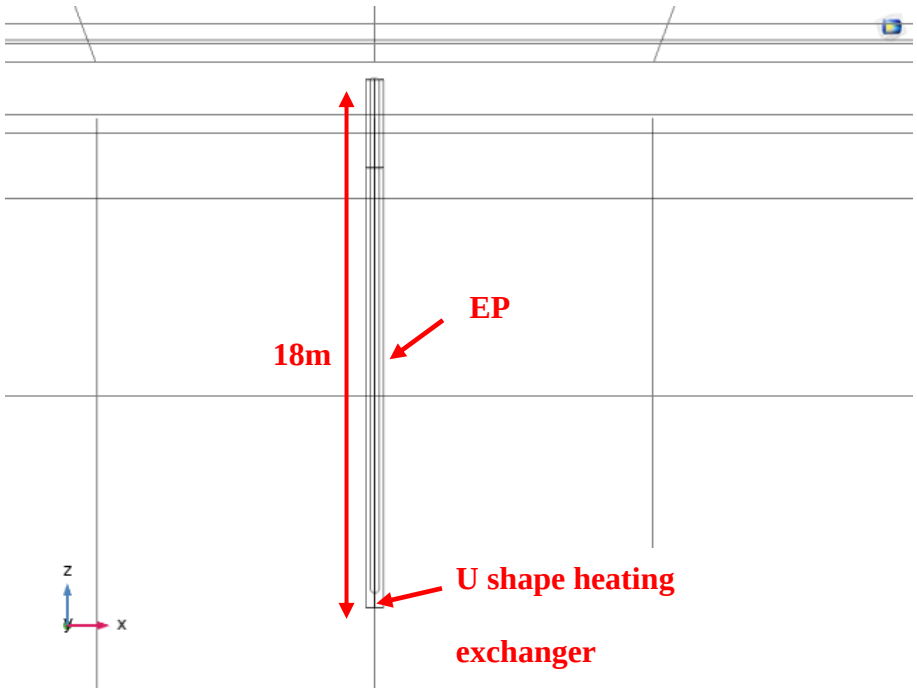

Figure 15. Details of the energy plie and U shape heating exchanger thermal-hydro model in COMSOL

5.2 Model Assumptions

1. The mudstone layer and glacial till layer are treated as a continuous medium, and the structure of individual fractures is not accounted for.
2. A local thermal equilibrium model is utilized to describe the energy transfer process (Nield and Bejan, 2006).
3. Fluid flow within the mudstone is considered as saturated single-phase fluid flow, following Darcy's Law, without considering chemical reactions between the fluid and the soil.
4. It is assumed that the mudstone and pile are homogeneous and isotropic materials. Heat transfer mechanisms in the mudstone include heat conduction and heat convection, while in the pile, heat transfer occurs through heat conduction, utilizing effective thermal conductivity in calculations.

5. In this thermal-hydro coupled model, the U-shaped heat exchanger pipe and the heat transfer fluid inside it are simplified as one-dimensional lines, with heat energy primarily transmitted in the normal direction.
6. The phase change process of the fluid within the soil layer is not considered.
7. Heat is transferred only through heat conduction and heat convection, without accounting for compression effects and viscous dissipation of the fluid, as well as thermo-mechanical dispersion and thermal radiation effects.

5.3 Governing Equations

The governing equations of solid heat transfer:

$$\rho_m C_m \frac{\partial T}{\partial t} + \nabla \cdot q = Q \quad (5.1)$$

$$q = -\lambda_m \nabla T \quad (5.2)$$

Combining the above equations yields:

$$\rho_m C_m \frac{\partial T}{\partial t} - \nabla \cdot (\lambda_m \nabla T) = Q \quad (5.3)$$

Where ρ_m is the solid density; C_m is solid specific heat capacity; T is temperature; t is time; λ_m solid thermal conductivity; ∇T is temperature gradient; Q is heating source; The subscript m denotes solid.

Mass conservation equation (the Darcy's law) :

$$\frac{\partial}{\partial t}(n_m \rho_w) + \nabla \cdot (\rho_w u) = Q_m \quad (5.4)$$

$$u = -\frac{k_m}{\mu_w}(\nabla p + \rho_w g) \quad (5.5)$$

Joining the above equations yields:

$$\frac{\partial}{\partial t}(n_m \rho_w) - \nabla \cdot \left(\frac{\rho_w k_m (\nabla p + \rho_w g)}{\mu_w}\right) = Q_m \quad (5.6)$$

Where n_m is the porosity of the soil; ρ_w is the density of the fluid; u is the fluid velocity; k_m is the

permeability of the soil;μ_w is the dynamic viscosity of the fluid; $\rho_w g$ is the gravity term in the z (negative axis) direction; Q_m is the source item; Subscripts m indicates soil phase; Subscripts w indicates fluid phase.

Governing equations for thermal convection (heat transfer in porous media):

$$(\rho C)_{\text{eff}} \frac{\partial T}{\partial t} + \rho_w C_w u \cdot \nabla T - \nabla \cdot \left(\lambda_{eff} \nabla T\right) = Q \quad (5.7)$$

$$(\rho C)_{eff} = n_m \rho_w C_w + (1 - n_m)\rho_m C_m \quad (5.8)$$

$$\lambda_{eff} = n_m \lambda_w + (1 - n_m)\lambda_m \quad (5.9)$$

where（ρC）$_{\text{eff}}$ is the effective heat capacity; λ_{eff} is the effective thermal conductivity; is the temperature; t is the time; ρ is the density; C is the constant-pressure heat capacity; λ is the thermal conductivity; u is the velocity vector; ∇T is the temperature gradient; n_m is the porosity of the soil; Q is the source term; Subscripts m indicates solid phase; Subscripts w indicates fluid phase.

Convective heat transfer and pipe wall heat transfer in U-type heat exchanger tubes are based on the non-isothermal pipe flow heat transfer model, and the pipe flow continuity equation can be expressed as follows(Ding et al., 2022):

$$\frac{\partial A \rho_f}{\partial t} + \nabla t\left(A \rho_f u \vec{e}_t\right) = 0 \quad (5.10)$$

The momentum conservation equation can be expressed as:

$$\rho_{\text{f}} \frac{\partial u}{\partial t} = -\nabla_t p \vec{e}_t - \frac{1}{2} f_D \frac{\rho_f}{d_h} |u| u \quad (5.11)$$

The energy conservation equation can be expressed as(Ding et al., 2022):

$$\rho_f A C_f \frac{\partial T_f}{\partial t} + \rho_f A C_f u \vec{e}_t \nabla_t T_f = \nabla_t \times \left(A k_f \nabla_t T_f\right) + \frac{1}{2} f_D \frac{\rho_f A}{d_h} |u| u^2 + Q_{wall} \quad (5.12)$$

Where ρ_{f} is the fluid density， A is the cross-sectional area of the pipe，u is the fluid velocity，

$\vec{e}_t$ is the tangential vector in the direction of the pipe， ∇t is a differential operator in pipe coordinates，f_D is the coefficient of friction that depends on the Reynolds number，dh is the diameter of the pipe，p is the pressure in the pipe.， T_f is the temperature of the fluid，$k_{f\,is}$ the thermal conductivity of the fluid， C_f is the specific heat capacity of the fluid， Q_{wall} is the efficiency of heat transfer per unit length through the pipe wall.

5.4 Boundary Condition

This model involves two working conditions:

1. Summer working conditions: the atmospheric temperature is 20°C, the soil temperature is 12°C, the fluid injection flow rate in the U-pipe is 2 m/s, the injection temperature is the same as the atmospheric temperature at that time of the year (the injection temperature is approximately equal to the atmospheric temperature), and the soil side wall is adiabatic.
2. Winter working conditions: the atmospheric temperature is -2°C, the soil temperature is 12°C, the fluid injection flow in the U-pipe is 2 m/s, the injection temperature is consistent with the atmospheric temperature at that time, the soil side wall is an adiabatic boundary, and all wall surfaces in contact with the fluid are assumed to be a fixed boundary.

The computational model in the thermal-hydro simulation uses a transient solver with a total computational duration of 3 months and a time step of 1 day for both winter and summer conditions.

System evaluation metrics-thermal extraction:

$$Q = \left(\rho C_p\right)_{eff} \cdot \mathrm{V} \cdot \nabla \mathrm{T} \quad (5.13)$$

Where: Q is the heat recovery rate; $(\rho Cp)_{eff}$ is the effective heat capacity; V is the volume of the solid mass; and is the temperature gradient.

5.5 Parameters of Simulation

The parameters of the simulation are shown in the following Table 3.

Table 3. Input parameter in the TH model

Parameters	value
Mudstone density	2200 kg/m^3
Mudstone thermal conductivity	2 W/(m·K)
Heat capacity of mudstone	500 J/(kg·K)
Mudstone permeability	1×10^{-14} m^2
Mudstone porosity	0.23
Mudstone layer thickness	47m
Top layer thickness	3m
Top layer density	2200 kg/m^3
Top layer thermal conductivity	1.65 W/(m·K)
Heat capacity of the top layer	1218.66 J/(kg·K)
Top layer permeability	1×10^{-13} m^2
Top layer porosity	0.2
Energy pile density	2300 kg/m^3
Thermal conductivity of energy piles	1.8 W/(m·K)
Energy pile heat capacity	880 J/(kg·K)
U-tube inner diameter	2 mm
U-tube wall thickness	1 mm
Inlet flow	2 m/s
Injection temperature (winter conditions)	-2℃

Injection temperature (summer conditions)	20℃

The parameters of water in this model are set as a functional equation related to the temperature T with the following expression：

$$\rho = 6.309e^{-5} \times T^{\wedge 3} - 0.0604 \times T^{\wedge 2} + 18.923 \times T - 950.704 \quad T \in [273.15 - 293.15]$$

$$\rho = 1.034e^{-5} \times T^{\wedge 3} - 0.0134 \times T^{\wedge 2} + 4.969 \times T + 432.257 \quad T \in [293.15 - 373.15]$$

$$Cp = 12010.147 - 80.407 \times T^{\wedge 1} + 0.31 \times T^{\wedge 2} - 5.382e^{-4} \times T^{\wedge 3} + 3.625e^{-7} \times T^{\wedge 4} \quad T \in [273.15 - 553.75]$$

$$\lambda = -0.869 + 0.0089 \times T^{\wedge 1} - 1.584e^{-5} \times T^{\wedge 2} + 7.975e^{-9} \times T^{\wedge 3} \quad T \in [273.15 - 553.75]$$

$$\mu = 2.79 \times [1.380 - 0.0212 \times T^{\wedge 1} + 1.360e^{-4} \times T^{\wedge 2} - 4.645e^{-7} \times T^{\wedge 3} + 8.904e^{-10} \times T^{\wedge 4} - 9.079e^{-13} \times T^{\wedge 5} + 3.846e^{-16} \times T^{\wedge 6}] \quad T \in [273.15 - 413.15]$$

$$\mu = 2.79 \times [0.00401 - 2.107e^{-5} \times T^{\wedge 1} + 3.858e^{-8} \times T^{\wedge 2} - 2.397e^{-11} \times T^{\wedge 3}] \quad T \in [413.15 - 553.75]$$

5.6 Mesh Analysis

The mesh of this model is customized by the user, with one-dimensional lines controlled by edges, and the concrete pile and surrounding soil mass divided into free tetrahedral meshes. In total, 469,988 tetrahedral elements were generated, with an average element quality of 0.6603. The refined mesh division resulted in a total of 1,881,003 tetrahedral elements, with an average element quality of 0.6623. Monitoring point A was set at position (20, 22, 35) in the model to observe the temperature and flow velocity values at this point under different mesh quantities.

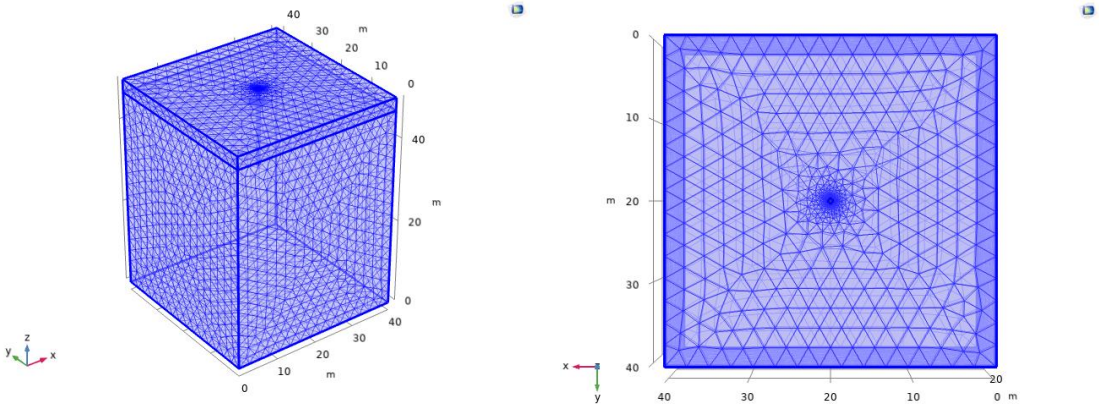

Figure 16. Detail of the 3D TH model mesh - normal grid (number of elements: 469988).

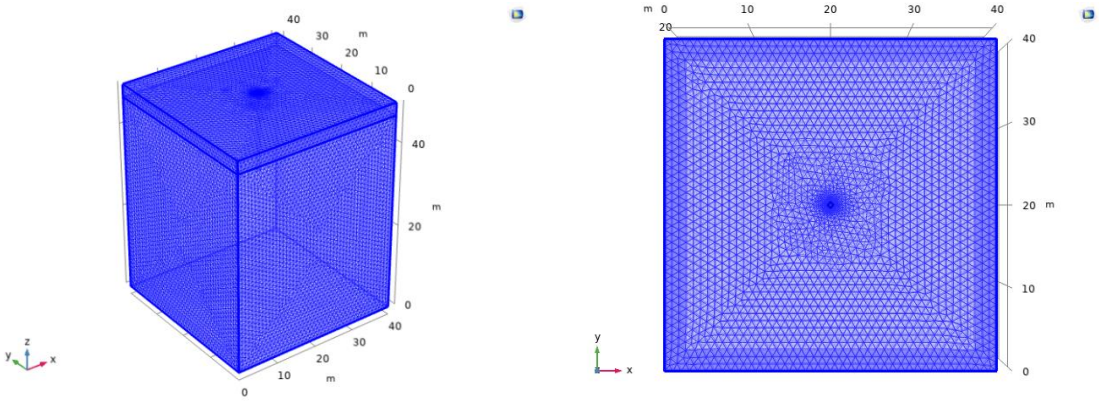

Figure 17. Detail of the 3D TH model mesh - fined grid (number of elements: 1881003).

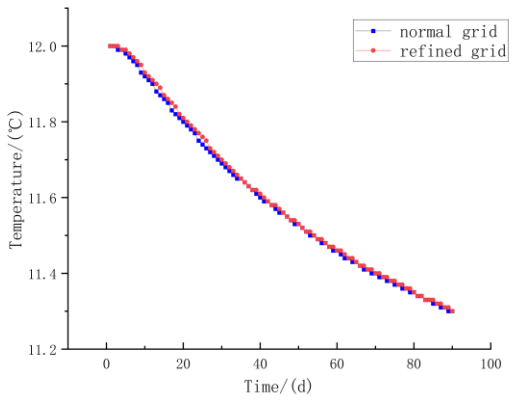

Figure 18. Temperature variation curve with time at monitoring point A

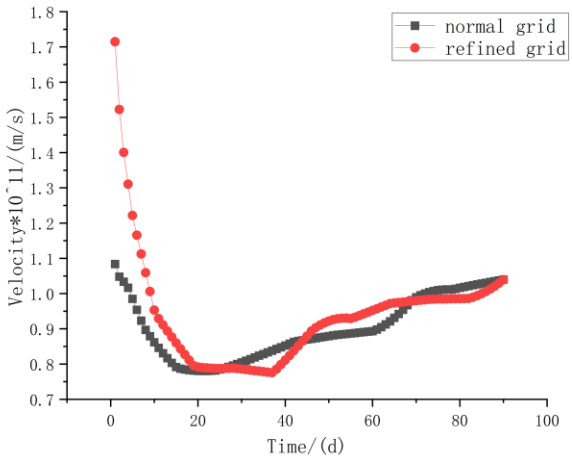

Figure 19. Darcy velocity versus time at monitoring point A

From the above change curves, it can be observed that the different numbers of grid cells have a certain influence on the numerical calculation results of the model. The temperature field values at monitoring point A are basically consistent, and the trend of the Darcy velocity field values is consistent as well. However, there exist some inaccuracies in their numerical solutions. Considering that the Darcy seepage field involves velocity changes on the order of 10^{-12}, the relative error values have minimal impact on the heat flow field. Therefore, in the numerical simulation of this chapter, 469,988 grid cells are used to improve the computational efficiency of the model.

5.7. Simulation Results

5.7.1 Winter Working Conditions

This section primarily studies the heat transfer process of energy piles under winter working conditions. A transient solver with a time step of 1 day and a total simulation duration of 90 days is used. The analysis focuses on the changes in the outlet water temperature of the energy piles, the temperature distribution of the pile and the surrounding soil, and the heat exchange efficiency.

The heat transfer fluid inside the U-shaped pipe is injected into the ground at a flow rate of 2 m/s.

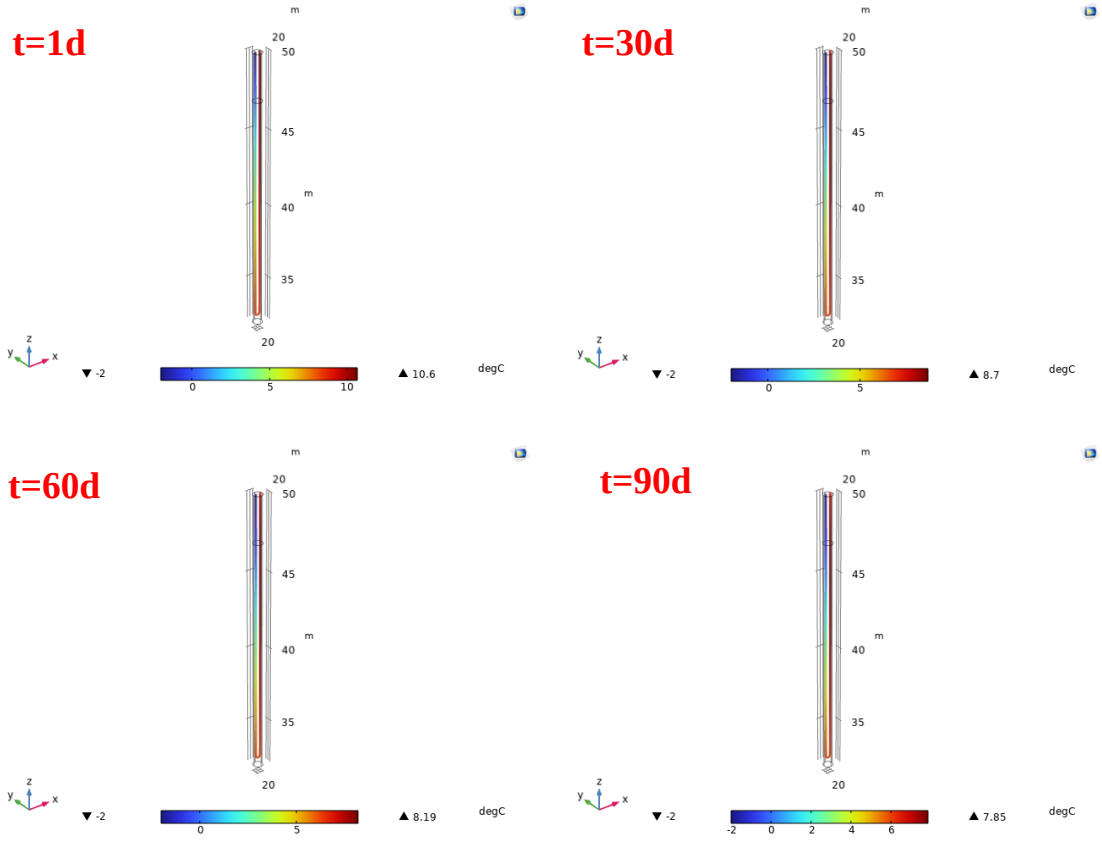

Figure 20. Temperature distribution of heat transfer fluid in U-tube.

As the soil temperature is higher than the surface temperature during winter, the cold fluid continuously absorbs heat from the surrounding soil layers. The sequence of heat transfer is as follows: soil → concrete energy pile → U-shaped heat exchanger pipe → cold heat transfer fluid. Since the length of the heat exchanger pipe is 36 meters and the fluid injection velocity is 2 m/s, the temperature field in the U-shaped pipe reaches a relatively stable state at t=1 day under the calculation time step.

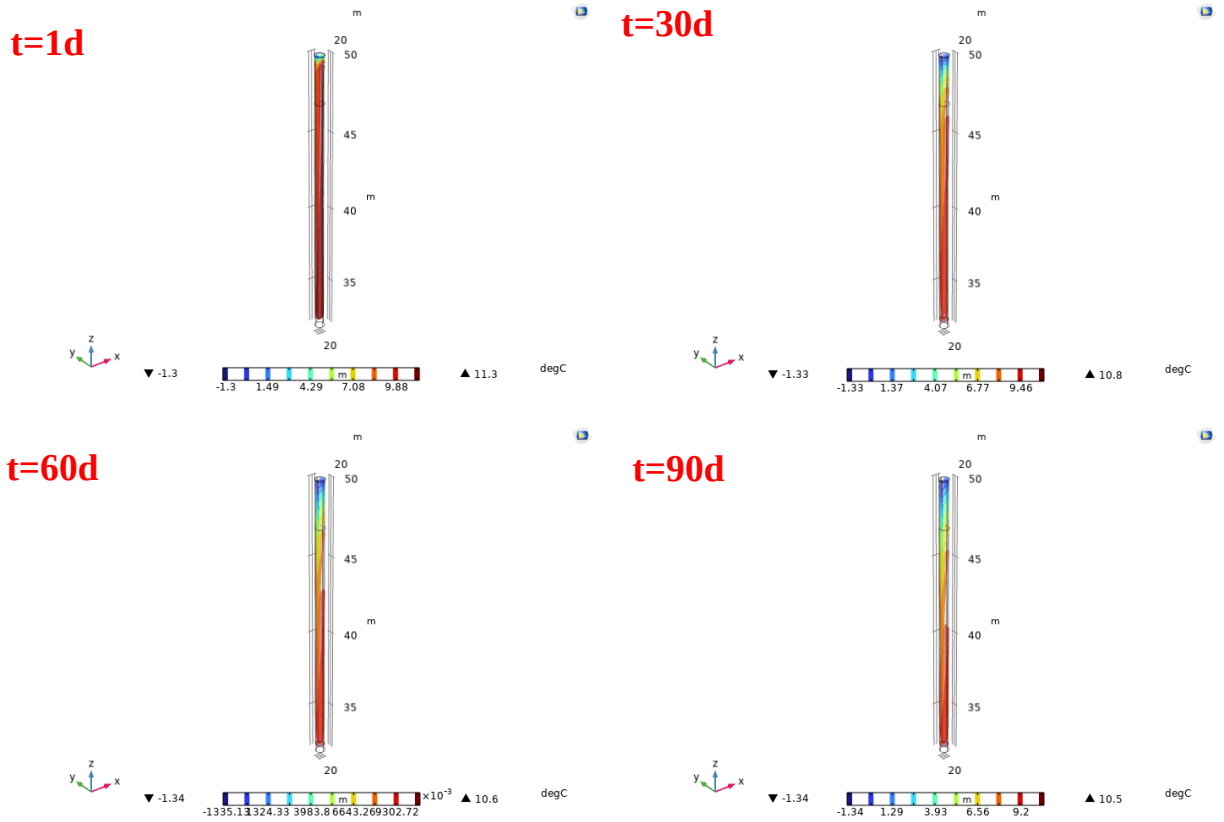

Figure 21. Temperature field of energy pile in the TH model

Due to the continuous increase in temperature of the cold heat transfer fluid inside the U-shaped pipe along the depth direction, the temperature distribution within the concrete energy pile becomes uneven. The fluid temperature is lowest at the injection point at the top of the pile, resulting in the greatest temperature decrease at that location. Conversely, at the bottom of the pile, the temperature of the heat transfer fluid inside the U-shaped pipe increases, and there is heat supplementation from the surrounding area, resulting in the smallest temperature decrease at that location.

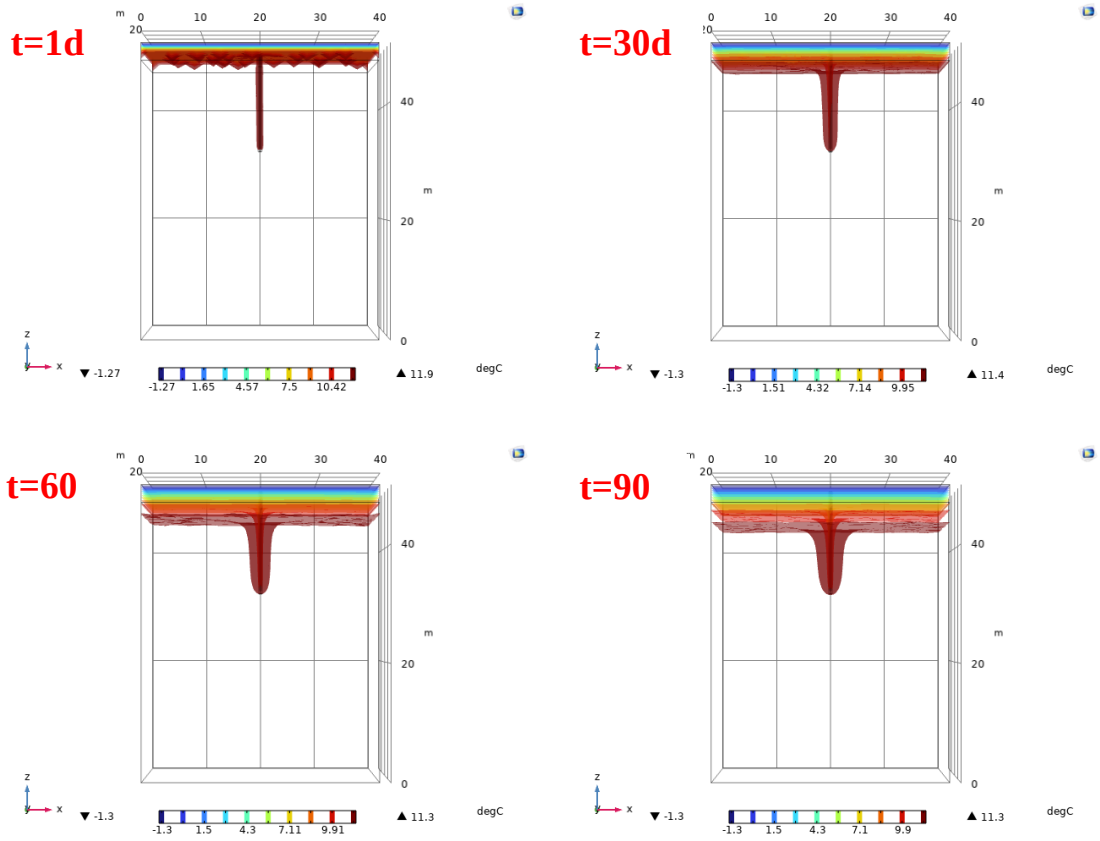

Figure 22. Soil temperature field in the TH model

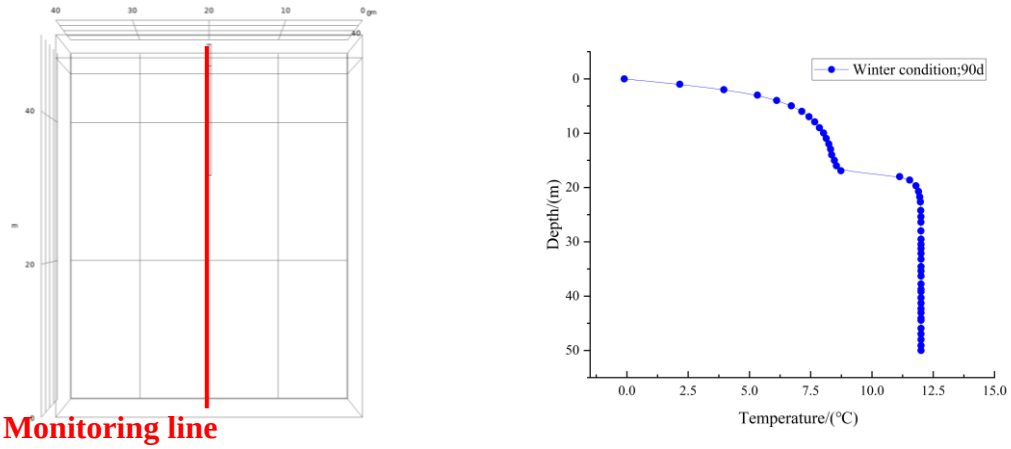

Figure 23. Monitoring line positions and temperature variation curves (90 Days)

In winter conditions, the surface temperature is lower than the temperature of the underground soil layers. The density of pore water at the surface is greater than that of the pore water in the deep

layers. This density difference drives natural convection: pore water at the surface sinks while the deeper pore water rises. Therefore, at t=1d, the isothermal surfaces exhibit a distinct "hill-shaped" distribution. The cold working fluid inside the U-tube continuously cools the surrounding pile and soil, but the cold front has not yet reached the distant soil (due to slow solid heat conduction). As a result, the soil temperature field shows a "funnel-shaped" distribution characteristic.

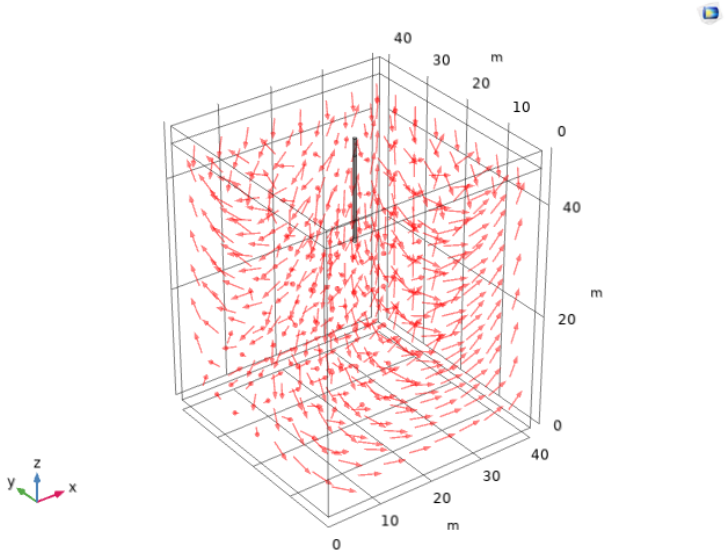

Figure 24. Darcy velocity field arrows in the TH model(t=90d)

The pore water within the soil is influenced by the temperature field, with higher temperatures in the deeper layers and lower temperatures near the surface. Driven by buoyancy, pore water flows from the deeper layers towards the surface, while surface pore water sinks, forming a groundwater flow path. Pore water near the U-tube is influenced by the cold front, with temperatures lower than the average at that depth, causing pore water to move downward.

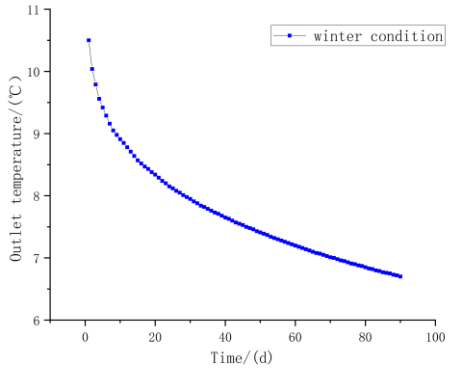

(a) Outlet temperature in winter

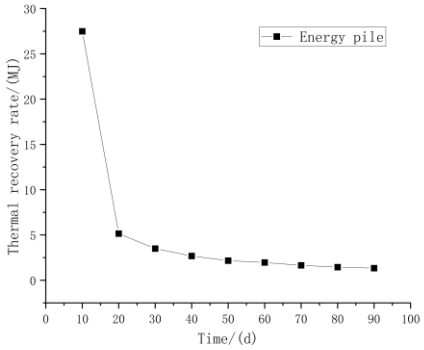

(b)The heat extraction of the energy pile

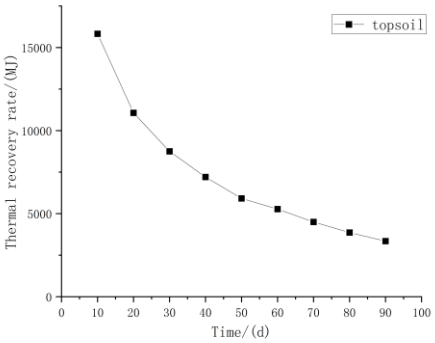

(c)Thermal extraction of the top layer

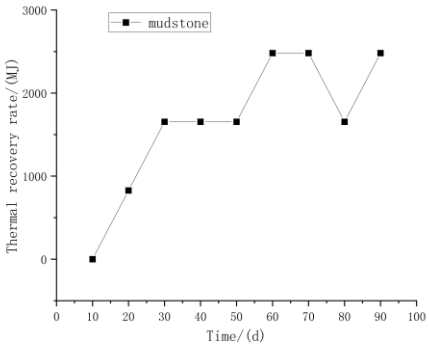

(d)Thermal extraction of the mudstone layer

Figure 25. Thermal extraction rate of the TH model

From the temperature and heat extraction rate curves described above, it can be observed that the cold working fluid undergoes sufficient heat exchange with the surrounding energy piles and soil within the 36-meter-long U-shaped heat exchange pipe. The water temperature increases from -2°C to approximately 10.5°C. Subsequently, as the heat dissipates from the surrounding energy piles and soil, the heating efficiency of the heat source decreases, leading to a continuous decline in the outlet temperature of the heat exchange pipe.

During the initial operation of the system, the working fluid experiences the greatest temperature difference with the surrounding soil, resulting in the highest heat exchange efficiency and maximum heat extraction. This efficiency gradually decreases over time. The top layer of soil

(with a thickness of 3 meters) is more influenced by the cold front of the heat exchange pipe compared to the deeper mudstone layer, and the temperature difference is greater. Therefore, during the initial operation of the system, the main heat extraction comes from the top layer of soil. As the temperature of the working fluid within the deep heat exchange pipe rises, its cooling effect on the surrounding mudstone weakens, resulting in relatively stable heat dissipation rates within the mudstone formation.

5.7.2 Summer Working Conditions

This section primarily investigates the heat transfer process of energy piles under summer conditions. A transient solver with a time step of 1 day and a total simulation duration of 90 days is utilized. The analysis focuses on the variations in outlet water temperature, the temperature distribution of the pile and surrounding soil, and the heat exchange efficiency.

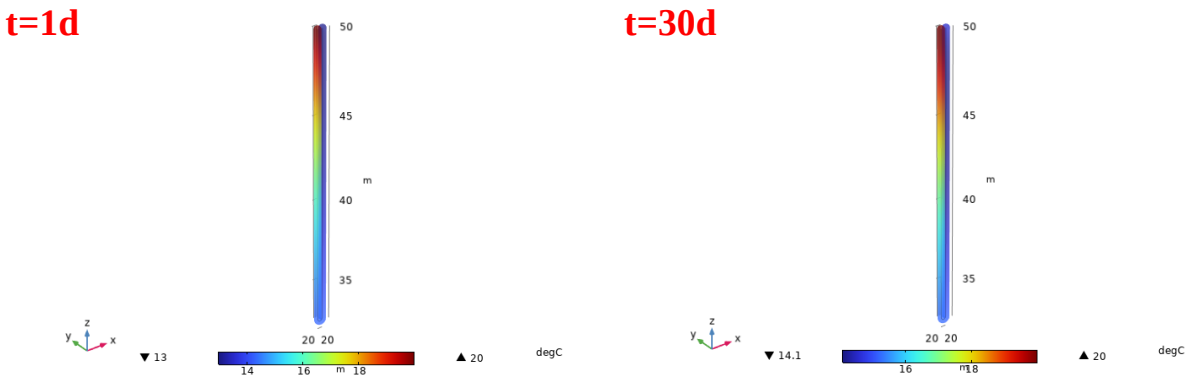

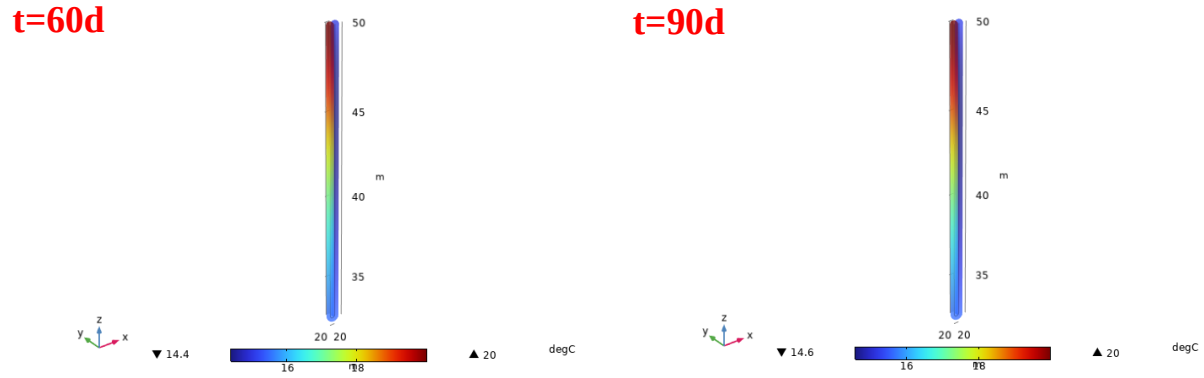

Figure 26. Temperature distribution of heat transfer fluid in U-tube

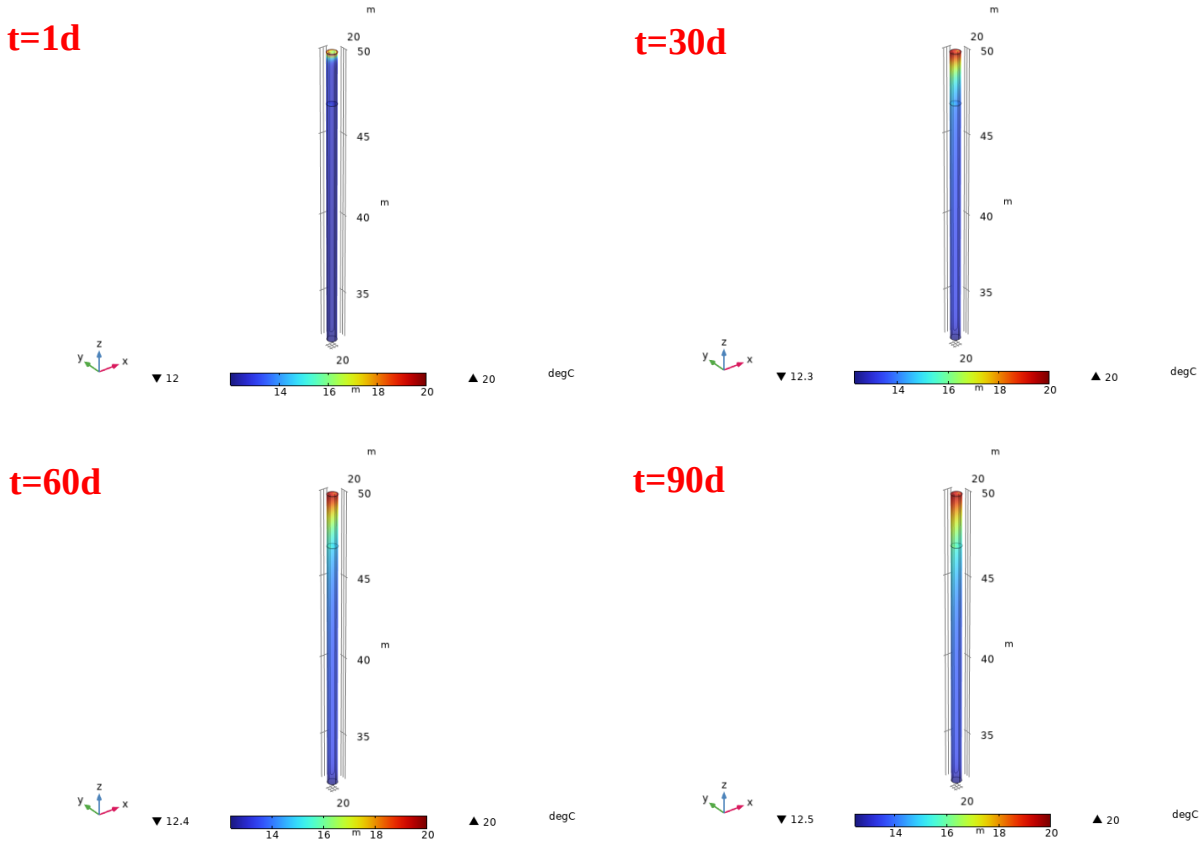

Figure 27. Temperature field of energy pile in the TH model

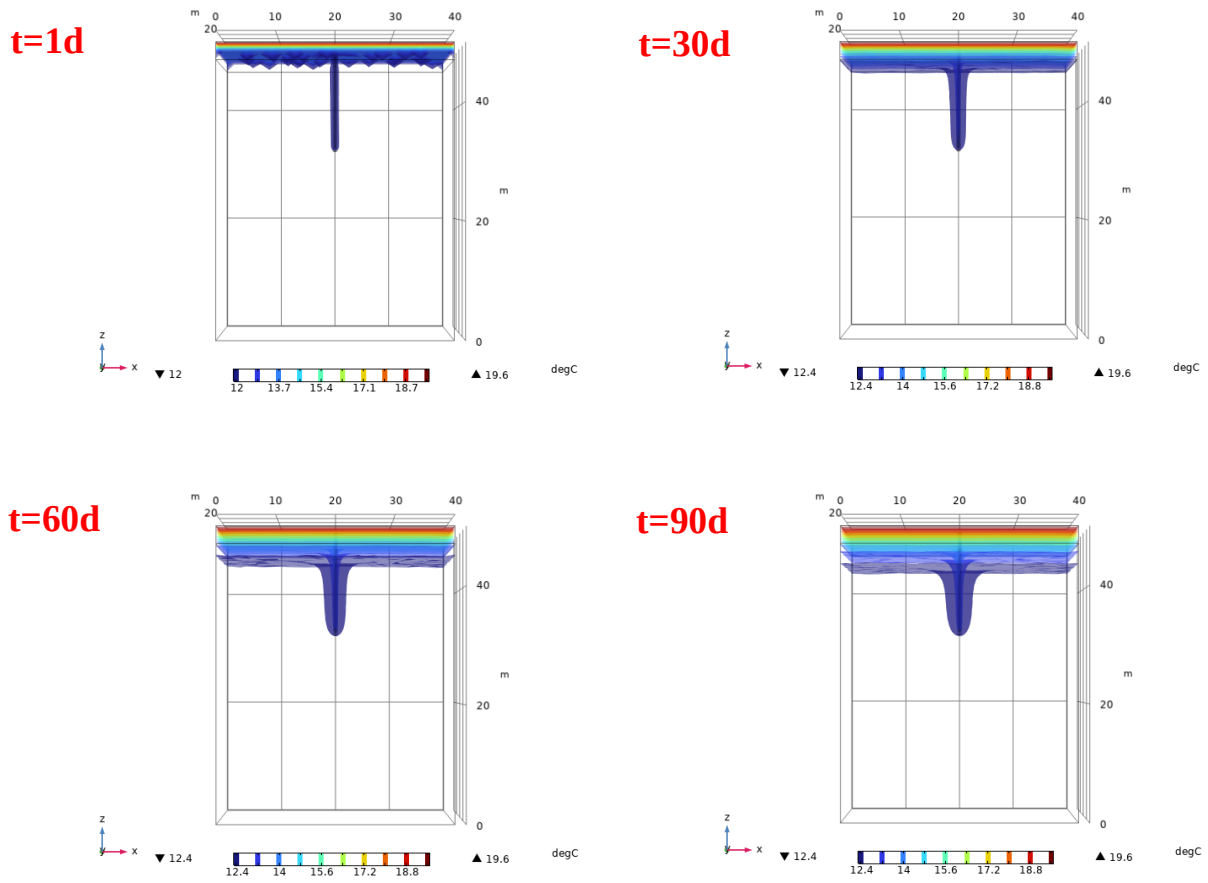

Figure 28. Temperature field distribution of ground in the TH model

During the summer conditions, the distribution patterns of temperature fields within the U-shaped pipe, energy piles, and surrounding soil are consistent with those during the winter conditions: 1. The thermal fluid inside the U-shaped pipe continuously transfers heat to the surrounding soil. The process of heat transfer occurs as follows: fluid → U-shaped pipe → energy piles → surrounding soil. 2. Along the flow direction of the U-shaped pipe, the contact area between the fluid and the energy piles continuously increases, leading to the continuous absorption of heat by the surrounding soil. However, the amount of heat exchange gradually decreases, resulting in a noticeable "spike" in the isotherms. 3. Under the combined influence of natural convection and warm fronts, the temperature field of the soil exhibits an overall "funnel-shaped" distribution with localized "hill-shaped" patterns.

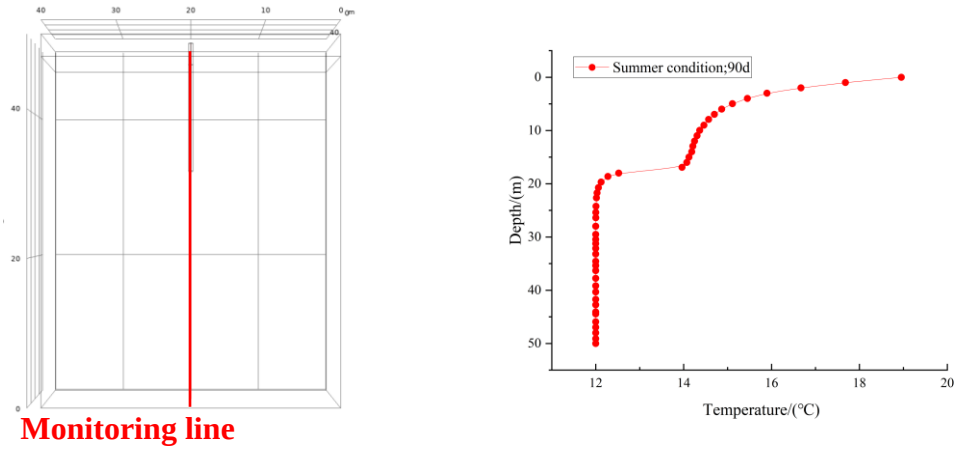

Figure 29. Monitoring line positions and temperature variation curves (90 Days)

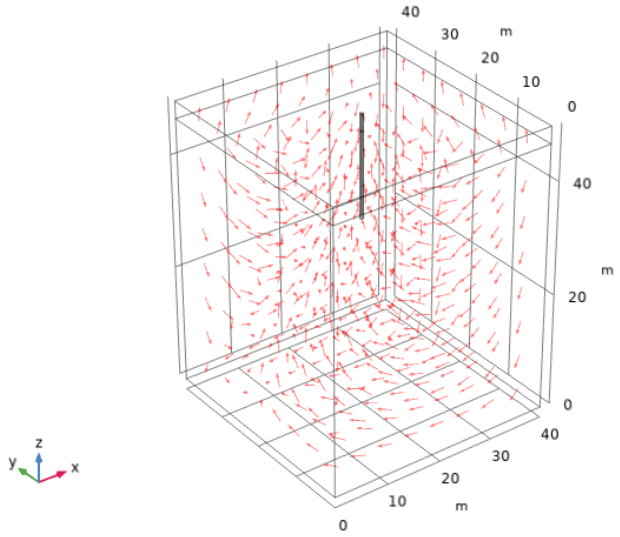

Figure 30. Darcy velocity field arrow（t=90d）

During summer conditions, the surface temperature and the injection temperature of the thermal fluid inside the U-shaped pipe are higher than those of the underground soil. The density of deep-seated pore water is greater than that of shallow pore water, resulting in natural convection driven by buoyancy. The heat transfer from the thermal fluid inside the U-shaped pipe causes localized temperature disturbances within the soil. As a result, the temperature of the pore water in the heat-disturbed region increases and flows upward, while the surrounding pore water moves toward the heat-disturbed area.

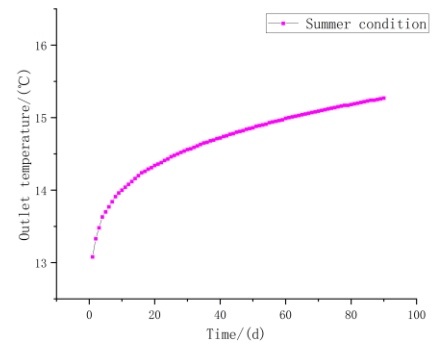

(a) Outlet temperature in summer

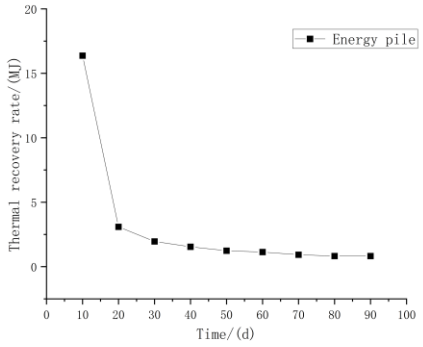

(b)Thermal extraction of energy pile

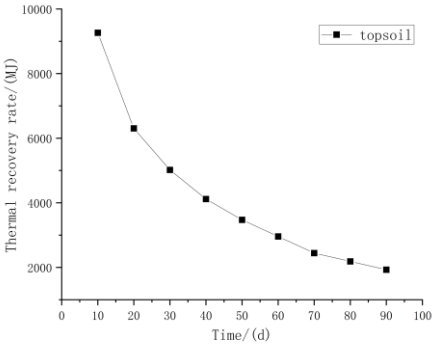

(c)Thermal extraction of the top layer

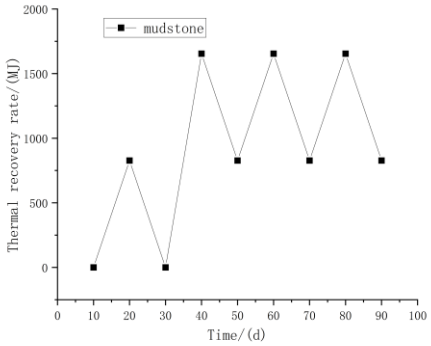

(d)Thermal extraction of mudstone

Figure 31. Thermal extraction in summer

During summer conditions, the thermal fluid with higher temperatures continuously absorbs heat from the surrounding cooler soil as it flows. The soil around the energy piles is heated and transfers heat to the surrounding soil through solid heat conduction, but the efficiency of heat conduction in porous media is low. The soil around the U-shaped pipe cannot promptly transfer heat to the surrounding soil, resulting in a decrease in the temperature difference between the thermal fluid and the surrounding soil, consequently reducing the heat exchange between them. Eventually, this leads to a gradual increase in the temperature of the thermal fluid inside the U-shaped pipe and a decrease in heat exchange efficiency.

5.8 Sensitivity Analysis

This section focuses on the sensitivity analysis of parameters such as the thermal conductivity of concrete piles and mudstone, the permeability of mudstone, and the injection velocity of the thermal fluid under winter conditions. The evaluation criteria for the system are as follows: (a) Heat extraction rate (Q) (b) Outlet temperature (T_out) of the U-shaped pipe.

5.8.1 Thermal Conductivity of Energy Piles and Mudstone

The heat transfer pathway of energy piles in the soil mass mainly consists of three components: thermal conduction and convection within the porous medium of the soil mass, solid thermal conduction of the energy piles, and thermal convection within the U-shaped pipe. From the analysis above, it is evident that both the energy piles and the soil mass play crucial roles in heat transfer. Therefore, this section focuses on investigating the heat transfer characteristics of energy piles and mudstone under different thermal conductivity combinations. Specific parameter settings are illustrated in Table 4.

Table 4. Parameter settings in the TH model

Parameter	A	B	C
Energy Pile Thermal Conductivity	1.2 W/(m·K)	1.8 W/(m·K)	2.0 W/(m·K)
Mudstone thermal conductivity	0.8 W/(m·K)	2.0 W/(m·K)	2.8 W/(m·K)

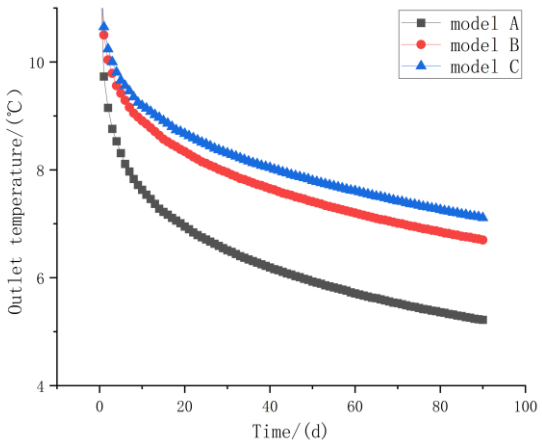

Figure 32. The outlet temperature change curve

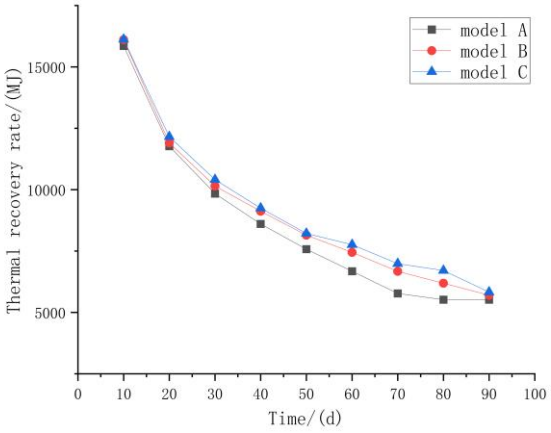

Figure 33. System thermal extraction in winter

From the above curves, it can be observed that the thermal conductivity of energy piles and mudstone has a significant impact on the efficiency of heat extraction. Higher thermal conductivity results in greater efficiency in soil thermal conduction, allowing the far-field soil mass to supplement heat to the near-field soil mass more quickly. As a result, the temperature decrease at the outlet of the U-shaped pipe is slower.

5.8.2 Permeability of Mudstone

The permeability of the soil directly affects the seepage velocity of the internal pore water, and pore water is an important carrier for heat transfer. Therefore, a sensitivity analysis of the permeability of the lower mudstone layer is necessary. In this section, four permeability values are selected: 1×10^{-14} m^2, 1×10^{-15} m^2, 1×10^{-16} m^2, and 1×10^{-17} m^2.

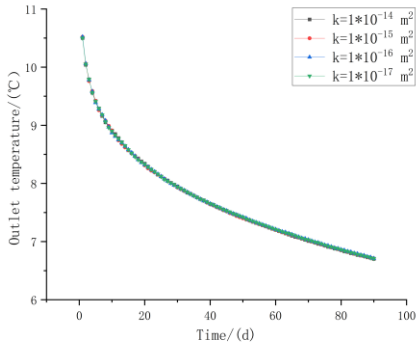

(a)The outlet temperature change curve with different permeability

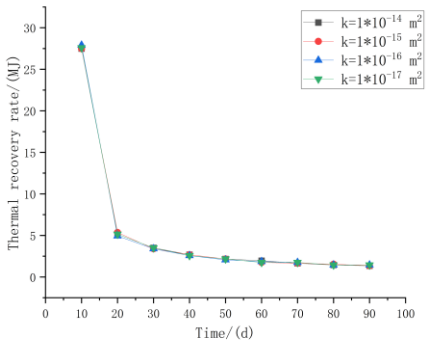

(b)Thermal extraction of energy pile with different permeability

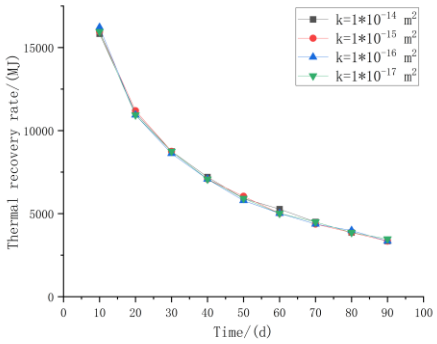

(c)Thermal extraction of the top layer with different permeability

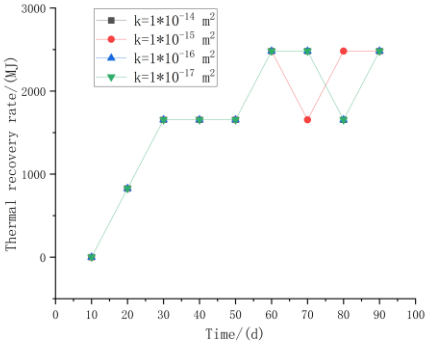

(d)Thermal extraction of mudstone with different permeability

Figure 34. Thermal extraction with different permeability

From the above curves, it can be observed that the permeability of the mudstone has a minor impact on the heat transfer process of the energy pile. The main reasons for this phenomenon are as follows: (1) The temperature difference between the fluid inside the U-shaped pipe and the deep

mudstone is small, only a few degrees Celsius. As a result, the thermal convection of the pore water in the mudstone is weak, making it difficult to significantly affect the heat transfer process. (2) The seepage velocity of the pore water in the mudstone is in the order of 10^{-12} m/s, resulting in relatively short fluid seepage paths within the short operating time.

5.8.3 U-tube Work Fluid Injection Flow Rates

In the U-shaped pipe, the working fluid is subjected to forced convection along the pipe wall under external pumping and gravity-driven forces. It undergoes convective heat exchange with the contact surface of the energy pile. The flow velocity directly affects the convective heat transfer coefficient, thereby influencing heat exchange. In this section, the injection flow velocities of the fluid are chosen to be 0.5 m/s, 1.5 m/s, and 2.0 m/s, respectively.

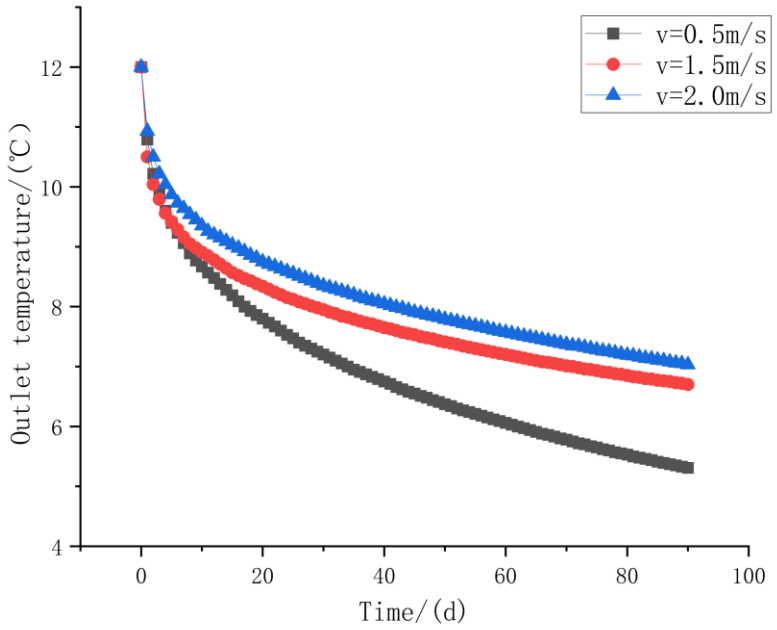

Figure 35. The outlet temperature change curve with different flow rate

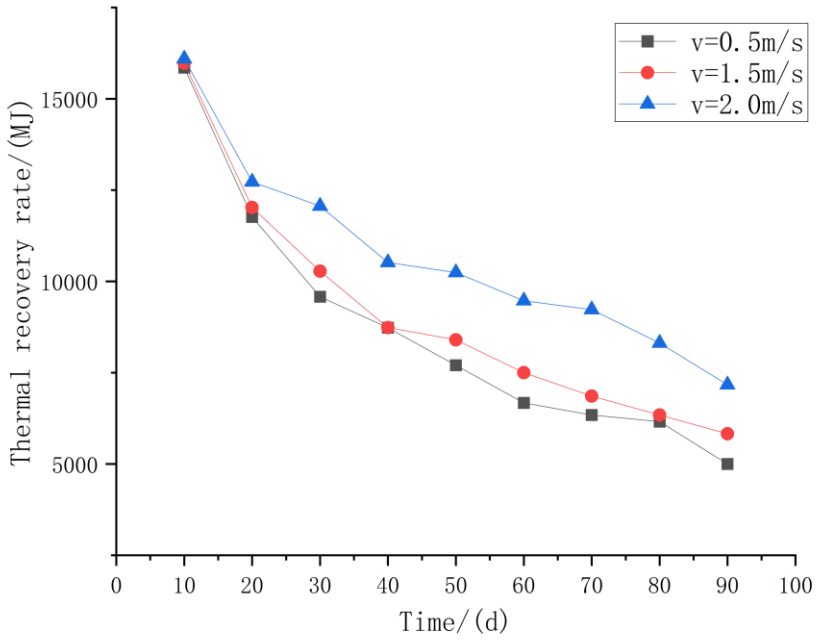

Figure 36. System thermal extraction with different flow rate

From the above figure, it can be observed that as the flow velocity of the working fluid inside the U-shaped pipe increases, the convective heat transfer coefficient between the working fluid and the energy pile also increases. Consequently, the amount of heat extracted per unit of time is larger, leading to a slower decrease in the outlet temperature.

5.8.4 Layout of Group Energy Pile

Common group pile models typically consist of 4 or more piles, and their arrangement can be classified into straight-line or staggered patterns based on the overall load-bearing requirements. Below are several common arrangements of group piles.

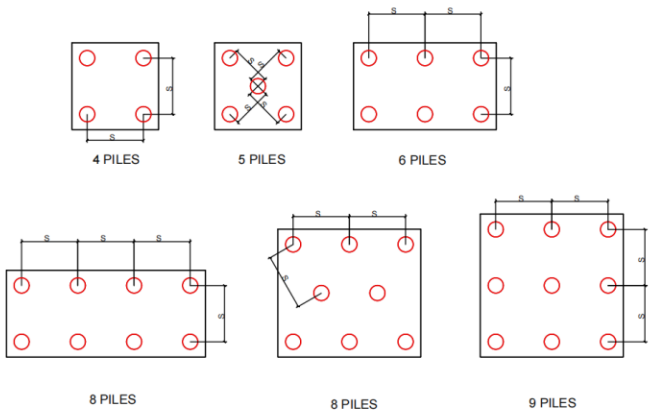

Figure 37. Common group pile arrangement

As this section focuses on the thermal performance of group piles (the thermal properties of each pile), it is important to consider the mutual influence of adjacent heat sources as they continuously transfer heat to their surroundings, leading to the formation of thermal disturbance zones at certain times. For group piles, the arrangement of 9 piles includes the placement of 3 piles, 5 piles, and piles as shown in Figure 37. Therefore, selecting 9 piles can be used to investigate the thermal disturbance effects among different group pile combinations. Based on the above analysis; to accurately model the operating conditions of energy group piles, a 9-pile grid arrangement is selected to establish the thermal transfer model for this group of energy piles.

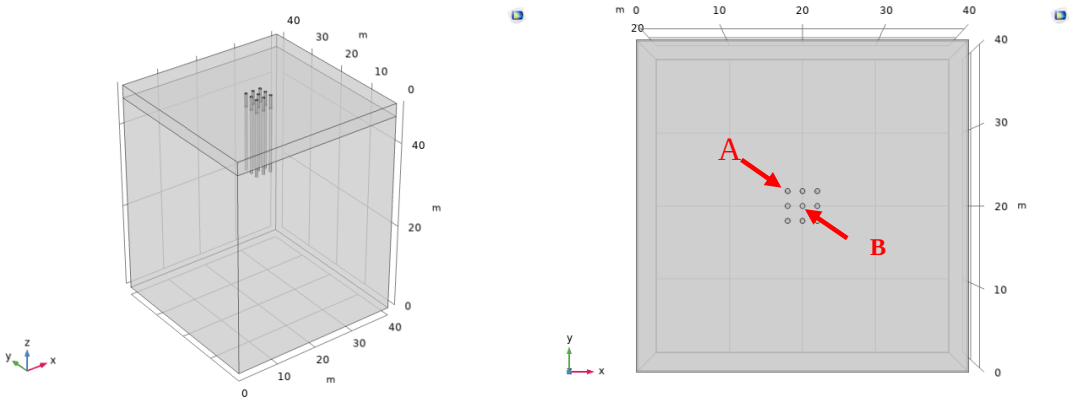

Figure 38. 3D model of 9 group piles in the TH model

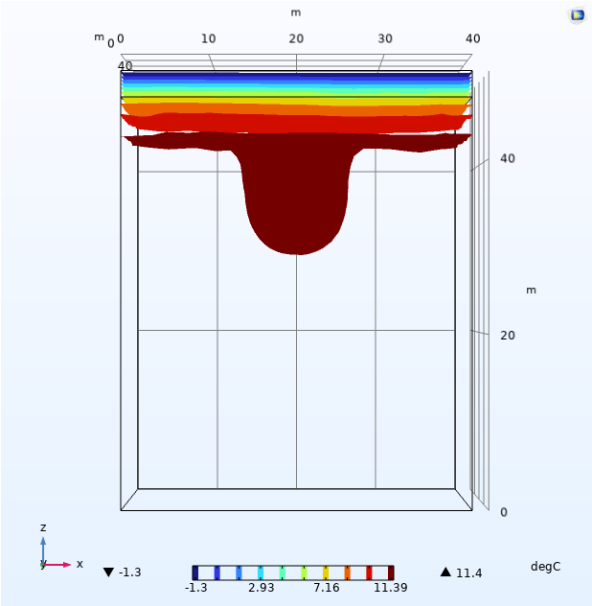

Figure 39. Temperature field of group pile in the TH model

The outlet temperatures of A and B piles in the group pile model are selected for comparison and analysis with the outlet temperature of the single pile model, and the curves are shown below.

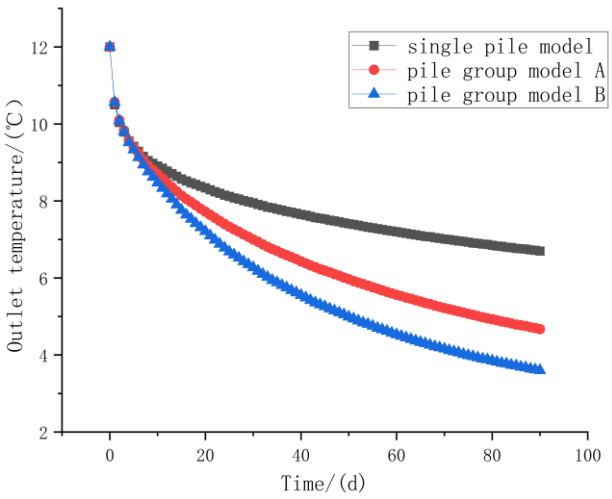

Figure 40. Variation of outlet temperature between group pile and single pile

The above curve demonstrates that there is mutual interference among the piles in the group pile model. The outlet temperature of the central pile decreases by half compared to that of the single

pile model, and the outlet temperature of the side piles is also lower than that of the single pile model. This is mainly attributed to the mutual thermal disturbance among the piles in the group pile model. The temperature reduction in the central region is faster while the replenishment of thermal energy is slower, resulting in a significant decrease in the heat exchange efficiency of each pile in the group pile system.

5.9 Conclusion

This chapter primarily simulated the heat transfer process of energy piles under two operating conditions: summer and winter. It analysed the variation patterns of heat transfer performance such as the outlet temperature of energy piles, the temperature of the pile and surrounding mudstone layer, and heat exchange efficiency. Furthermore, it explored the seepage characteristics of pore water in the soil under the driving force of natural convection. Based on the numerical calculations:

1. The temperature field of the soil exhibits an overall "funnel-shaped" distribution under the combined influence of natural convection and warm/cold fronts, with localized "hill-shaped" patterns.
2. The thermal energy of concrete energy piles gradually depletes or accumulates during the initial stage of system operation, subsequently affecting the heat transfer in the surrounding soil. Therefore, the heat transfer performance of energy piles is crucial for the overall system.
3. Higher thermal conductivity in both concrete energy piles and mudstone enhances solid heat conduction efficiency, leading to reduced temperature decay at the heat exchanger outlet and increased heat extraction efficiency.
4. A faster flow velocity of the working fluid inside the U-shaped pipe leads to a higher convective heat transfer coefficient between the working fluid and the energy pile, thus

increasing the heat extraction rate.

5. Pore water in the soil undergoes natural convection driven by density differences, with a flow velocity magnitude of 10^{-12} m/s. The impact of different mudstone permeabilities on the heat transfer process of energy piles is minimal.
6. During group pile heat transfer, neighboring piles experience thermal interference, and the heat exchange efficiency between piles is relatively lower compared to single-pile operation.

6 3D FEA Thermal-mechanical Coupling Modelling of Energy Pile

The previous chapter mainly focused on studying the heat transfer and efficiency of energy piles. However, under thermal loading, the stress behaviour of energy piles differs significantly from that of conventional piles. Moreover, as the main load-bearing component of buildings, it is crucial to study the thermo-mechanical response of the pile and the surrounding soil. Under thermal loading, there exist complex interactions between piles, which can impact the design of energy piles. Due to limitations in experimental conditions, to explore the potential impact of soil thermal expansion coefficients and elastic moduli on the thermo-mechanical response of energy piles, this chapter utilizes COMSOL Multiphysics to establish a three-dimensional thermo-mechanical coupling numerical model.

6.1 Numerical Model

The model consists of a U-tube heat exchanger, concrete energy piles, and surrounding soil. The dimensions of the surrounding soil model are 15m × 15m × 28m (with distances from the outer boundaries to the pile axis greater than 10D) to minimize the influence of boundaries on the simulation results. The diameter of the concrete energy piles is 0.6m, and the length of the piles is 18m. The U-tube heat exchanger is simplified as a one-dimensional line, with a single-sided length of 17.5m.

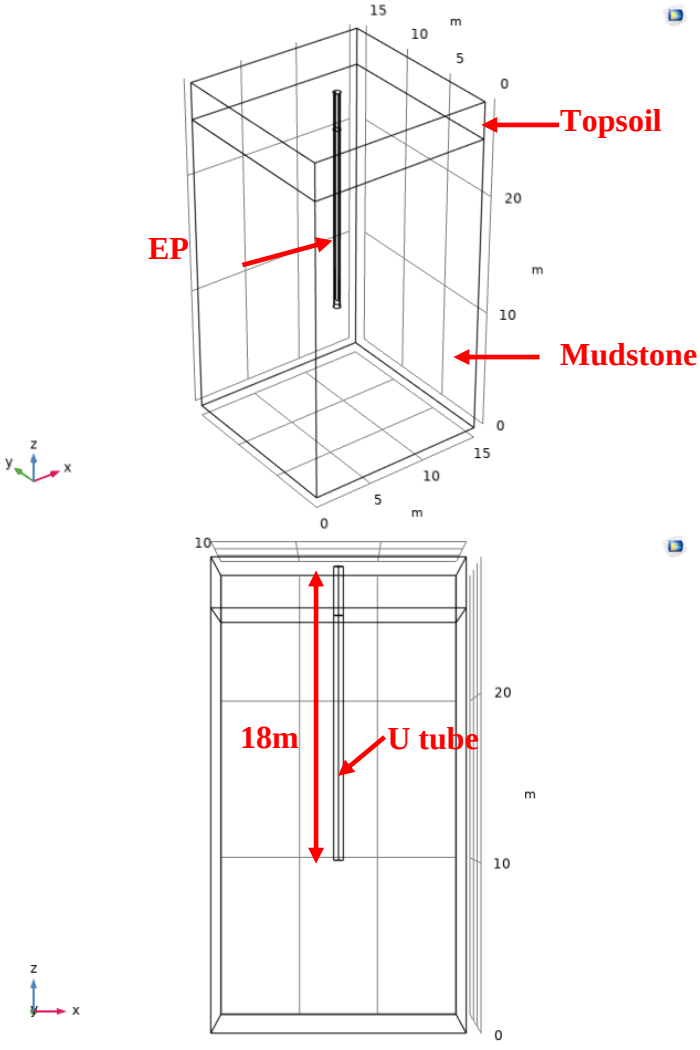

Figure 41. 3D thermal-mechanical coupling model

6.2 Model Assumptions

1. Concrete energy piles are assumed to be isotropic, elastic, and incompressible.
2. Energy piles and surrounding soil are linear thermally elastic materials.
3. The influence of relevant loads on fluid pressure in the soil is ignored.
4. Non-isothermal pipe flow simulation is employed to model the flow and heat transfer process of the heat transfer fluid in the U-tube. Heat transfer between energy piles and soil occurs primarily through conduction.
5. The interface between the piles and the surrounding media forms a composite unit where

they share common nodes at their contact surfaces, ensuring conformity. Frictional contact between the energy piles and the surrounding media (excluding relative sliding) is not considered in the analysis.

6.3 Governing Equations

Equation of heat conduction in solids:

$$\rho_m C_m \frac{\partial T}{\partial t} + \nabla \cdot q = Q \text{ (6.1)}$$

$$q = -\lambda_m \nabla T \text{ (6.2)}$$

Joining the above equations:

$$\rho_m C_m \frac{\partial T}{\partial t} - \nabla \cdot (\lambda_m \nabla T) = Q \text{ (6.3)}$$

Where ρ_m is the density of the solid pile; C_m is the constant pressure heat capacity of the pile; T is the temperature; t is the time; λ_m is the thermal conductivity of the solid pile;∇T is the temperature gradient; Q is the heat source term; m denotes solid.

Equations for solid mechanics(Nield and Bejan, 2006):

$$F_v + \nabla \cdot \left(C \cdot \left(\varepsilon_{ij} - \alpha \cdot \Delta T \right) \right) = 0 \text{ (6.4)}$$

Where Fv is the volumetric force factor，∇ is the dispersion，C is the stiffness tensor determined by the combination of the modulus of elasticity and Poisson's ratio，ε_{ij} is the strain tensor，α is the linear coefficient of thermal expansion，ΔT is the temperature gradient.

U-type heat exchanger tube convection heat transfer and wall heat transfer using a "non-isothermal pipe flow heat transfer model", the pipe flow continuity equation can be expressed as:

$$\frac{\partial A\rho_f}{\partial t} + \nabla t\left(A\rho_f u\vec{e}_t\right) = 0 \text{ (6.5)}$$

The momentum conservation equation can be expressed as:

$$\rho_f \frac{\partial u}{\partial t} = -\nabla_t p\vec{e}_t - \frac{1}{2} f_D \frac{\rho_f}{d_h}|u|u \text{ (6.6)}$$

The energy conservation equation can be expressed as (Ding et al., 2022):

$$\rho_f AC_f \frac{\partial T_f}{\partial t} + \rho_f AC_f u\vec{e}_t \nabla_t T_f = \nabla_t \times \left(Ak_f \nabla_t T_f\right) + \frac{1}{2} f_D \frac{\rho_f A}{d_h}|u|u^2 + Q_{wall} \text{ (6.7)}$$

Where: ρ_f is the fluid density, A is the cross-sectional area of the pipe,u is the fluid velocity, $\vec{e}t$ is the tangential vector in the direction of the pipe, ∇t is the differential operator of the pipe coordinates, f_D is the friction coefficient depending on the Reynolds number, dh is the diameter of the pipe, p is the pressure inside the pipe, T_f is the temperature of the fluid, k_f is the thermal conductivity of the fluid, C_f is the specific heat capacity of the fluid, Q_{wall} represents the heat transfer efficiency per unit length through the pipe wall.

6.4 Boundary Condition

Solid mechanics boundary: The bottom of the soil surrounding the pile is set to have fixed constraints, completely restricting vertical and horizontal displacements. Roll conditions are placed around the soil on all sides to limit horizontal displacements. No constraints or mechanical loads are applied at the top of the model.

Heat transfer boundary: In summer conditions, assuming an atmospheric temperature of 20°C and a soil temperature of 12°C, the fluid injection rate inside the U-shaped pipe is 1 m/s, with the injection temperature matching the atmospheric temperature for that period. The sidewall of the soil is treated as an adiabatic boundary.

In winter conditions, assuming an atmospheric temperature of -2°C and a soil temperature of 12°C, the fluid injection rate inside the U-shaped pipe is 1.5 m/s, with the injection temperature matching the atmospheric temperature for that period. The sidewall of the soil is treated as an adiabatic boundary.

6.5 Parameters of Simulation

The computational model in this chapter utilizes a transient solver, with a total calculation duration of 30 days for both winter and summer conditions and a time step of 1 day.

Table 5. Input of simulation parameters in the TM model

Parameters	Value
Top layer density	2200 kg/m^3
Top layer thermal conductivity	1.65 W/(m·K)
Constant pressure heat capacity of the top layer	1218.66 J/(kg·K)
Coefficient of thermal expansion of the top layer	1×10^{-4} 1/K
Young's modulus of the top layer	2.5×10^{8} Pa
Top layer Poisson's ratio	0.33
Top layer thickness	3m
Mudstone layer thickness	25m
Mudstone density	2200 kg/m^3
Mudstone thermal conductivity	2 W/(m·K)
Constant pressure heat capacity of mudstone	500 J/(kg·K)
Coefficient of thermal expansion of mudstone	1×10^{-5} 1/K
Young's modulus of mudstone	7×10^{9} Pa
Poisson's ratio for mudstone	0.33
Energy pile density	2300 kg/m^3
Energy pile thermal conductivity	1.8 W/(m·K)
Energy pile constant pressure heat capacity	880 J/(kg·K)

Coefficient of thermal expansion of energy piles	1×10^{-5} 1/K
Young's modulus of energy pile	4×10^{10} Pa
Energy pile Poisson's ratio	0.2
U-tube inner diameter	2 mm
U-tube wall thickness	1 mm
Injection flow rate	1.5 m/s
Injection temperature (winter conditions)	-2℃
Injection temperature (summer conditions)	20℃

6.6 Mesh Analysis

The model mesh is user-defined, with one-dimensional lines as edges, and the concrete piles and soil layers are meshed with free tetrahedra, generating a total of 131,008 tetrahedral units with an average unit quality of 0.65. Extremely fine meshing generates a total of 319,996 tetrahedral units with an average unit quality of 0.66.

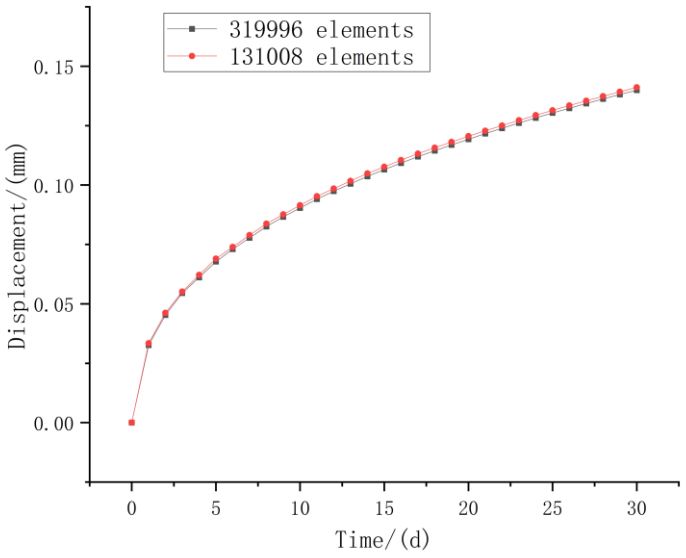

Figure 42. Pile axial displacement with time (energy pile head)

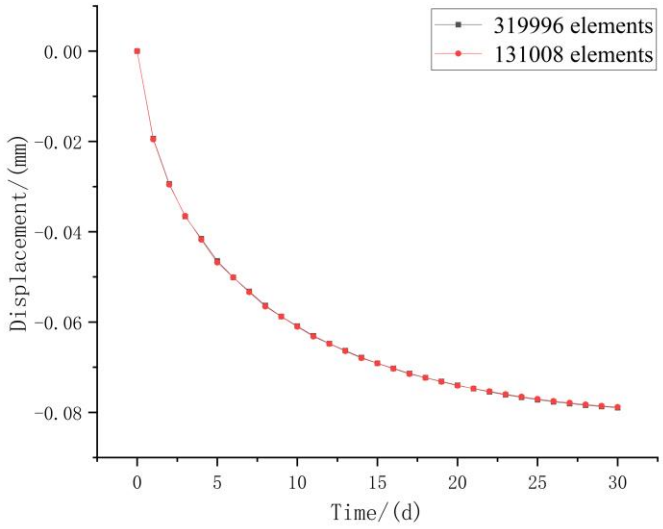

Figure 43. Pile axial displacement with time (energy pile bottom)

From the above figure, it is observed that the mesh density has little effect on the axial displacement of the pile body. Therefore, 131,008 tetrahedral unit models are used for numerical analyses in this section to improve computational efficiency.

6.7. Simulation Results

This section primarily investigates the influence of thermal disturbances on the mechanical characteristics of energy piles and surrounding media under summer and winter conditions. It analyses the stress distribution along the energy pile body, examines displacement variations, and conducts sensitivity analyses on key parameters such as the thermal conductivity of mudstone, the thermal expansion coefficient, and the elastic modulus.

6.7.1 Thermal-mechanical Coupling Effects of Energy Piles

In the absence of friction shaft resistance, a pile with free boundary conditions is free to expand or contract under temperature changes in the pile body without additional thermal stresses. This assumes that the temperature change between points in each cross-section of the pile is uniform

and that there is no temperature gradient, as non-uniformity in the temperature gradient would result in additional stresses in the pile. The magnitude of the expansion deformation depends on the thermophysical properties of the pile and can be calculated as:

$$\varepsilon_{T-\text{free}} = \alpha \Delta T \quad (6.8)$$

Where $\varepsilon_{\text{T-free}}$ is the axial thermal strain of the pile under free boundary conditions; ignore friction at the pile-soil interface; α is the thermal expansion coefficient of the pile.

When the pile is restrained in the axial direction, the pile length does not change, and a uniform axial strain is generated in the pile:

$$P = EA\varepsilon_{T-\text{free}} \quad (6.9)$$

Where E is the elastic modulus of the pile, A is the cross-sectional area of the pile.

Some or all of the thermal deformation (strain) is limited when the pile is subjected to frictional contact at the pile-soil interface, fixed at the pile head, and ground restraint at the pile end, preventing it from moving completely freely. As a result, the actual thermal strain in the pile is less than the calculated value of thermal strain in a free pile. This actual value varies significantly with the degree of restriction at the pile head, pile end, and friction shaft, and with the temperature of the pile, as expressed below:

$$\varepsilon_{T-O\text{bs}} \leq \varepsilon_{T-free} \quad (6.10)$$

$$\varepsilon_{T-Rstr} = \varepsilon_{T-free} - \varepsilon_{T-Obs} \quad (6.11)$$

To resist thermal strain, an axial thermal stress is induced in the pile:

$$P = EA\varepsilon_{T-R\text{str}} \quad (6.12)$$

6.7.2 Summer Working Conditions

This subsection primarily investigates the influence of thermal disturbances on the mechanical characteristics of energy piles and surrounding rock-soil media during summer conditions, specifically focusing on the injection of high-temperature working fluids into the rock-soil mass. A transient solver is employed with a time step of 1 day, totalling 30 days of computation. The analysis includes studying the stress distribution along the energy pile body and analysing the patterns of displacement variations.

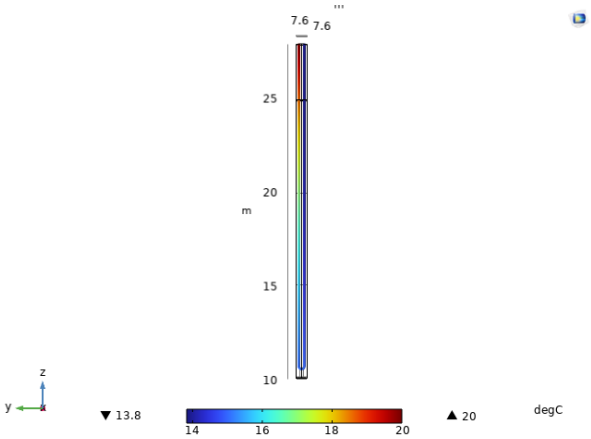

Figure 44. U-tube temperature field in summer(30d)

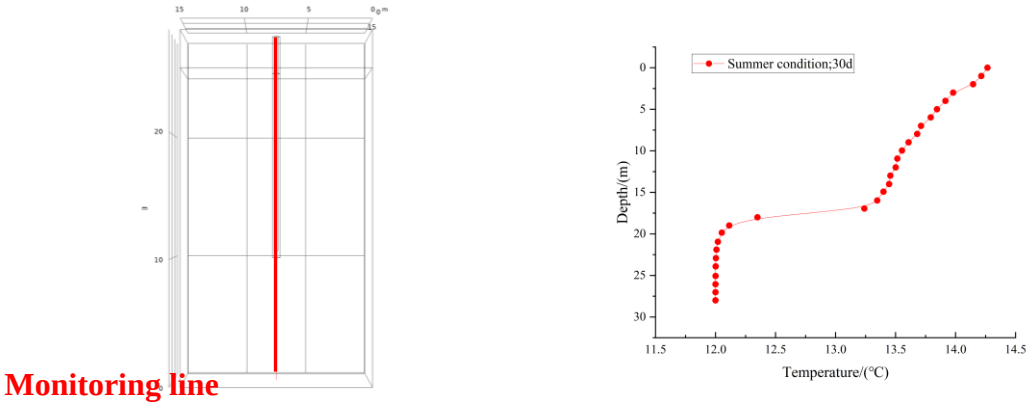

Figure 45. Monitoring line positions and temperature variation curves (30 Days)

The heat exchanger working fluid inside the U-tube is injected into the ground at a flow rate of 1.5 m/s. Since the temperature of the soil is lower than the U-tube temperature in summer, the

surrounding soil continuously absorbs the heat energy inside the heat exchanger fluid, and the heat energy transfer sequence is heat exchanger fluid → U-tube → energy pile → surrounding soil. With the increase in calculation time, the temperature of the surrounding soil gradually rises to a relatively stable state, and the temperature at the outlet of the U-shaped pipe gradually increases.

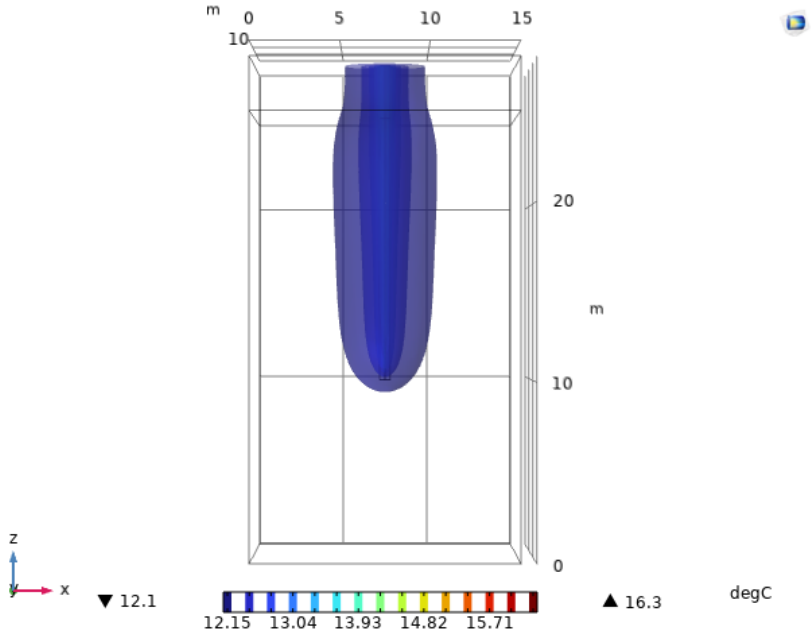

Figure 46. Soil isotherm in summer (30d)

The working fluid in the U-tube continuously heats the pile and the surrounding soil, and the warm front has not yet reached the farther soil (since solid heat conduction is slow). As a result, the temperature field of the soil body shows a "funnel-shaped" distribution characteristic.

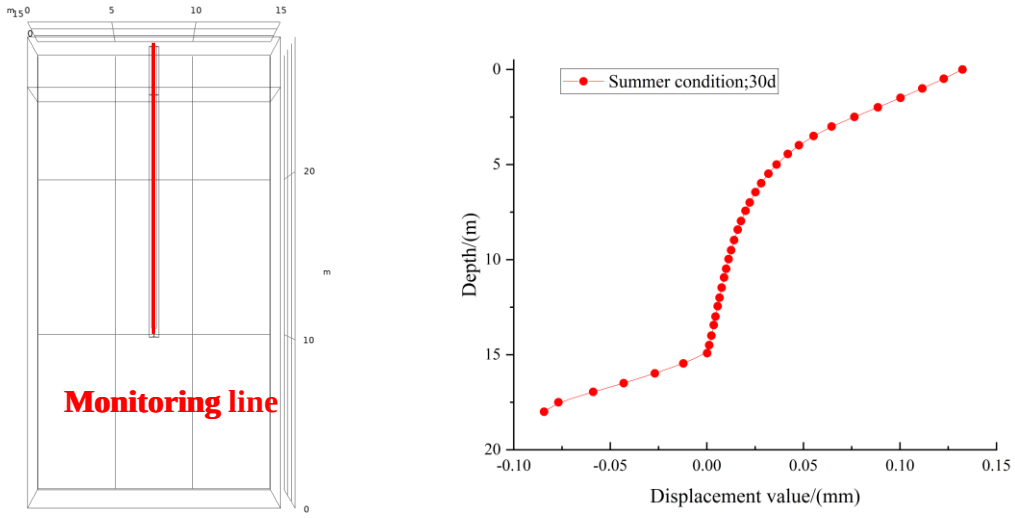

Figure 47. Monitoring line positions and deformation variation curves (30 Days)

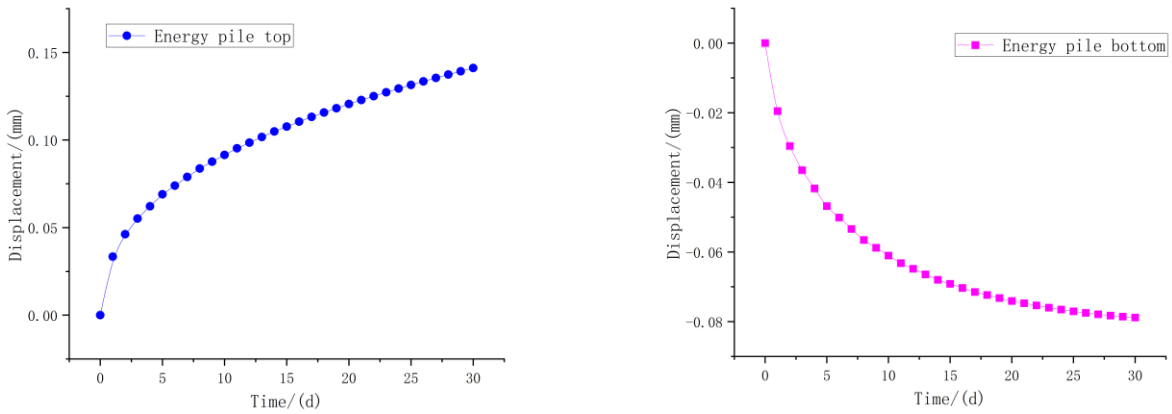

Figure 48. Change in energy pile displacement (Z-axis)

The graph above illustrates the displacement variations at the top and bottom of the energy pile over a 30-day period of system operation. Positive displacement values indicate upward movement, while negative values denote downward movement. As the duration of heating in the U-shaped pipe increases, the upward displacement at the pile top continuously increases, reaching 0.141 mm after 30 days. Similarly, the downward displacement at the pile bottom also increases progressively.

However, due to constraints imposed by the underlying mudstone, the absolute displacement value at the pile bottom is less than that at the pile top, with a displacement of 0.078 mm after 30 days.

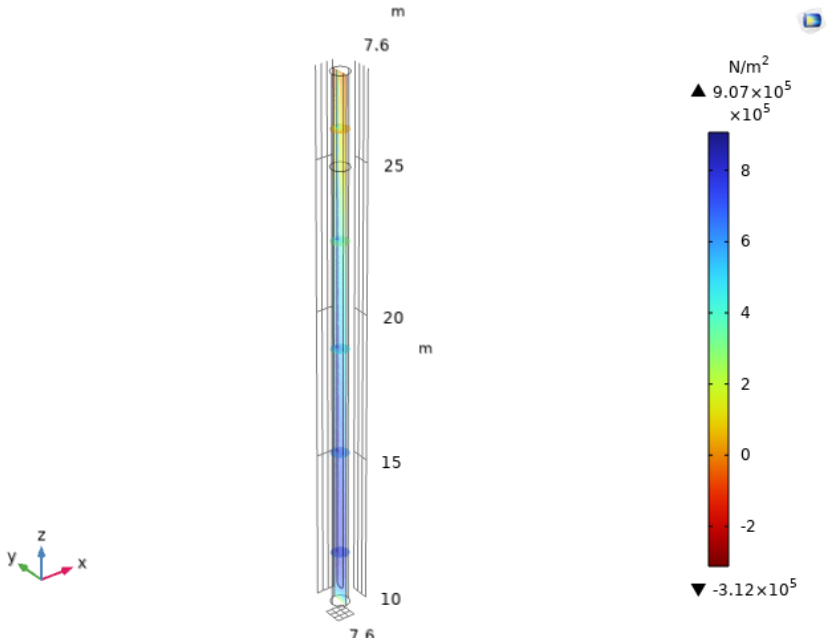

Figure 49. Energy pile stress distribution (30d)

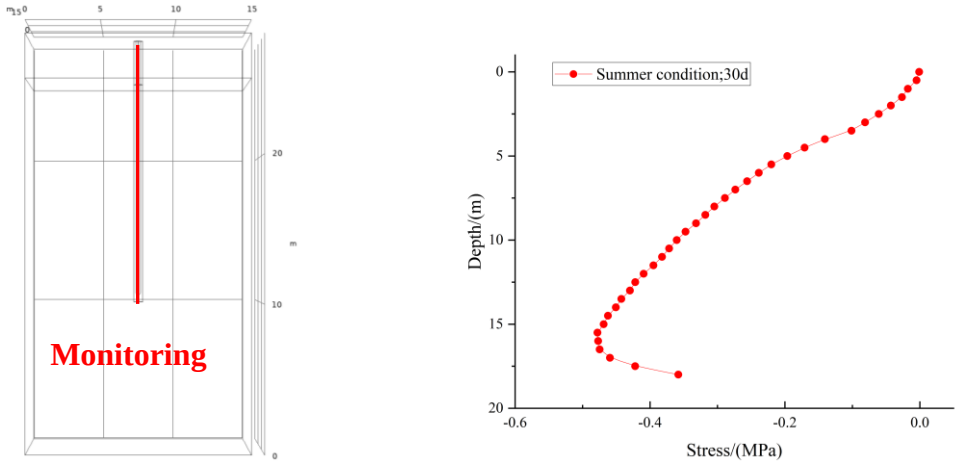

Figure 50. Monitoring line positions and stress variation curves (30 Days)

The stress distribution map at the end of heating is depicted in the above figure. Based on the numerical trends, the thermal stress distribution along the pile can be divided into three regions: two transitional zones with high amplitude fluctuations at the top and bottom of the pile, and a stable region in the middle. The thermal stress reaches its maximum value at a depth of 0.7 times

the pile length, peaking before gradually decreasing. Considering the trend of pile displacement changes, the maximum thermal stress is located near the zero-displacement point of the pile.

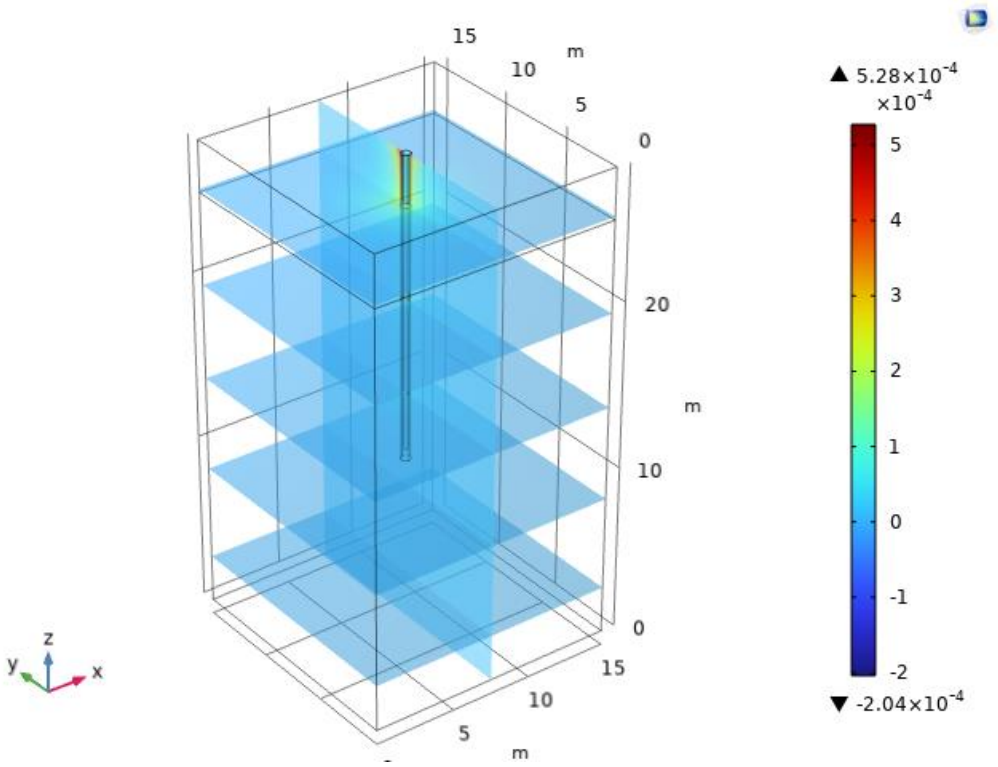

Figure 51. Energy pile and soil layer strain maps in summer

The above figure reveals that the maximum temperature increases and, consequently, the maximum strain occurs at the injection point of the U-shaped pipe into the top layer. Moving along the depth direction, the influence range of the warm front gradually diminishes, resulting in a reduction in the strain of the pile and surrounding media. At the same depth, significant differences in strain occur due to the different temperature values within the U-shaped pipe on both sides.

Based on the above analysis, it can be inferred that when an energy pile absorbs heat energy from the working fluid in the U-shaped pipe, it undergoes expansion, leading to additional displacement in the pile. Different conditions of pile-soil contact and support layers at the pile end resist some of the displacement, resulting in displacement occurring between partial and full constraint. After

heating, the pile exhibits tensile deformation along its axial direction, with the deformation gradually extending towards both ends as the temperature increases. The upper part of the pile tends to rise relative to the soil, while the lower part tends to descend. Since the pile top is a free boundary, it experiences minimal constraint on expansion deformation, resulting in the largest displacement at that location. The midsection of the energy pile is constrained in both upward and downward directions, resulting in a relatively smaller displacement with a zero-displacement point. Finally, a relatively large downward displacement is observed at the pile end.

6.7.3 Winter Working Conditions

This subsection primarily investigates the mechanical impact of thermal disturbances on energy piles and the surrounding rock-soil mass during winter conditions, particularly when injecting low-temperature working fluids into the surrounding media. A transient solver is employed with a time step of 1 day, totalling 30 days of computation. The analysis focuses on studying the stress distribution along the energy pile body and analysing patterns of displacement variations.

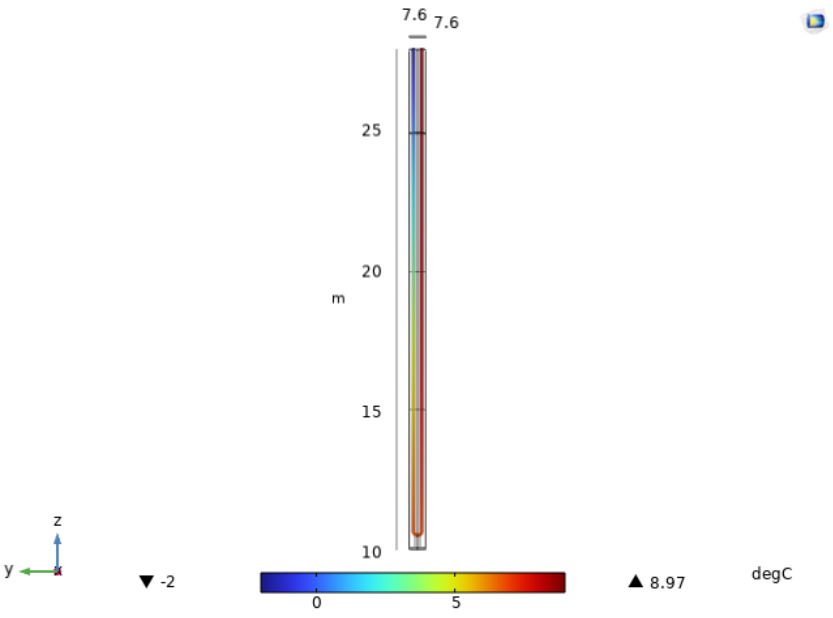

Figure 52. U-tube temperature field in winter (30d)

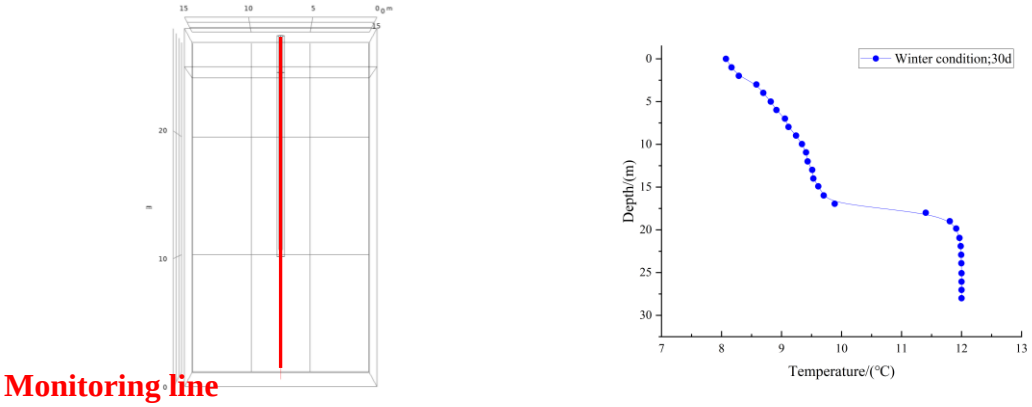

Figure 53. Monitoring line positions and temperature variation curves (30 Days)

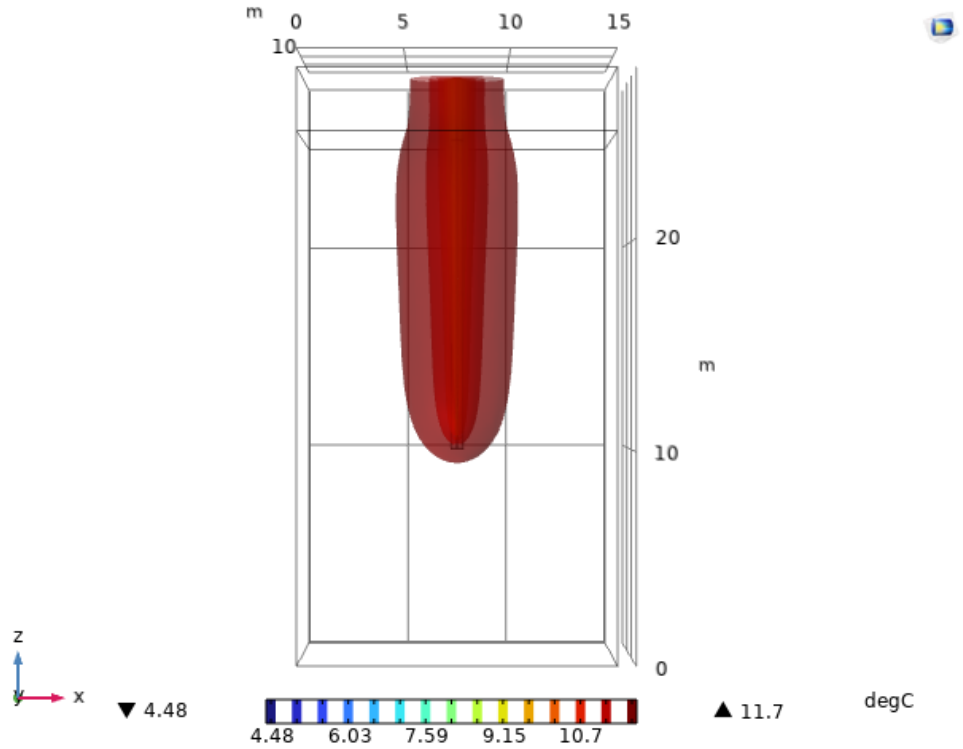

Figure 54. Soil isotherm in winter (30d)

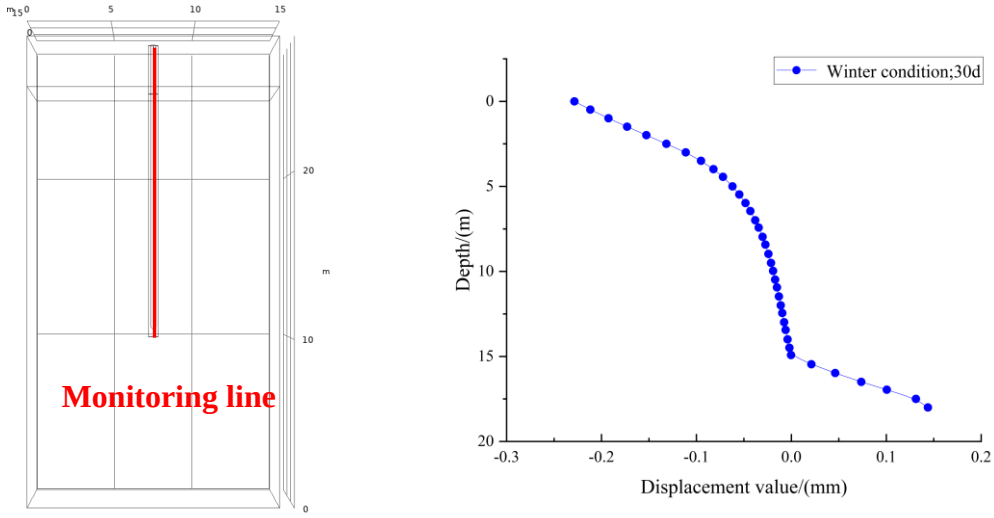

Figure 55. Monitoring line positions and deformation variation curves (30 Days)

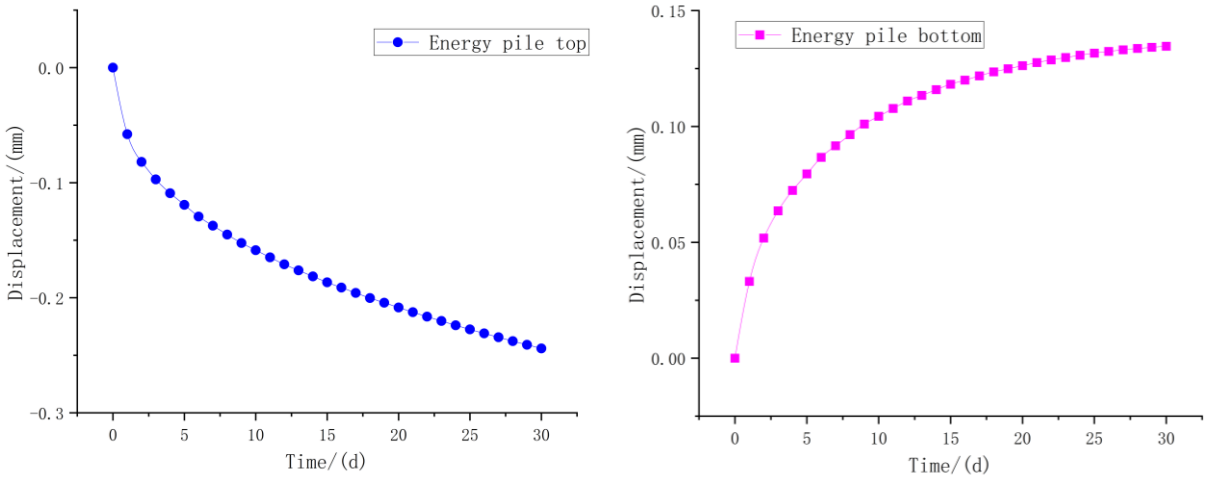

Figure 56. Change in energy pile displacement (Z-axis)

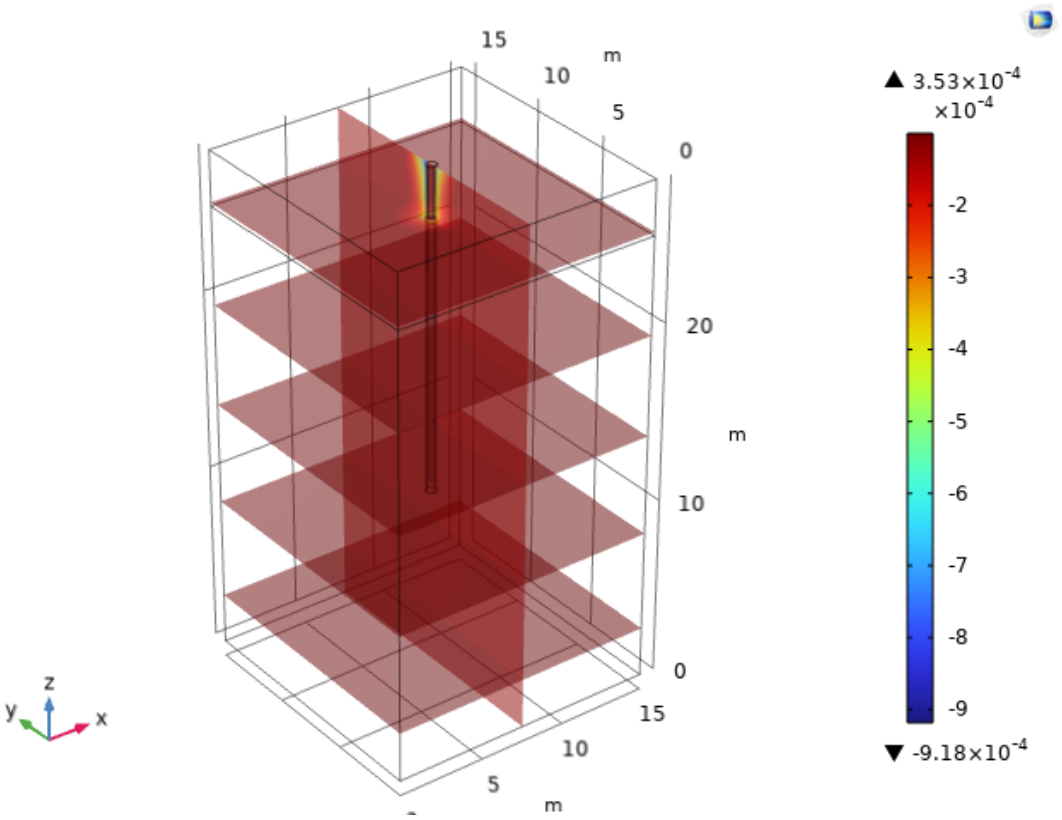

Figure 57. Energy pile and soil layer strain maps in winter

During winter operation, the cooling working fluid in the U-shaped pipe is injected into the soil at a higher temperature. Consequently, the thermal energy of the pile and soil is continuously extracted by the working fluid, causing the pile and soil to cool and contract, resulting in additional displacement of the pile structure. After cooling, the pile undergoes axial shrinkage deformation, with the deformation gradually contracting towards the center as the temperature decreases. The upper part of the pile tends to move downward relative to the soil, while the lower part tends to move upward. Since the pile head is a free boundary, it has the weakest constraint on shrinkage deformation, resulting in the largest absolute displacement at that point. The middle part of the energy pile is constrained in both upward and downward directions, resulting in relatively smaller displacement values and zero-displacement points. Lastly, a relatively large upward displacement is observed at the pile toe.

6.8 Sensitivity Analysis

6.8.1 Coefficient of Thermal Expansion of Mudstone

The thermal expansion coefficient, an important material property parameter for soil expansion during heating and contraction during cooling, plays a significant role in the mechanical response mechanism of soil under temperature disturbances. Therefore, in this section, three types of mudstone thermal expansion coefficients are selected for numerical analysis, namely $\alpha = 1\times10^{-6}$ 1/K, 1×10^{-5} 1/K, and 5×10^{-5} 1/K.

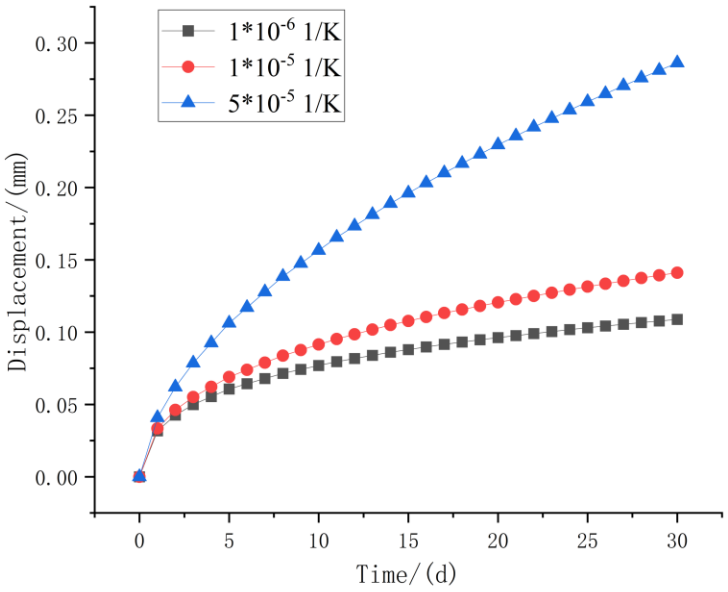

Figure 58. Pile axial displacement with time (energy pile head)

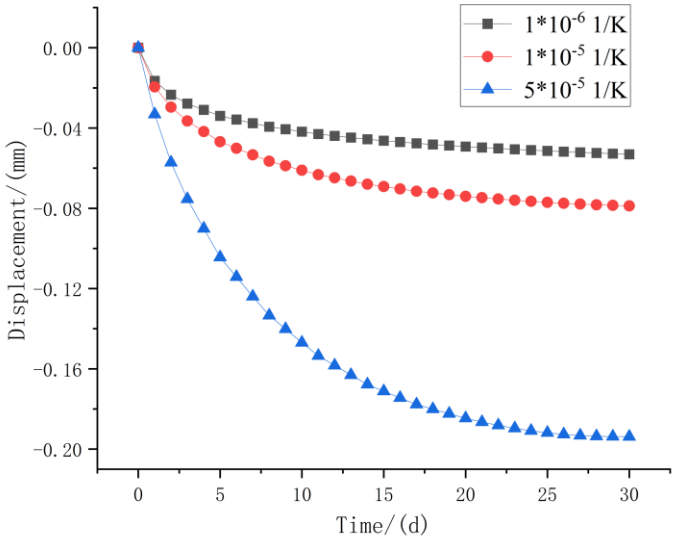

Figure 59. Pile axial displacement with time (energy pile bottom)

Analysis of the above figures reveals that as the thermal expansion coefficient of the mudstone increases from 1×10^{-6} 1/K to 5×10^{-5} 1/K, the ratio of thermal expansion coefficients between the soil and concrete increases, leading to a decrease in thermal compressive stress and an increase in displacement at both ends of the pile. This is mainly because heating-induced soil expansion generates additional tensile stress on the pile, thereby reducing the thermal compressive stress on the pile body.

6.8.2 Mudstone Modulus of Elasticity

The soil's elastic modulus is a crucial parameter that measures the soil's deformation capacity. A higher elastic modulus indicates that, under the same load conditions, the soil will experience less deformation. To investigate the effect of the elastic modulus of mudstone on pile displacement and thermal stress, values of E=7×10^{8} Pa, 7×10^{9} Pa, and 7×10^{10} Pa were selected for analysis.

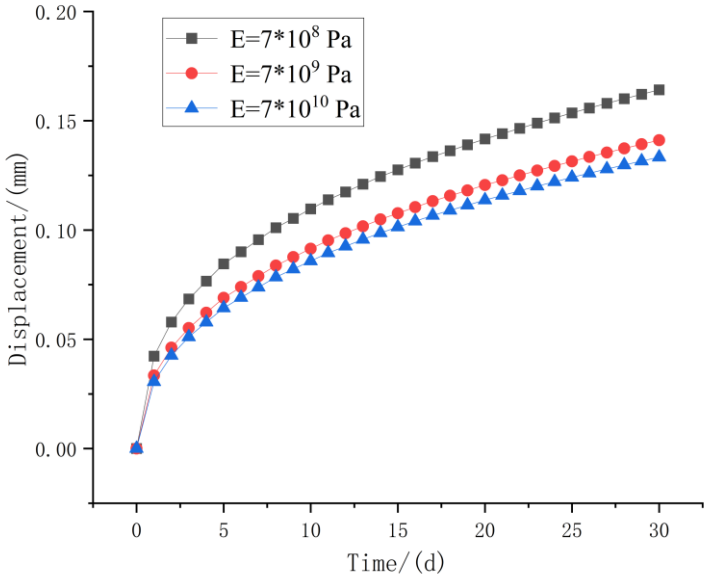

Figure 60. Pile axial displacement with time (energy pile head)

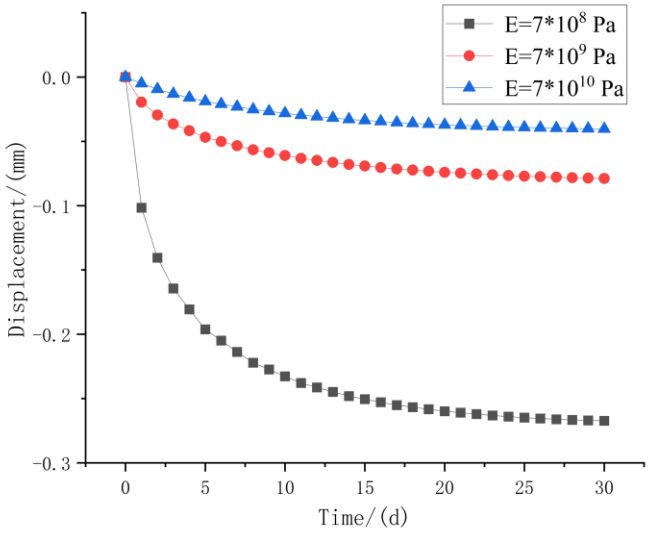

Figure 61. Pile axial displacement with time (energy pile bottom)

From the above graphs, it can be observed that as the elastic modulus of the mudstone layer increases, the constraint exerted by the mudstone on the pile increases, resulting in an increase in thermal stress within the pile. Consequently, the displacement values at the top ends of the pile decrease. When the elastic modulus of the mudstone increases from 7×10^{8} Pa to 7×10^{9} Pa, the

thermal stress at the location (7.5, 7.5, 13) at the end of heating increases from -594 kPa to -741 kPa. Meanwhile, the upward displacement at the pile top decreases from 0.16 mm to 0.14 mm, and the downward displacement at the pile bottom decreases from 0.26 mm to 0.07 mm.

6.8.3 Thermal Conductivity of Mudstone

From the analysis results in Chapter 5, it is evident that the greater the thermal conductivity of the soil, the higher its solid heat conduction efficiency, resulting in faster temperature changes. This, in turn, affects the mechanical response of both the pile and the soil. Therefore, this section investigates the influence of the thermal conductivity of mudstone on the axial deformation of the pile. Three values of thermal conductivity are selected: k=0.5 W/(m·K), 1.5 W/(m·K), and 2.0 W/(m·K). Monitoring points A (8,8,10) and B (8,8,27) are selected to monitor the temperature field changes near the bottom and top of the pile, respectively.

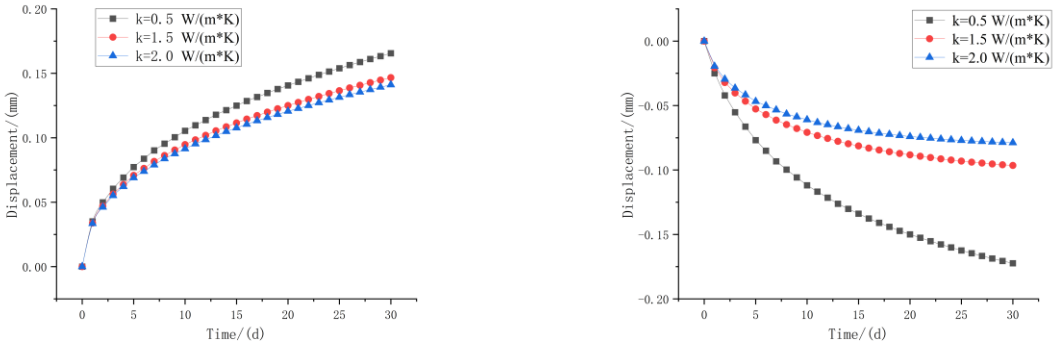

Energy pile head *Energy pile bottom*

Figure 62. Pile axial displacement with time

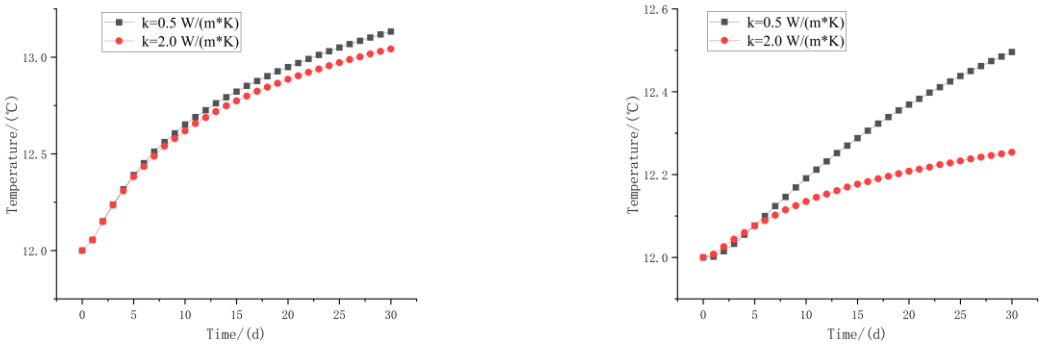

Energy pile head *Energy pile bottom*

Figure 63. Temperature at monitoring points A and B

The trend depicted in the above figure indicates that when the thermal conductivity of mudstone is higher, the efficiency of solid heat conduction increases. Consequently, the heating rate of the soil near the pile decreases, resulting in a reduction in the axial displacement of the pile caused by thermal expansion.

6.8.4 U-tube Flow Velocity

Similarly, as concluded from the analysis in Chapter 5, the flow velocity of the working fluid in the U-tube significantly affects the temperature distribution of the energy pile and the surrounding soil layer, thereby influencing their mechanical response. Therefore, in this section, three different flow velocities, set at v=0.5 m/s, 1.5 m/s, and 2.0 m/s, are selected for investigation.

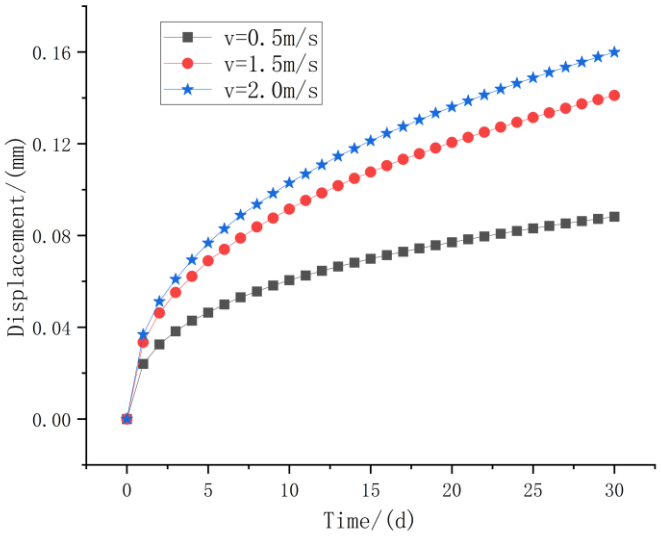

Figure 64. Pile axial displacement with time (energy pile head)

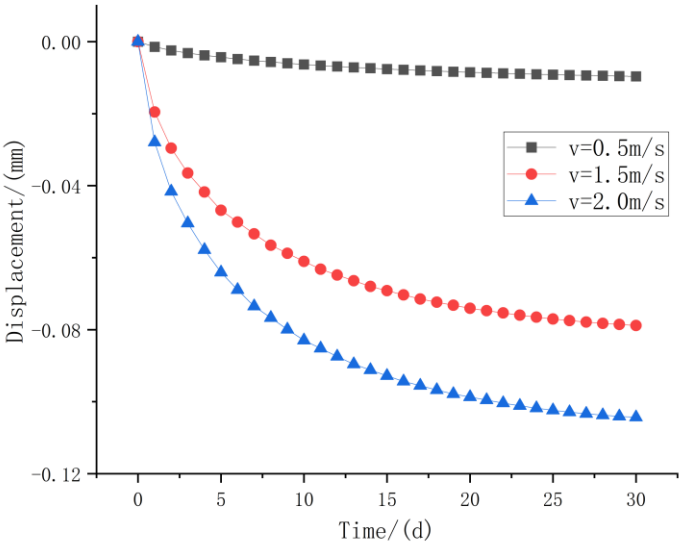

Figure 65. Pile axial displacement with time (energy pile bottom)

The above figure illustrates that at varying injection rates, the pile experiences deformation characterized by expansion and stretching towards both ends. Specifically, the upper section of the pile tends to rise relative to the mudstone layer, while the lower section tends to descend relative to the mudstone layer.

As the injection speed of the working fluid in the U-tube increases, the displacement of the pile towards both ends, either upward or downward, becomes greater. This is primarily because higher flow velocities can effectively enhance the heat exchange efficiency of the energy pile, resulting in a greater increase in pile-soil temperature, consequently leading to larger deformations under the influence of thermal stress.

6.9 Verification

In Chapter 5, the accuracy of TH model simulations was not specifically validated because the equations involved are Darcy's law and thermal equilibrium equations. The accuracy of these equations in the COMSOL Thermal and Flow simulation module is widely accepted, hence additional validation in this context is unnecessary.

Thermal-mechanical coupled models involve complex computations, necessitating validation to ensure the applicability of the assumptions and equations used in the simulations. This section aims to validate the accuracy of the thermal-mechanical model simulation results. The results obtained from the FEA model are compared with the experimental results conducted by Nguyen et al. (2017). Through this comparative analysis, the reliability of the model can be evaluated.

6.9.1 The Verification Model

The verification model comprises an energy pile and surrounding dry sand. The dry sand forms a cylindrical shape with a diameter of 548 mm and a height of 900 mm, while the energy pile is cylindrical with a diameter of 20 mm and a length of 600 mm. To reduce the number of mesh elements and improve computational efficiency, a symmetry model was employed for numerical calculations. Point A (0, 0, 900) was selected to monitor the displacement changes at the top of the energy pile. The calculations were performed using the solid mechanics and heat transfer modules

of COMSOL. A user-defined mesh was created, resulting in a total of 51,860 elements with an average element quality of 0.658.

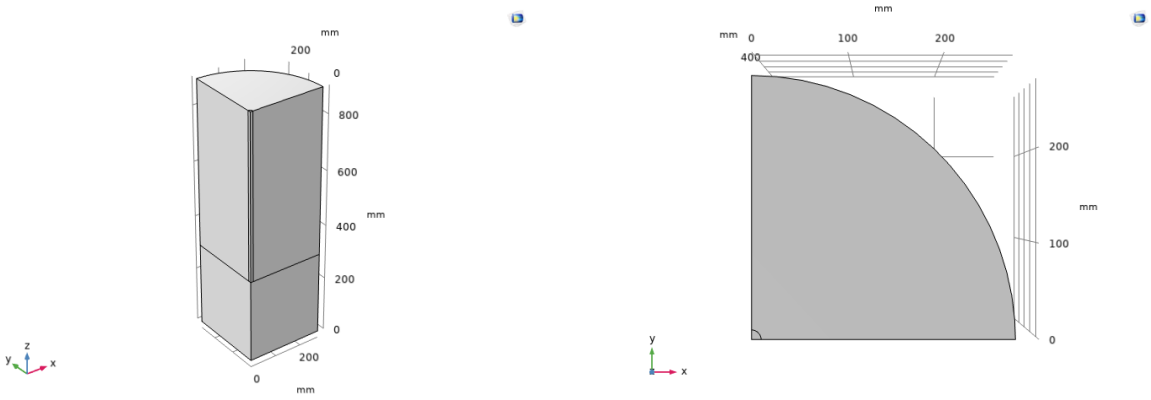

Figure 66. The verification model

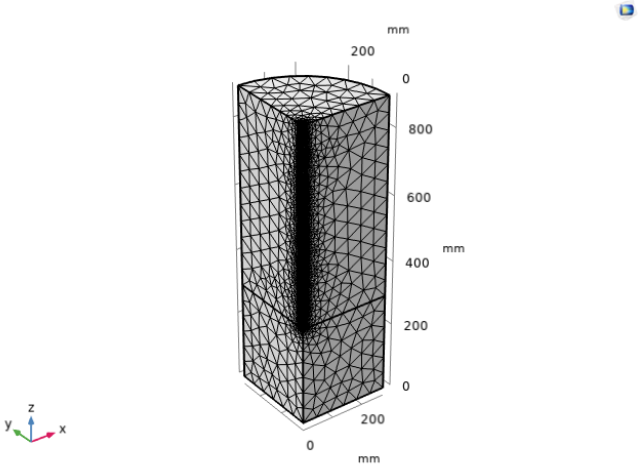

Figure 67. The verification model mesh

6.9.2 Parameters of Simulation

The parameters of the simulation are shown in the following Table 6.

Table 6. Input of the verification model

Parameters	Value
Sand density	1500 kg/m^3
Thermal conductivity of sand	1.90 W/(m·K)
The heat capacity of sand	500 J/(kg·K)
Permeability of sand	1×10^{-13} m^2
Porosity of sand	0.35
Coefficient of thermal expansion of sand	3×10^{-5} 1/K
Young's modulus of sand	3×10^{8} Pa
Poisson's ratio of sand	0.36
Pile density	2300 kg/m^3
Thermal conductivity of pile	1.8 W/(m·K)
Heat capacity of pile	880 J/(kg·K)
Coefficient of thermal expansion of pile	1×10^{-6} 1/K
Young's modulus of pile	2×10^{11} Pa
Poisson's ratio of pile	0.20
Initial temperature	20 ℃

6.9.3 Boundary Condition

(a) Heat transfer boundary

The initial temperature of the energy pile and dry sand is 20°C. The model is divided symmetrically, with the energy pile temperature varying over time as shown in Figure 59. The remaining boundaries are thermally insulated.

(b) Solid mechanics boundary

The pile and the bottom of the dry sand are fixed to fully restrict vertical and horizontal displacements. Roller conditions are set for the dry sand on all sides to limit horizontal displacement. A mechanical load of 100 N (20% of the pile resistance) is applied to the top of the

pile head.

In this section, a transient solver is employed for model validation, with a computation time step of 1 hour and a total of 14 hours of computation steps.

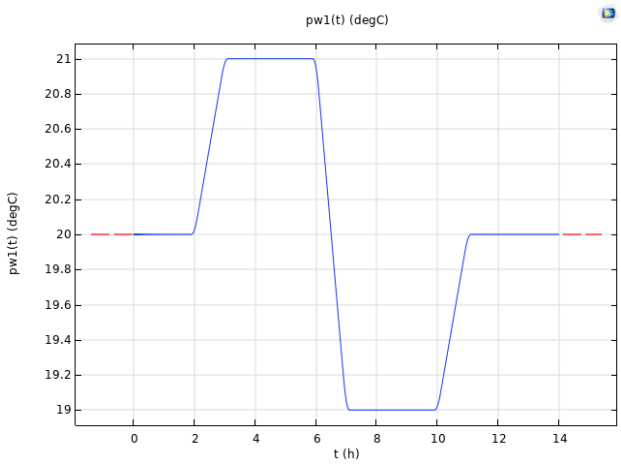

Figure 68. Input temperature of the verification model

6.9.4 Analysis of simulation results

The simulation results of the validation model are depicted in Figures 69 and 70. Figure 69 illustrates the temperature contour map and isothermal surfaces at 4 hours. Figure 70 shows the variation in pile head displacement over time.

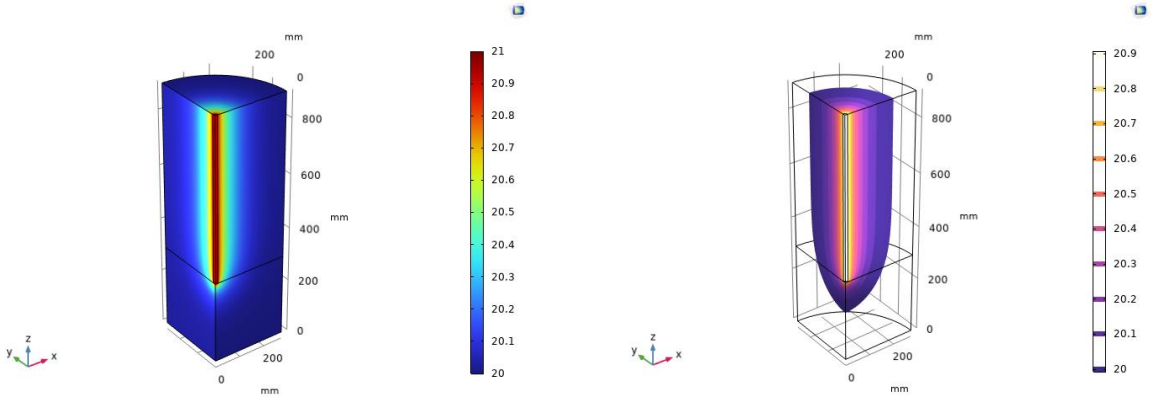

Figure 69. Temperature Field (4h) and Isothermal Surface (4h)

The temperature maps below depict the conditions of the dry sand and energy pile at the 4th hour.

The temperature of the energy pile stabilizes at 21°C, while the dry sand starts at 20°C. Thermal energy is transferred from the energy pile to the dry sand through solid conduction, as Figure 61 illustrates.

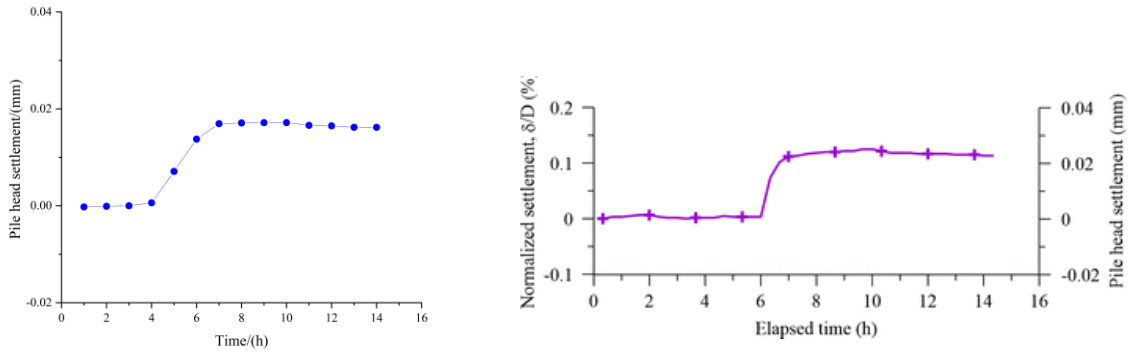

Figure 70. Numerical Simulation Results vs. Experimental Results (Nguyen et al., 2017)

From Figure 70, it is evident that as the temperature of the energy pile increases, there is an upward movement at the pile head, and subsequent short-term cooling has minimal impact on the displacement at the pile head. The numerical simulation conducted using COMSOL shows that the variation curve of pile head displacement over time closely matches the trends observed in experimental studies of long-term thermomechanical behaviour in dry sand. The displacement error is approximately 10%. This confirms the accuracy of the model, as validated against the findings of Nguyen et al. (2017).

6.10 Conclusion

This chapter utilized COMSOL to establish a three-dimensional numerical model to investigate the heat exchange of energy piles in soil layers, exploring the effects of thermal disturbances on the piles and soil during winter and summer conditions The focus was primarily on analysing the impacts of input parameters such as the thermal expansion coefficient of mudstone, the thermal conductivity of mudstone, and the injection rate of the working fluid on the mechanical response of the piles and surrounding media. The following conclusions were drawn from the analysis:

1. Under the thermal disturbance of the working fluid in the U-shaped pipe, energy piles undergo thermal expansion or contraction, resulting in additional displacement of the pile structure. In summer conditions, the pile undergoes significant tensile deformation along its axial direction when heated, with deformation gradually increasing towards both ends as the temperature rises. The upper portion of the pile tends to ascend relative to the soil, whereas the lower portion tends to descend. As the pile top represents a free boundary, it experiences the weakest constraint against expansion deformation, resulting in the largest displacement at that location. The middle portion of the energy pile is constrained in both upward and downward directions, resulting in smaller displacements with a zero point. Finally, a relatively large downward displacement is also observed at the pile base.
2. In the summer condition, the thermal expansion of the pile is constrained by the surrounding soil, resulting in compressive stress. When the soil's elastic modulus is greater, its constraint on the pile becomes more significant, leading to higher thermal stress on the pile and smaller displacements at the pile end. Additionally, the soil exerts additional tensile stress on the pile due to thermal expansion. As the ratio of thermal expansion coefficients between the soil and the pile increases, the resulting compressive stress decreases, leading to larger displacements at the pile end.
3. When the thermal conductivity of the mudstone layer is greater, the efficiency of solid heat conduction is higher, resulting in a slower heating rate of the soil near the pile, and consequently reducing the axial displacement of the pile caused by thermal expansion.
4. A faster injection rate of the working fluid in the U-shaped pipe leads to higher heat exchange efficiency of the energy pile. This results in a greater increase in pile and soil temperature, leading to larger deformations under the influence of thermal stress.

5. Compared to soils, mudstone layers exhibit characteristics such as low permeability, high elastic modulus, and low thermal expansion. Based on the conclusions drawn from the sensitivity analysis of parameters in this chapter, it is evident that under similar thermal disturbance conditions, energy piles in mudstone regions experience greater constraint and higher thermal stresses compared to shallow soil types like clay. Consequently, the displacement at the pile ends is smaller, which is more favorable for the structural safety of upper buildings.

7. 2D FEA THM Coupled Energy Piles Model

In Chapter 6, the reliability of the single-pile model has been verified. To enhance the efficiency of the analysis and broaden the range of applicable scenarios, this section simplifies the model from 3D to 2D and transitions to a more common group pile model. Given the substantial computational demand of THM (thermal-hydraulic-mechanical) coupled models, which require high-performance computing, this simplification aims to reduce computational load and processing time. The design details are derived from the conceptual model presented in Chapter 5 (Figure 13). The model will be developed in COMSOL software, as shown in Figure 71.

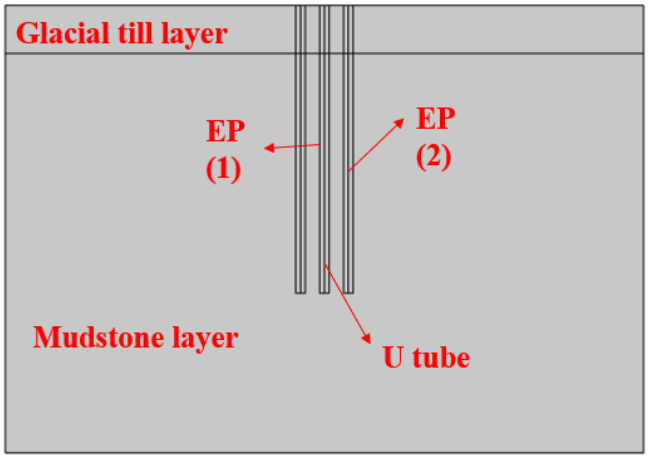

Figure 71. 2D thermal-hydro-mechanical coupling model

In this chapter, a 2D THM group pile model will be used to explore two different operational scenarios for energy piles, demonstrating the potential applications of this THM-coupled energy pile model during the construction design phase. These scenarios will help to understand the feasibility and applicability of the model in various engineering contexts, thus supporting the design of real engineering projects.

The objective of this research is to develop a specialized analysis model for the analysis of the thermomechanical behaviour of an energy pile conceptual model based on the ground conditions of the Woodsmith project area in the UK under mechanical and thermal loads. This numerical study aims to provide a reliable reference for the future application of energy piles in the construction practices of this region.

7.1 Numerical Model

This chapter establishes a transient finite element numerical model for 2D group piles to simulate the heat exchange process between energy piles (EP) and surrounding soils (glacial till and mudstone) over the course of a year (400 days), predicting the thermo-mechanical behavior of the group energy piles and surrounding soils. In this model, both the soil and concrete piles are treated as porous media for heat transfer, following Darcy's law. The U-shaped heat exchanger is simplified as a one-dimensional line source, and the heat flux is simplified as a temperature function dependent on time.

The model consists of the heat exchanger, concrete energy piles, and surrounding soil layers. The dimensions of the surrounding soil layer model are 40m × 28m, with the concrete energy piles having a diameter of 0.6m and a length of 18m. There are three energy piles in total, spaced at a center-to-center distance of 1.5m. The U-shaped heat exchanger is simplified as a one-dimensional line with a length consistent with the pile length of 18m.

7.2 Model Assumptions

Due to the THM coupling model in the 2D model, in addition to the assumptions in Chapters 5 and 6, the following assumptions should also be considered:

1. In this 2D model, the U-shaped heat exchanger and the internal heat transfer fluid are

simplified as a one-dimensional line, acting on the vertical section line of the energy pile, ignoring the thermal performance of the heat exchanger. Heat energy is mainly transferred in the normal direction.

2. Soils below the groundwater level are considered to be fully saturated biphasic materials (solid and water).
3. The pile is modeled as an isotropic thermoelastic porous material.
4. The fluid phase and soil particles are considered incompressible.

7.3 Governing Equation

The 2D model adopts the THM coupling equations. The governing equations involve the mechanical behavior of the solid skeleton, heat conduction, and convection between the energy piles and the soil, as well as hydraulic flow in the soil.

$$\text{M: } G\nabla^2\dot{\boldsymbol{d}} + \left(\frac{G}{1-2\theta}\right)\nabla\left(\nabla\cdot\dot{\boldsymbol{d}}\right) - \zeta\nabla\dot{p} - K\beta_T\nabla\dot{T} = 0 \quad (7.1)$$

$$\text{H: } \zeta\dot{\varepsilon}_{ii} + \nabla\cdot\boldsymbol{u} + \left(\frac{\phi}{K_f} + \frac{\zeta-\phi}{K_s}\right)\dot{p}^f + \left((\phi-\zeta)\alpha_s - \phi\alpha_f\right)\dot{T} = 0 \quad (7.2)$$

$$\text{T: } \left((1-\phi)\rho_s^s C^s T\right) + \left(\phi\rho_f^f C^f T\right) - \nabla\cdot(\lambda\nabla T) + \nabla\cdot C^f T\rho_f^f\boldsymbol{u} = 0 \quad (7.3)$$

Where α_s being the thermal expansion coefficient of the solid. $K_f = \frac{1}{\rho_f^f}\left(\frac{\partial\rho_f^f}{\partial p^f}\right)_T$ is the bulk modulus of the fluid.$\alpha_f = -\frac{1}{\rho_f^f}\left(\frac{\partial\rho_f^f}{\partial T}\right)_{p^f}$ is the thermal expansion coefficient of the fluid.ζ is biot coefficient.

7.4 Model Boundary

Solid mechanics boundary conditions: A structural load of 1000 kN is applied to the pile head. The top of the soil layer is considered a free boundary, while the bottom of the soil layer is fixed.

The lateral boundaries of the soil layer are set to roller conditions. The Darcy boundary: No flow conditions are applied at the left and right boundaries of the soil layer bottom, with the groundwater level set at the ground surface, and zero pore water pressure applied. Heat transfer in porous media boundary: The initial temperature of both the soil layer and the pile is set to 16.9°C. A temperature boundary is applied to the pile's internal line source, following a function of temperature variation over time (Adinolfi et al., 2018).

Two scenarios are modelled: Scenario 1 does not consider the heat exchanger and ignores daily variations. Scenario 2 considers the daily operation time of the energy pile, inputting temperature changes averaged over time instead of the heat exchanger's daily variations. The model boundaries are referenced from the study by Adinolfi et al. (2018) to compare the deformation trends of the model, ensuring consistency with the research model by Adinolfi et al. (2018), and serving as additional evidence for the reliability of the model presented in this chapter.

7.5 Model Input Parameters

The parameters of the simulation are shown in the following Table 8.

Table 7. Input parameters the of THM model.

Property	Value
Mudstone density	2200 kg/m^3
Mudstone thermal conductivity	2 W/(m·K)
Heat capacity of mudstone	500 J/(kg·K)
Mudstone permeability	1×10^{-14} m^2
Mudstone porosity	0.23
Mudstone coefficient of thermal expansion	1×10^{-5} 1/K
Young's modulus of mudstone	7×10^{9} Pa
Poisson's ratio of mudstone	0.33
Dynamic viscosity of mudstone	8.9×10^{-4} Pa·s

Compressibility of fluid of mudstone	4.5×10^{-10} 1/Pa
Top layer density	2200 kg/m^3
Top layer thermal conductivity	1.65 W/(m·K)
heat capacity of the top layer	1218.66 J/(kg·K)
Top layer permeability	1×10^{-13} m^2
Top layer porosity	0.2
Top layer coefficient of thermal expansion	3×10^{-5} 1/K
Young's modulus of the top layer	2.5×10^{8} Pa
Poisson's ratio of the top layer	0.33
Dynamic viscosity of the top layer	1.7×10^{-5} Pa·s
Compressibility of fluid of the top layer	4.5×10^{-10} 1/Pa
Concrete density	2300 kg/m^3
Thermal conductivity of concrete	1.8 W/(m·K)
Concrete heat capacity	880 J/(kg·K)
Concrete coefficient of thermal expansion	2.6×10^{-5} 1/K
Young's modulus of concrete	2×10^{10} Pa
Poisson's ratio of concrete	0.20
Dynamic viscosity of concrete	8.9×10^{-4} Pa·s
Initial temperature	16.9℃

The system evaluation indicators will focus on the following aspects:

- Energy Pile Stability Analysis: Taking into account the applied mechanical load and the increase in pile temperature, the deformation of the pile will be studied to assess the stability of the energy pile.
- Energy Efficiency Analysis: Modeling the process of extracting underground thermal energy by the energy pile aids in evaluating the thermal energy utilization potential of the energy pile in winter conditions.
- Pore Pressure and Darcy Velocity Analysis: This analysis helps in understanding how the

thermal conductivity and hydraulic properties of the surrounding soil respond to the temperature changes of the pile.

7.6 Scenario 1

Scenario 1: In this scenario, the most unfavourable operational condition is assumed, where the energy pile operates continuously for 24 hours each day, resulting in a constant daily temperature variation of the pile body within the same season. Therefore, this numerical simulation does not consider daily temperature changes. During the heat extraction phase, a temperature of 10°C is applied inside the pile's heat exchanger, while during the heat injection phase, a temperature of 28°C is applied. From day 0 to 41, no thermal load is applied, only mechanical load. Starting from day 41, the winter heat extraction phase begins, with the heat exchanger temperature set to 10°C, and this heat extraction state is maintained until day 181. After 181 days, the temperature is kept constant for one month, and then the heat injection phase begins, with the heat exchanger temperature raised to 28°C until day 364. For the next 35 days, the heat exchanger stops applying heat load for the recovery phase, which lasts until day 400.

7.6.1 Loading Schedule, Pile Head Displacement and Pile Temperature Variation.

To ensure structural stability, it is essential to monitor the soil deformation patterns around the energy piles, helping verify that the superstructure's deformation remains within the geotechnical design tolerances. Thus, Fig. 58 examines the displacement resulting from thermo-mechanical loading of energy piles (1) and (2) when the daily thermal load variation is ignored.

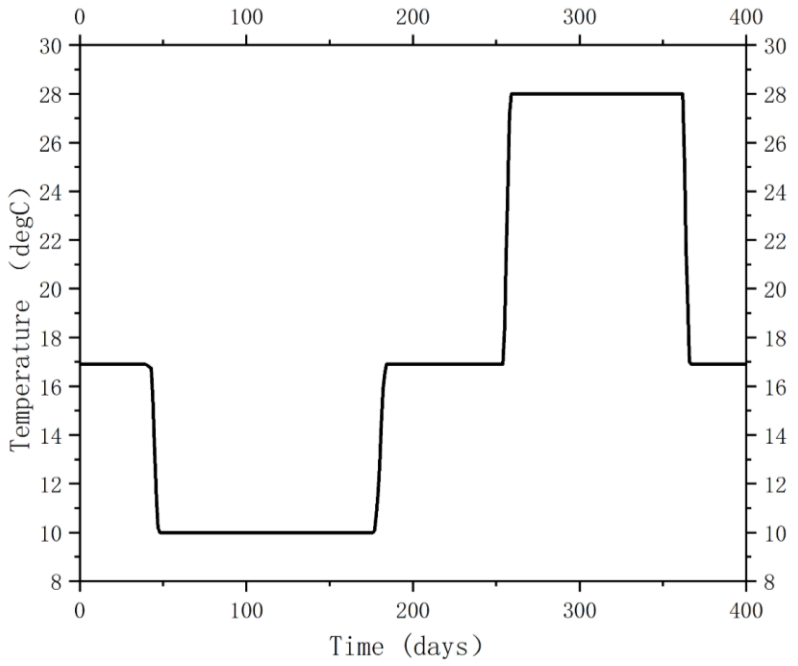

Figure 72. Energy pile heat exchanger long-term temperature input, ignoring daily variations

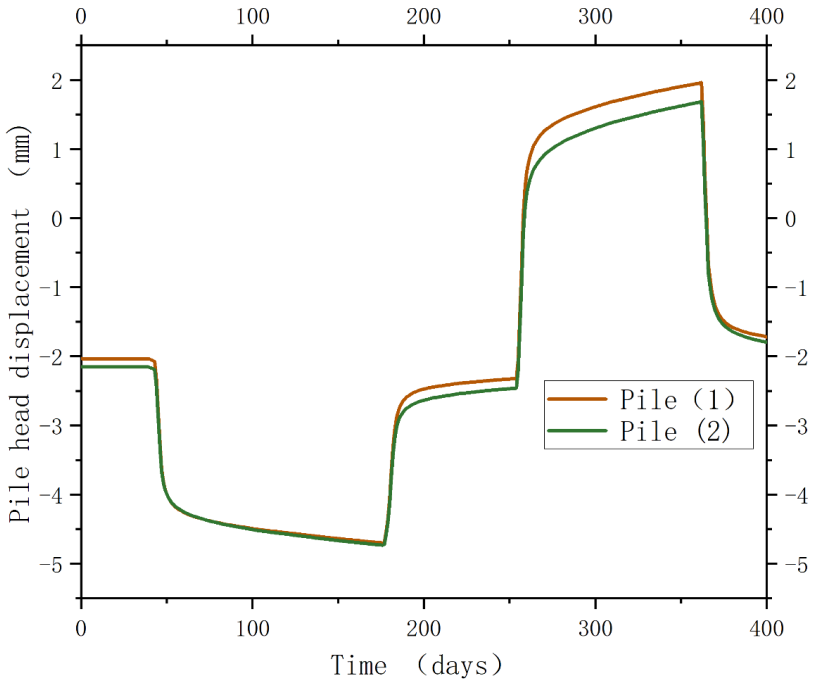

Figure 73. Energy Pile head settlement ignoring daily variations

Since scenario 1 piles neglect daily variations, the temperature experienced by the piles represents the highest and lowest temperatures, resulting in the highest upward and downward movement among the two situations. The mechanical load distribution at the pile head causes an initial settlement of -1.50mm. The variations in pile head displacement are attributed to temperature changes in the heating and cooling phases of the heat exchanger. During the heating phase, further settlement occurs, with pile (1) settling further from -1.50 mm to -4.19 mm and pile (2) further settling to -4.27 mm. In the cooling phase, as the heat exchanger temperature rises, the pile undergoes thermal expansion, causing the pile head to rise.

Compared to the initial settlement induced by mechanical loads of -1.50mm, the settlement of piles (1) and (2) rises to 2.62 mm and 2.23mm, respectively. Due to consolidation processes and plastic effects, after the recovery phase from day 365 to day 400, the residual vertical displacement of pile heads (1) and (2) is -0.18 mm and -0.22 mm, respectively. Compared to individual piles, the variation in settlement induced by the heating and cooling of pile groups depends on the position of the piles. The temperature of the central pile (1) during both the heating and cooling phases is slightly higher than that of the outer piles (2), resulting in a smaller contraction variation for pile (1) during the heating phase compared to the outer piles (2). Conversely, during the cooling phase, the expansion variation of the central pile (1) is greater than that of the outer piles (2)

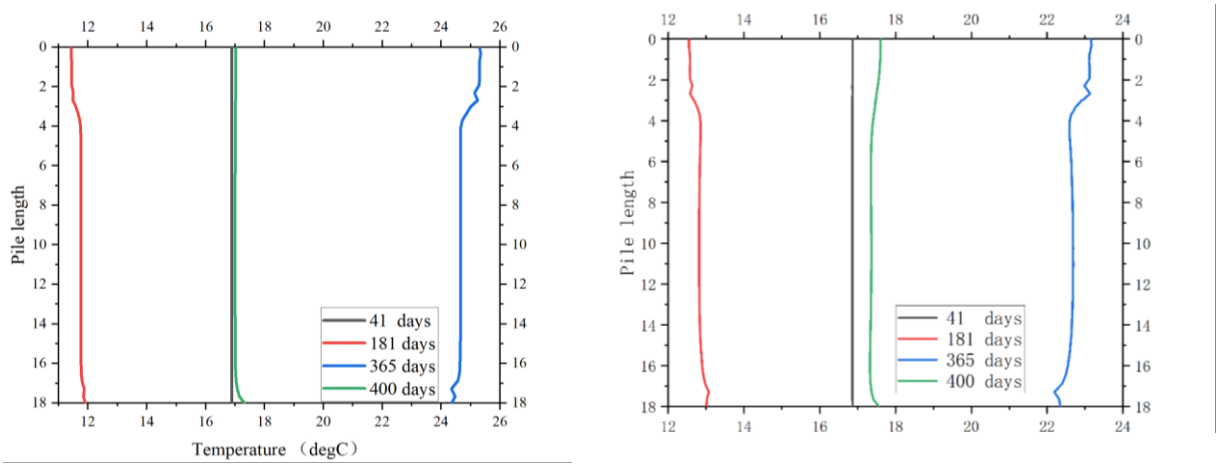

Figure 74. Temperature distribution of energy piles at different locations: left, energy pile (1); right, energy pile (2)

Figure 74 illustrates the temperature variation curves along the length of energy piles (1) and (2), covering different heating and cooling periods of 41 days, 181 days, 365 days, and 400 days. From the graph, it can be observed that the temperature trends of energy piles (1) and (2) are consistent. During the initial stage, when the heat exchangers are inactive, the soil-pile interface of energy piles (1) and (2) maintains a constant temperature. The subsequent heating phase results in a temperature drop from 16.9°C by 4.4°C to 12.5°C. At the end of the heating phase, temperatures increase from 8.6°C to 25.5°C compared to the initial stage**.** After 400 days, the temperature distribution at the pile-soil interface returns to its initial values. The temperature along the length of the piles is almost uniform, although temperature fluctuations occur at the interface between the mudstone and glacial till layers. It is noteworthy that the top temperature of the energy piles is slightly higher than the bottom temperature, likely due to the topsoil's lower thermal conductivity compared to the thermal conductivity of the mudstone region.

Furthermore, the average temperature at position (1) of the energy pile is higher than at position (2). This difference may be attributed to variations in the heat transfer capacity at different pile locations and may be caused by the collective heat transfer of the pile group. The central pile

exhibits lower heat transfer capacity, while the peripheral piles demonstrate higher heat transfer capability.

7.6.2 Vertical Displacements

This section focuses on the vertical displacements of energy piles during the heating and cooling phases, highlighting the impact of thermal expansion and contraction on pile movements. During the heating phase, thermal expansion causes the pile to move upwards, while during the cooling phase, the pile body moves downwards.

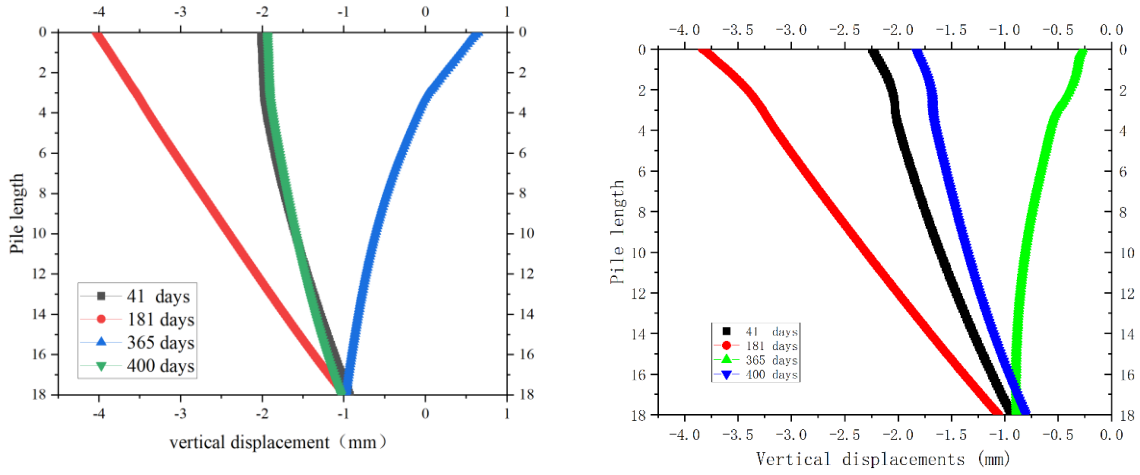

Figure 75. Vertical displacements(mm) at different operating temperatures: left pile (1); right pile (2)

Figure 75 illustrates the vertical displacement trend along the pile axis. During the cooling phase, the maximum deformation (downward displacement) at the pile head of pile (1) is -3.9 mm, compared to the initial maximum downward displacement of -2.1 mm, resulting in a change of -1.6 mm. During the heating phase, the maximum displacement (upward movement) at the pile head of pile (1) is 0.6 mm, compared to the initial -1.6 mm, resulting in a displacement change of 2.0 mm. During the cooling phase, the maximum settlement at the pile head of pile (2) is -3.9 mm, compared to the initial maximum downward displacement of -2.25 mm, resulting in a displacement change of -1.65 mm. During the heating phase, the maximum displacement (upward movement)

at the pile head of pile (2) is 0.4 mm, compared to the initial -2.25 mm, resulting in a displacement change of 2.65 mm.

The thermal expansion of the pile material during the heating process causes the pile head to move upwards, resulting in positive displacement. Conversely, during the cooling process, the contraction of the pile material leads to downward movement of the pile head, resulting in negative displacement. This cyclical displacement variation is closely related to the heating and cooling processes of energy piles, indicating the influence of temperature changes on pile displacement.

7.6.3 Pore Water Pressure and Temperature Profile

The impact of heat transfer on the surrounding soil needs to be considered because, when saturated soil is heated, the coefficient of thermal expansion of water is higher than that of the solid soil skeleton, which may lead to an increase in pore water pressure. Therefore, heating may result in a decrease in effective normal stress, while cooling may reduce pore water pressure and increase effective normal stress in the soil. Depending on the soil permeability and heating rate, excess pore water pressure can dissipate over a relatively short period of time.

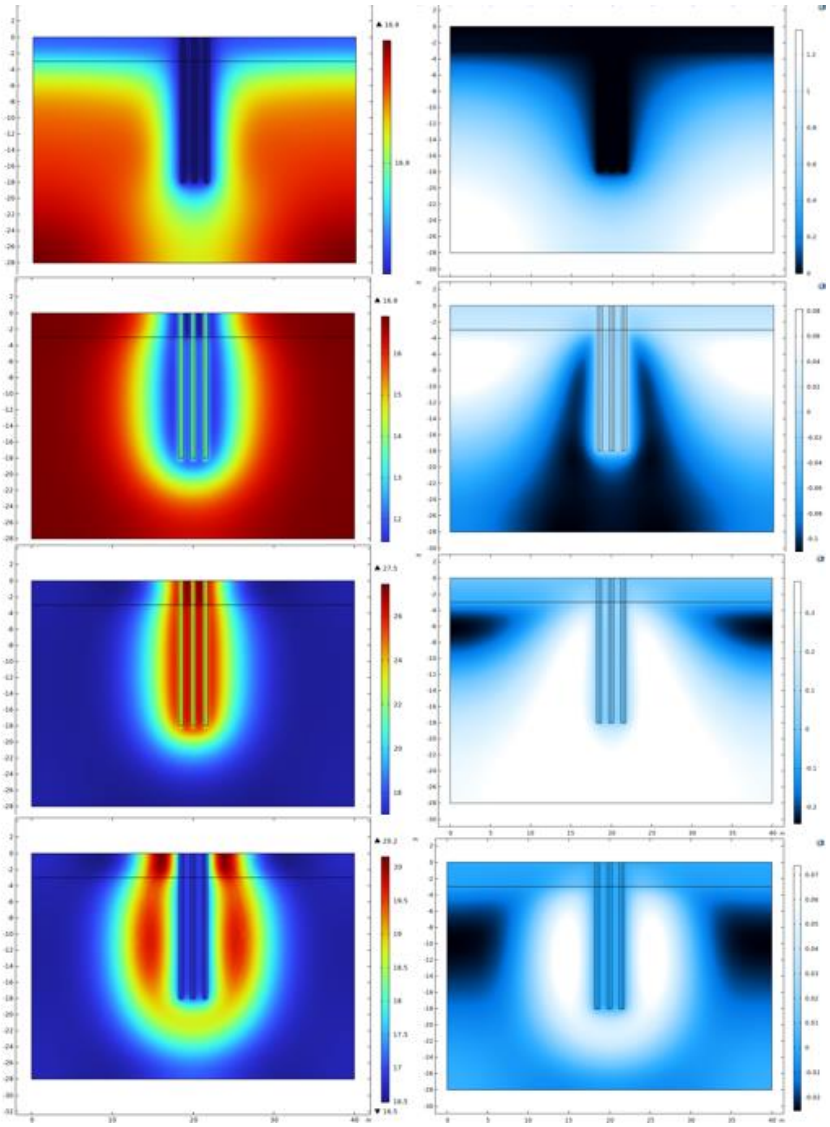

Figure 76. Temperature field and pore water pressure

Figure 76 illustrates the pore water pressure and temperature field. In scenario 1, during the initial period of 0-41 days, the system remains static, with pore water pressure dissipating around the pile to 0 Pa. As the cooling process progresses, the pore water pressure gradually decreases to -0.1 Pa by 181 days. During subsequent heating phases, the pore pressure further increases to 0.8 Pa by 365 days, then within the following 35 days, as the heat exchanger temperature drops from 28°C to the initial temperature of 16.9°C, there remains a residual 0.07 Pa yet to dissipate. Considering the relatively slow pore water dissipation due to the small permeability of the mudstone, it will

eventually dissipate over an elongated time step. Despite variations in pore water pressure values due to heat conduction and convection processes, these variations do not adversely affect the stability of the pile.

7.7 Scenario 2

Scenario 2: Similar to Scenario 1, Scenario 2 assumes that the pile maintains a constant daily temperature during the cooling and heating stages, with no cyclic thermal load variation due to changes in the temperature of the heat exchanger over time. However, the daily temperature variations in the thermal load are replaced by the weighted average temperature. During the winter heating stage, the pile's heat exchanger operates for 11 hours daily at 10°C. After weighted averaging, the daily average temperature is calculated as 14°C, aligning with Scenario 1's temperature change time points. In the summer heat injection stage, with the energy pile operating for 6 hours daily at 28°C, the weighted average calculation shows the heat exchanger's daily average operating temperature to be 20°C.

In this scenario, the daytime downtime of the energy pile is ignored, using only the weighted average daily temperature as the input function. This simplification deviates from actual operational conditions but greatly reduces the computational complexity associated with daily temperature cycles.

7.7.1 Loading Schedule, Pile Head Displacement, and Pile Temperature Variation.

This section focuses on the vertical displacements caused by the heating and cooling phases. Despite the smaller thermal load variation in Scenario 2 compared to Scenario 1, Figure 77 illustrates the displacements caused by thermal-mechanical loads on piles (1) and (2), using the

weighted average temperature instead of direct thermal load variations. This allows for monitoring deformation patterns in the surrounding ground layers around the energy pile.

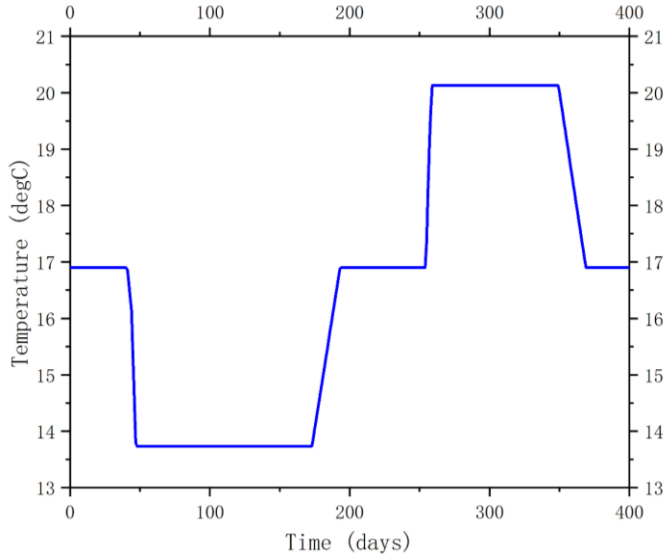

Figure 77. Energy pile heat exchanger long-term temperature input, ignoring daily variations

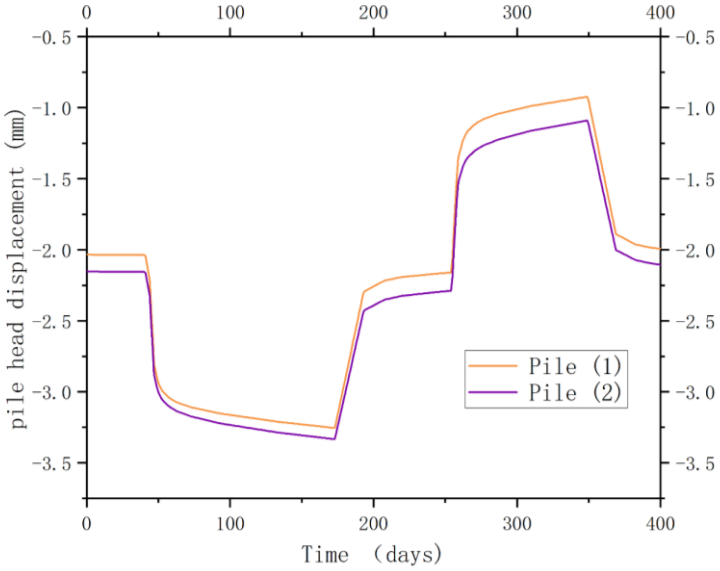

Figure 78. Energy Pile head settlement

In Scenario 2, the daily temperature variations of the piles are replaced by the weighted average temperature, resulting in temperatures experienced by the piles being lower than those in Scenario 1. Comparing the results of Scenarios 1 and 2 reveals similar response trends in both upward and

downward settlement variations at the pile heads in both scenarios. The mechanical loads distributed in the pile head area result in an initial settlement of -1.51 mm for the pile head (1). During the heat extraction phase, this leads to further settlement, increasing the settlement of pile (1) from -1.51 mm to -2.75 mm. During the heat injection phase, thermal expansion causes the pile head (1) to move upward to -0.36 mm.

The initial settlement of pile head (2) is -1.64 mm, which increases to -2.81 mm by the end of the heat extraction phase and then moves upward to -0.54 mm during the heat injection phase. The residual changes in vertical displacement for pile heads (1) and (2) are -0.03 mm and -0.04 mm, respectively. Both Scenarios 1 and 2 indicate that the settlement of the pile heads is influenced by temperature, with settlement changes following the trend of temperature variations. Moreover, due to the strength of the soil, the thermal-mechanical displacement changes are minimal and therefore do not adversely affect the safety of the structure.

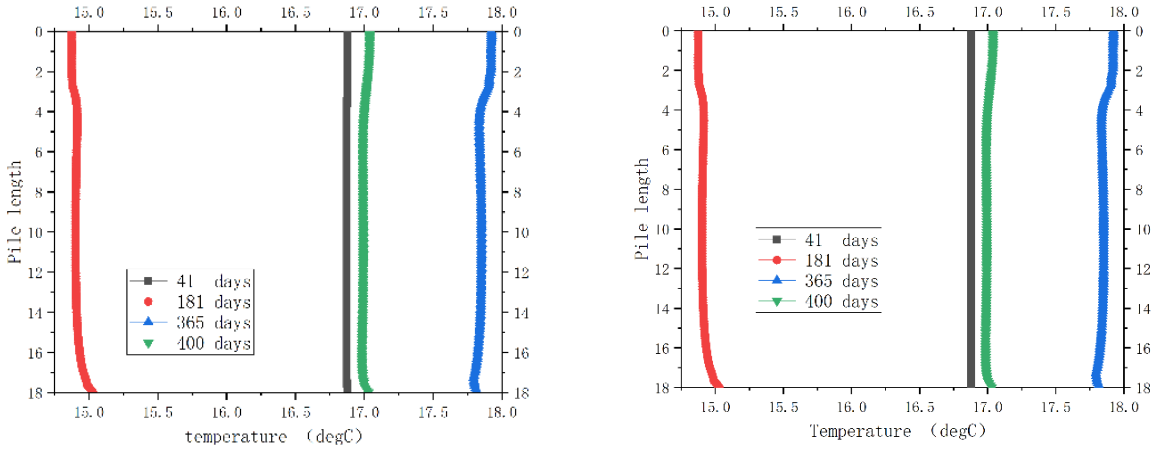

Figure 79. Temperature distribution of energy piles at different locations: left, energy pile (1); right, energy pile (2)

Figure 79 depicts the temperature variation along the length of energy piles (1) and (2) at different time points, after applying the weighted average temperature. From the graph, it can be observed that the temperature trends for energy piles (1) and (2) are consistent. The side piles exhibit the highest heat exchange capacity, with temperature variations during the heating phase being higher than those of the central piles. Initially, the temperature at the heat exchanger matches the ambient temperature, standing at 16.9°C. At the end of the heat extraction phase (181 days), the temperatures decrease to 14.8°C and 15°C, respectively. Conversely, at the end of the heat injection phase (365 days), the temperatures of piles (1) and (2) rise from their initial values to 17.65°C and 17.82°C. This indicates that side piles have higher heat exchange capacity, with temperature variations during the thermal expansion phase being higher than those of central piles. Additionally, comparing the temperature curves at 41 days and 400 days reveals temperature residuals of 0.02 and 0.2 at the pile-soil interfaces for piles (1) and (2), respectively. The temperature residual at the energy pile location (1) is lower than that at the peripheral pile (2), which is attributed to the presence of high-temperature zones between piles during group pile heating, causing temperature interference.

7.7.2 Vertical Displacement

Vertical displacement analysis in this section focuses on the thermal-mechanical behaviour of energy piles. Figure 80 illustrates the vertical displacements at different operational temperatures for pile (1) and pile (2).

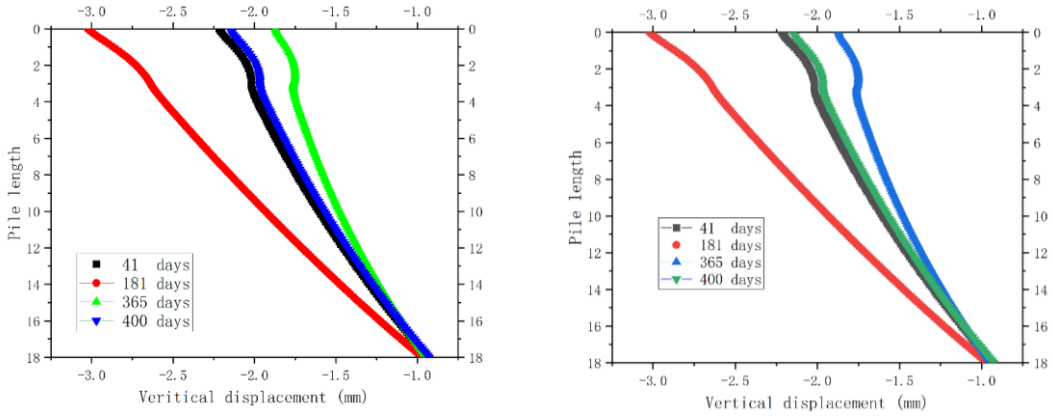

Figure 80. Vertical displacements(mm) at different operating temperatures: left pile (1); right pile (2)

As a result of thermal expansion and contraction, the pile ascends during the heating phase and descends during the cooling phase. At the initial stage, the downward displacement of the pile heads is -2.10 mm and -2.20 mm, respectively. During the cooling phase, the downward displacement at both pile heads (1) and (2) is -2.82 mm and -3.10 mm, respectively. Compared to the initial displacement, this results in changes of -0.72 mm and 0.90 mm, respectively. During the heating phase, the upward displacement of pile heads (1) and (2) is -1.60 mm and -1.79 mm, respectively. The changes in upward displacement (ΔS) at pile heads (1) and (2) are 0.50 mm and 0.41 mm, respectively. The displacement pattern for Scheme 2 is similar to Scenario 1 but with noticeably smaller changes.

7.7.3 Pore Water Pressure and Temperature Profile

Figure 81 depicts the pore water pressure and temperature field at various time points in Scenario 2. During the initial 0-41 days in this mode, the system remains static, with the pore water pressure around the pile at 0 Pa. From day 41 to 181, following the winter heat extraction phase, the pore water pressure around the pile gradually decreases to -0.12 Pa.

After the summer heat injection phase concludes (365 days), the pore water pressure rises to 0.04 Pa due to temperature effects and subsequently decreases to nearly zero residual pore water

pressure ($16x10^{-3}$ Pa) over the next 35 days as the heat exchanger temperature drops from 28°C to its initial temperature of 16.9°C. Compared to other scenarios, heating saturated soil can result in excessively high pore water pressures, whereas cooling reduces pore water pressure. Across all scenarios, the variations in pore water pressure are negligible (less than 10 Pa), indicating that thermal conduction and convection processes have no significant impact on the safety of the structure.

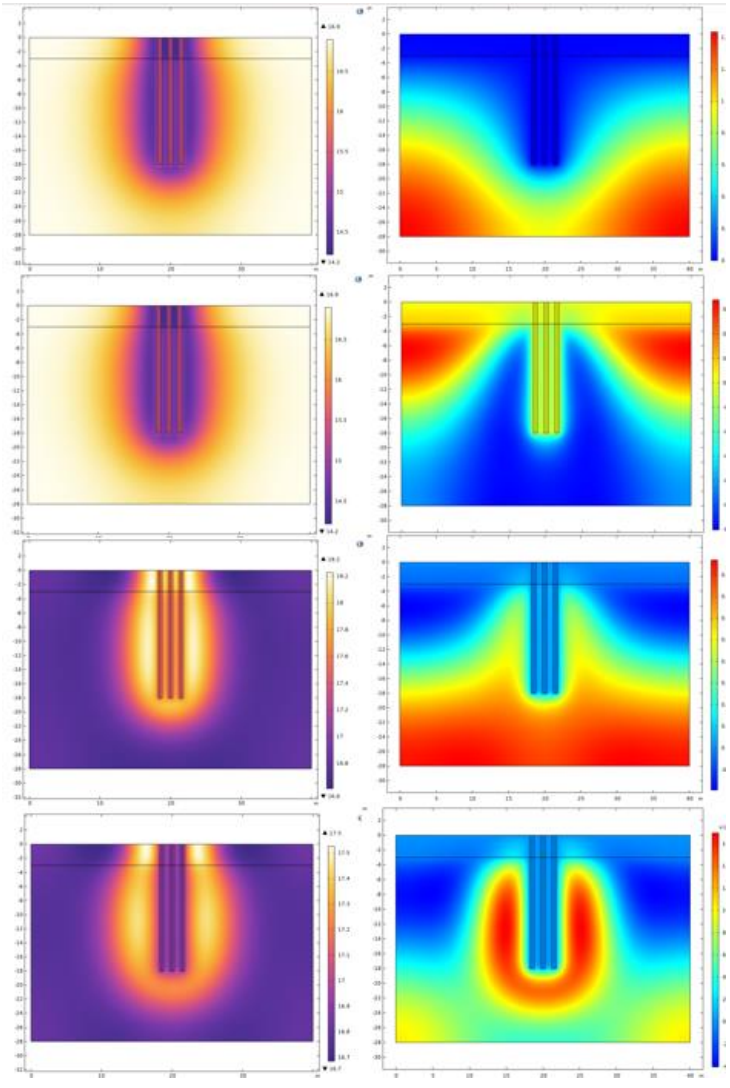

Figure 81. Temperature field and pore water pressure

7.8 Conclusion

In Chapters 5 and 6, the thermal-hydro and thermal-mechanical simulation results of energy piles were investigated. Chapter 7 comprehensively considers the thermal-hydro-mechanical coupling of energy piles. To reduce the number of model calculations and improve analysis efficiency, the THM coupling model is developed as a 2D model, primarily focusing on the group pile model to ensure broader applicability. The following conclusions can be drawn from the application of two different cases:

1. Scenario 1 disregards the temperature fluctuations during the daily operation of the energy pile, considering only the maximum and minimum operating temperatures. According to this condition, it is determined that the head of the energy pile will move upward during the heating phase and downward during the cooling phase, with a displacement of approximately 2 mm. The change in pore water pressure caused by the temperature field variation will eventually dissipate over time.
2. A comparison of the two scenarios indicates that thermal-induced displacements, stresses, and pore water pressures may be overestimated if the daily working time of the energy piles is not considered. Therefore, Scenario 1 calculations can be chosen for the conservative design, while Scenario 2 can be selected for simulations requiring accuracy.
3. The variations associated with thermal cycling in both scenarios fall within safe limits and do not pose a risk to structural stability. Therefore, energy piles can be applied in the mudstone stratigraphic environment where the model is situated.

8 Conclusion and Future Expectations

This study employed numerical simulation to investigate the operational efficiency and deformation of energy piles installed in mudstone areas. Three different coupled models of energy piles were established using the finite element software COMSOL to meet the research requirements. The 3D TH coupled model was numerically simulated to analyse the temperature changes of the energy piles and surrounding soil, as well as the effects of parameters such as working fluid temperature and flow rate on the heat transfer performance of energy piles and the seepage situation of the surrounding soil. Subsequently, the 3D TM coupled model was constructed to analyse the effects of thermal parameters of energy piles and surrounding soil on the thermal-hydraulic coupling effect of energy piles. Finally, the 2D THM-coupled simplified model was utilized to simulate the working conditions of energy piles over 400 days and evaluate the long-term performance of energy piles through simulation results. The following conclusions were drawn:

1. Under the thermal disturbance of the working fluid in the U-shaped pipe, the energy pile undergoes thermal expansion or contraction, resulting in additional displacement of the pile structure. In summer conditions, the heated pile exhibits significant tensile deformation, with the upper part tending to move upward and the lower part downward. The greater the soil's elastic modulus, the stronger the constraint on the pile, leading to smaller displacements at the pile ends.
2. Larger thermal conductivity of energy piles and soil corresponds to higher solid heat conduction efficiency, slower temperature attenuation at the outlet of heat exchange pipes, and higher efficiency in extracting thermal energy. Additionally, the heating rate of the soil near the pile decreases, thereby reducing the axial displacement of the pile caused by

thermal expansion.

3. A faster flow rate of the working fluid inside the U-shaped pipe results in a higher heat extraction rate for energy piles. This leads to a greater increase in pile-soil temperature, resulting in larger deformations under thermal stress.
4. Convection of pore water in the soil, driven by density differences, occurs at a flow rate of approximately 10^{-12} m/s. The influence of different clay permeabilities on the heat transfer process of energy piles is relatively minor.
5. In the long-term operation of energy piles, the temperature variation function of the heat exchanger will affect the prediction of pile displacements and soil pore water pressure. Therefore, during the design phase of energy piles, it is essential to account for the working duration of the energy piles. Selecting an appropriate temperature variation function based on the specific working hours of the energy piles ensures that the model analysis accurately reflects the deformations and pore water pressures, preventing underestimation.
6. Compared to soils, mudstone layers exhibit characteristics such as low permeability, high elastic modulus, and low thermal expansion. Based on the conclusions drawn from the sensitivity analysis of parameters in this chapter, it is evident that under similar thermal disturbance conditions, energy piles in mudstone regions experience greater constraint and higher thermal stresses compared to shallow soil types like clay. Consequently, the displacement at the pile ends is smaller, which is more favorable for the structural safety of upper buildings.

The THM coupling analysis of energy piles in mudstone areas is a challenging research topic with significant engineering implications. It involves solving multiple coupled physical fields, including temperature, seepage, and mechanics. In the process of numerical simulation, the numerical model was necessarily simplified, and some minor factors were disregarded. Therefore, future research can further refine the results by addressing the following aspects:

1. The current study employs a linear elastic model for the surrendering media, which does not account for the nonlinear, strain-hardening, elastoplastic, and dilatant mechanical characteristics of the soil under stress. To extend the applicability of the model, future research should upgrade the constitutive model to an elastoplastic model, considering the plastic deformation of mudstone.
2. This study does not consider the frictional contact between the energy pile and the surrendering media, thus failing to examine the impact of pile-soil friction on the stress and strain of the energy pile. Future research should focus on this aspect to provide a more comprehensive understanding.
3. The 2D model used in this study cannot accurately represent the complex stress-strain and pore water pressure dynamics within the energy pile and surrendering media under thermal disturbance. Therefore, future research should involve 3D THM coupling analysis to capture these intricate phenomena more realistically.

Reference

ADINOLFI, M., MAIORANO, R. M. S., MAURO, A., MASSAROTTI, N. & AVERSA, S. 2018. On the influence of thermal cycles on the yearly performance of an energy pile. *Geomechanics for Energy and the Environment,* 16**,** 32-44.

AGAR, R. 1954. GLACIAL AND POST-GLACIAL GEOLOGY OF MIDDLESBROUGH AND THE TEES ESTUARY. *Proceedings of the Yorkshire Geological Society,* 29**,** 237-253.

AMATYA, B. L., SOGA, K., BOURNE-WEBB, P. J., AMIS, T. & LALOUI, L. 2012. Thermo-mechanical behaviour of energy piles. *Géotechnique,* 62**,** 503-519.

ARZANFUDI, M. M., AL-KHOURY, R., SLUYS, L. J. & SCHREPPERS, G. M. A. 2020. A thermo-hydro-mechanical model for energy piles under cyclic thermal loading. *Computers and Geotechnics,* 125**,** 103560.

BOON, D. P., FARR, G. J. & HOUGH, E. 2021. Thermal properties of Triassic Sherwood (Bunter) Sandstone Group and Mercia Mudstone Group (Keuper Marl) lithologies. 2021**,** 1-5.

BOURNE-WEBB, P. J., AMATYA, B., SOGA, K., AMIS, T., DAVIDSON, C. & PAYNE, P. 2009. Energy pile test at Lambeth College, London: geotechnical and thermodynamic aspects of pile response to heat cycles. *Géotechnique,* 59**,** 237-248.

BOURNE-WEBB, P. J., FREITAS, T. M. B. & ASSUNçãO, R. M. F. 2016. Soil–pile thermal interactions in energy foundations. *Géotechnique,* 66**,** 167-171.

BOZIS, D., PAPAKOSTAS, K. & KYRIAKIS, N. 2011. On the evaluation of design parameters effects on the heat transfer efficiency of energy piles. *Energy and Buildings,* 43**,** 1020-1029.

BRANDL, H. 2006. Energy foundations and other thermo-active ground structures. *Géotechnique,* 56**,** 81-122.

CAROTENUTO, A., MAROTTA, P., MASSAROTTI, N., MAURO, A. & NORMINO, G. 2017. Energy piles for ground source heat pump applications: Comparison of heat transfer performance for different design and operating parameters. *Applied Thermal Engineering,* 124**,** 1492-1504.

CECINATO, F. & LOVERIDGE, F. A. 2015. Influences on the thermal efficiency of energy piles. *Energy,* 82**,** 1021-1033.

CHEN, Z., YAO, J., PAN, P., XIAO, H. & MA, Q. 2021. Research on the heat exchange characteristics of the deeply buried pipe type of energy pile. *Case Studies in Thermal Engineering,* 27**,** 101268.

CLARKE, B. G. 2018. The engineering properties of glacial tills. *Geotechnical Research,* 5**,** 262-277.

CUI, P., JIA, L., ZHOU, X., YANG, W. & ZHANG, W. 2020. Heat transfer analysis of energy piles with parallel U-Tubes. *Renewable Energy,* 161**,** 1046-1058.

DING, X., PENG, C., WANG, C. & KONG, G. 2022. Heat transfer performance of energy piles in seasonally frozen soil areas. *Renewable Energy,* 190**,** 903-918.

FADEJEV, J., SIMSON, R., KURNITSKI, J. & HAGHIGHAT, F. 2017. A review on energy piles design, sizing and modelling. *Energy,* 122.

GAO, J., ZHANG, X., LIU, J., LI, K. & YANG, J. 2008. Numerical and experimental assessment of thermal performance of vertical energy piles: An application. *Applied Energy,* 85**,** 901-910.

GSCHNITZER, E., WENGER, J. & RAINE, A. 2020. Woodsmith project – Construction of a 37 km long mineral transport system for the world's largest Polyhalite resource. *Geomechanics and Tunnelling,* 13**,** 643-649.

GUTIERREZ, M. & MAKURAT, A. 1997. Coupled HTM modelling of cold water injection in fractured hydrocarbon reservoirs. *International Journal of Rock Mechanics and Mining Sciences,* 34**,** 113.e1-113.e15.

HASSANI NEZHAD GASHTI, E., MALASKA, M. & KUJALA, K. 2014. Evaluation of thermo-mechanical behaviour of composite energy piles during heating/cooling operations. *Engineering Structures,* 75**,** 363-373.

HOBBS, P. R. N., HALLAM, J. R., FORSTER, A., ENTWISLE, D., JONES, L., CRIPPS, A. C., NORTHMORE, K. J., SELF, S. & MEAKIN, J. L. Engineering geology of British rocks and soils : mudstones of the Mercia Mudstone Group. 2002.

HOUBEN, M. E., VAN EEDEN, J. C. M., BARNHOORN, A. & HANGX, S. J. T. 2020. Fracture-Induced Permeability in Whitby Mudstone. *Environmental Science & Technology,* 54**,** 9564-9572.

LALOUI, L., NUTH, M. & VULLIET, L. 2006. Experimental and numerical investigations of the behaviour of a heat exchanger pile. *International Journal for Numerical and Analytical Methods in Geomechanics,* 30**,** 763-781.

LI, G.-C., QI, C.-C., SUN, Y.-T., TANG, X.-L. & HOU, B.-Q. 2017. Experimental Study on the Softening Characteristics of Sandstone and Mudstone in Relation to Moisture Content. *Shock and Vibration,* 2017**,** 4010376.

LIU, B., YANG, H. & KAREKAL, S. 2020. Effect of Water Content on Argillization of Mudstone During the Tunnelling process. *Rock Mechanics and Rock Engineering,* 53**,** 799-813.

LIU, C.-D., CHENG, Y., JIAO, Y.-Y., ZHANG, G.-H., ZHANG, W.-S., OU, G.-Z. & TAN, F. 2021. Experimental study on the effect of water on mechanical properties of swelling mudstone. *Engineering Geology,* 295**,** 106448.

LOVERIDGE, F. & POWRIE, W. 2013. Pile heat exchangers: thermal behaviour and interactions. *Proceedings of the Institution of Civil Engineers - Geotechnical Engineering,* 166**,** 178-196.

LUO, J., ZHAO, H., GUI, S., XIANG, W., ROHN, J. & BLUM, P. 2016. Thermo-economic analysis of four different types of ground heat exchangers in energy piles. *Applied Thermal Engineering,* 108**,** 11-19.

MAN, Y., QU, Y., WANG, Z. & FANG, Z. 2017. Design and analytical analysis of foundation pile ground heat exchanger with spiral coils.

MOHAMAD, Z., FARDOUN, F. & MEFTAH, F. 2021. A review on energy piles design, evaluation, and optimization. *Journal of Cleaner Production,* 292**,** 125802.

NEW, B. M. & BOWERS, K. H. 1994. Ground movement model validation at the Heathrow Express trial tunnel. *In:* ARTHUR, L. J., DARBY, A. W., RAFONEKE, B., DAWS, G., MACDONALD, D., INNAURATO, N., MANCINI, R., RONDENA, E., ZANINETTI, A., COUTTS, A. W. P., DAVIES, H. R., CURTIS, R. S., FINCH, A. P., LOVAT, R. P., DEANE, A. P., BURGESS, K. T., KNIGHTS, M. C., OSWELL, M. A., FARMER, I. W., MAK, B. W. L., MORFELDT, D., MARTIN, C. J. H., PAKES, G., FINNSSON, S., JANZON, H. A., LAUGHTON, C., NELSON, P. P., ABD AL-JALIL, Y.,

REMINGTON, R., CASPE, H. P., KIM, A. Y., BERGEN, L. J., ARAUJO, J. R., HARPF, R., AXHAUSEN, K., HELLINGS, J. E., MAIR, R. J., HARRIS, D. I., LOVE, J. P., BLAKEY, D., KETTLE, C., NEW, B. M., BOWERS, K. H., AARVOLD, V., CHUDLEIGH, I. L. J., WEBB, N. S., FEATHERSTONE, G. A., BANDMANN, M., RAMISCH, H., BECKMANN, U., COLE, B. J., LEES, H. J., DIETZ, W., FAWCETT, D. F., REMINGTON, R., CHAPMAN, P. J., BARRATT, D. A., O'REILLY, M. P., TEMPORAL, J., BASTON-PITT, J., FREDRIKSEN, F. J., AABøE, R., HASLE, G. J., HOBSON, D. A., GILCHRIST, D. C., JANCSECZ, S., STEINER, W., FARROW, J. P., CLAYE, P. M., WARREN, R. B., GINARY, M. A., MATTHEWS, R., KRUIZENGA, H., WEEKS, C. R., WINTERTON, T. R., LEBLAIS, Y., LEBLOND, L., MALIOS, Y., PERON, J. Y., MARCHESELLI, P., CATLING, P., SCHOLEY, J., MURRAY, A. D., MARRAI, B., DAVIES, P. G., TIBAU, G., GUTENWIK, E., SANTANA, M., PELLEGRI, P. J., FOWELL, R. J., RICHARDSON, G., GOLLICK, M. J., BEATTY, J. G., GANEY, R. J. & KILLINGSWORTH, J. E. (eds.) *Tunnelling '94: Papers presented at the seventh international symposium, 'Tunnelling'94'.* Boston, MA: Springer US.

NGUYEN, V. T., TANG, A. M. & PEREIRA, J.-M. 2017. Long-term thermo-mechanical behavior of energy pile in dry sand. *Acta Geotechnica,* 12**,** 729-737.

NIELD, D. A. & BEJAN, A. 2006. *Convection in porous media,* Springer.

OLGUN, G., OZUDOGRU, T., ABDELAZIZ, S. & SENOL, A. 2015. Long-term performance of heat exchanger piles. *Acta Geotechnica,* 10**,** 553-569.

PARK, S., LEE, D., LEE, S., CHAUCHOIS, A. & CHOI, H. 2017. Experimental and numerical analysis on thermal performance of large-diameter cast-in-place energy pile constructed in soft ground. *Energy,* 118**,** 297-311.

PARKES, D., BUSBY, J., KEMP, S. J., PETITCLERC, E. & MOUNTENEY, I. 2021. The thermal properties of the Mercia Mudstone Group. *Quarterly Journal of Engineering Geology and Hydrogeology,* 54**,** qjegh2020-098.

REES, S. J. 2016. 1 - An introduction to ground-source heat pump technology. *In:* REES, S. J. (ed.) *Advances in Ground-Source Heat Pump Systems.* Woodhead Publishing.

REITER, M. B., JELLO, J. & BASER, T. 2023. Thermo-hydro-mechanical behavior of energy foundations in saturated glacial tills. *Geothermics,* 108**,** 102614.

SADEGHI, H. & SINGH, R. M. 2023. Driven precast concrete geothermal energy piles: Current state of knowledge. *Building and Environment,* 228**,** 109790.

SANI, A. K., SINGH, R. M., AMIS, T. & CAVARRETTA, I. 2019. A review on the performance of geothermal energy pile foundation, its design process and applications. *Renewable and Sustainable Energy Reviews,* 106**,** 54-78.

SLATER, S. M., WELLMAN, C. H., ROMANO, M. & VAJDA, V. 2018. Dinosaur-plant interactions within a Middle Jurassic ecosystem—palynology of the Burniston Bay dinosaur footprint locality, Yorkshire, UK. *Palaeobiodiversity and Palaeoenvironments,* 98**,** 139-151.

SUMBLER, M. G., MORIGI, A. N. & BARRON, A. J. M. 2000. *Geology of the Cirencester district,* London, Stationery Office.

TIMMEN, C., BROWN, L., HEAP, M. & HORNUNG, A. 2023. Depositional environment and aquifer properties of the Sherwood Sandstone Group in the Cleveland Basin based on investigations at Woodsmith Mine. *Quarterly Journal of Engineering Geology and Hydrogeology,* 56**,** qjegh2022-041.

TINSLEY, J. & PAVíA, S. 2019. Thermal performance and fitness of glacial till for rammed earth construction. *Journal of Building Engineering,* 24**,** 100727.

TORTIKE, W. S. & ALI, S. M. F. 1993. Reservoir Simulation Integrated with Geomechanics. *Journal of Canadian Petroleum Technology,* 32.

VAZIRI, H. H. 1988. Coupled Fluid Flow And Stress Analysis Of Oil Sands Subject To Heating. *Journal of Canadian Petroleum Technology,* 27.

WANG, K., ZHOU, J., MA, Y., DING, A. & CHEN, X. 2023. Constitutive and numerical modeling for the coupled thermal-hydro-mechanical processes in dual-porosity geothermal reservoir. *Applied Thermal Engineering,* 223**,** 120027.

YANG, S.-Q., TIAN, W.-L., JING, H.-W., HUANG, Y.-H., YANG, X.-X. & MENG, B. 2019. Deformation and Damage Failure Behavior of Mudstone Specimens Under Single-Stage and Multi-stage Triaxial Compression. *Rock Mechanics and Rock Engineering,* 52**,** 673-689.

YANG, Y. & APLIN, A. C. 2010. A permeability–porosity relationship for mudstones. *Marine and Petroleum Geology,* 27**,** 1692-1697.

YOON, S., LEE, S.-R., XUE, J., ZOSSEDER, K., GO, G.-H. & PARK, H. 2015. Evaluation of the thermal efficiency and a cost analysis of different types of ground heat exchangers in energy piles. *Energy Conversion and Management,* 105**,** 393-402.

ZHANG, C. L., WIECZOREK, K. & XIE, M. L. 2010. Swelling experiments on mudstones. *Journal of Rock Mechanics and Geotechnical Engineering,* 2**,** 44-51.

ZHANG, W., CUI, P., LIU, J. & LIU, X. 2017. Study on heat transfer experiments and mathematical models of the energy pile of building. *Energy and Buildings,* 152**,** 643-652.

ZHANG, W., YANG, H., CUI, P., LU, L., DIAO, N. & FANG, Z. 2015. Study on spiral source models revealing groundwater transfusion effects on pile foundation ground heat exchangers. *International Journal of Heat and Mass Transfer,* 84**,** 119-129.

ZHAO, Q., LIU, F., LIU, C., TIAN, M. & CHEN, B. 2017. Influence of spiral pitch on the thermal behaviors of energy piles with spiral-tube heat exchanger. *Applied Thermal Engineering,* 125**,** 1280-1290.